NASA CR-54679
HRL-6278-SA

ION THRUSTOR ELECTRODE SURFACE PHYSICS STUDIES

by

R. G. Wilson

prepared for

NATIONAL AERONAUTICS AND SPACE ADMINISTRATION

CONTRACT NAS 3-6278

HUGHES

HUGHES AIRCRAFT COMPANY

RESEARCH LABORATORIES

NASA CR-54679
HRL-6278-SA

SEMIANNUAL REPORT

ION THRUSTOR ELECTRODE SURFACE PHYSICS STUDIES

by

R. G. Wilson

prepared for

NATIONAL AERONAUTICS AND SPACE ADMINISTRATION

Submitted
June 1965

Approved
October 1965

CONTRACT NAS 3-6278

Technical Management
NASA-Lewis Research Center
Cleveland, Ohio
John Ferrante

HUGHES RESEARCH LABORATORIES

Malibu, California

BLANK PAGE

TABLE OF CONTENTS

	LIST OF ILLUSTRATIONS	v
	ABSTRACT	ix
I.	INTRODUCTION AND SUMMARY	1
II.	THEORETICAL CALCULATIONS	5
III.	EXPERIMENTAL MEASUREMENTS	27
	A. Vacuum Work Functions	27
	B. Cesiated Electron Emission	40
	C. Cesium Ion Emission	55
	D. Emitter Fabrication	69
	REFERENCES	73
	APPENDIX	
	DISTRIBUTION LIST	

BLANK PAGE

LIST OF ILLUSTRATIONS

Fig. 1.	Experimental tube geometry	3
Fig. 2.	Composite surface work function versus arrival flux for 27 adsorbate atoms on tungsten	6
Fig. 3.	Composite surface work function versus arrival flux for 27 adsorbate atoms on iridium	7
Fig. 4.	Composite surface work function versus arrival flux for 27 adsorbate atoms on rhenium	8
Fig. 5.	Composite surface work function versus arrival flux for 27 adsorbate atoms on rhodium	9
Fig. 6.	Composite surface work function versus arrival flux for 27 adsorbate atoms on nickel	11
Fig. 7.	Composite surface work function versus arrival flux for 27 adsorbate atoms on platinum	12
Fig. 8.	Composite surface work function versus arrival flux for 27 adsorbate atoms on osmium	13
Fig. 9.	Composite surface work function versus arrival flux for 27 adsorbate atoms on molybdenum	15
Fig. 10.	Composite surface work function versus arrival flux for 27 adsorbate atoms on tantalum	17
Fig. 11.	Composite surface work function versus arrival flux for beryllium on nine substrate surfaces	19
Fig. 12.	Composite surface work function versus arrival flux for copper on nine substrate surfaces	20

Fig. 13. Composite surface work function versus arrival flux for nickel on nine substrate surfaces 21

Fig. 14. Composite surface work function versus arrival flux for adsorbate atoms of aluminum, iron, copper, and nickel on a tungsten surface at the four surface temperatures 1300, 1400, 1500, and 1600 K 22

Fig. 15. Composite surface work function versus arrival flux for the five adsorbate atoms beryllium, aluminum, iron, nickel, and copper on a tungsten surface (no surface coverage limitation) 23

Fig. 16. Composite surface work function versus arrival flux for the five adsorbate atoms beryllium, aluminum, iron, nickel, and copper on a rhenium surface (no surface coverage limitation) 24

Fig. 17. Composite surface work function versus arrival flux for the five adsorbate atoms beryllium, aluminum, iron, nickel, and copper on an iridium surface (no surface coverage limitation) . . 25

Fig. 18. Electron emission from cesiated beryllium 41

Fig. 19. Electron emission from cesiated titanium 43

Fig. 20. Electron emission from cesiated chromium 44

Fig. 21. Electron emission from cesiated nickel 45

Fig. 22. Electron emission from cesiated copper 47

Fig. 23. Electron emission from cesiated rhenium 48

Fig. 24. Electron emission from cesiated iridium 49

Fig. 25. Electron emission from cesiated platinum 50

Fig. 26. Electron emission from cesiated 304 stainless steel 52

Fig. 27. Electron emission from cesiated Lucalox aluminum oxide (decreasing temperature) 53

Fig. 28. Electron emission from Lucalox aluminum oxide (increasing temperature) 54

Fig. 29. Cesium ion emission from beryllium 56

Fig. 30. Cesium ion emission from titanium 57

Fig. 31. Cesium ion emission from chromium 59

Fig. 32. Cesium ion emission from nickel 60

Fig. 33. Cesium ion emission from copper 61

Fig. 34. Cesium ion emission from rhenium 63

Fig. 35. Cesium ion emission from iridium 64

Fig. 36. Cesium ion emission from platinum 65

Fig. 37. Cesium ion emission from 304 stainless steel 67

Fig. 38. Cesium ion emission from Lucalox aluminum oxide (actual data) 68

Fig. 39. Cesium ion emission from Lucalox aluminum oxide (smoothed-out data) 70

ION THRUSTOR ELECTRODE SURFACE PHYSICS STUDIES

by R. G. Wilson

ABSTRACT

23820

Experimental data concerning electron and ion emission from cesiated (and vacuum) surfaces of beryllium, titanium, chromium, nickel, copper, rhenium, iridium, platinum, 304 stainless steel, and Lucalox are reported. Included are vacuum work functions, electron emission S curves, cesium ion emission and critical temperature envelopes, and ion desorption energies. The range of cesium arrival flux is 10^{13} to 10^{17} atoms/cm^2-sec. Iridium and rhenium hold promise of being better cesium contact ionizers. No material clearly superior to copper has yet been found for accel electrodes. Because aluminum oxide is an insulator and was studied in bulk form rather than as a thin film, the emission measurements have not unequivocably proved it to be a superior focus electrode material. Theoretical computer calculations are reported for surface work function, cesium atom desorption energy, and cesium ion desorption energy versus surface coverage for cesium adsorbed on 27 metal substrates and for 21 other adsorbates on each of nine metal substrates. Residence times for 11 adsorbates on each of nine substrates versus surface temperature for six values of coverage from zero to one monolayer and the same residence times versus adsorbate arrival flux (to 10^{21} atoms/cm^2-sec) for several values of surface temperature are also included. Three separate volumes comprise this report. Author

1. INTRODUCTION AND SUMMARY

This Semiannual Report on Contract NAS 3-6278 consists of three volumes: this volume contains the technical discussion and two additional volumes contain supplementary analytical calculations. This contract has the objective of improving the lifetime and efficiency of cesium surface contact ionization electrostatic thrustors by providing experimental and analytical information necessary for the selection of materials from which to fabricate improved thrustor electrodes.

The experimental information to be provided consists of the electron and ion emission properties of a variety of cesiated surfaces, and vacuum emission data. Parameters being measured are vacuum work functions, electron emission versus surface temperature for cesium arrival fluxes between 10^{13} and 10^{17} atoms/cm^2-sec, and cesium surface ionization current densities versus surface temperature for the same cesium arrival fluxes. These last measurements yield surface ionization critical temperature envelopes and cesium ion desorption energies at low coverage. The materials to be studied under this contract, and those studied under Contract NAS 3-5249, are listed in Table I.

A theoretical phase of the program involves analytical calculations of composite surface work functions, atom and ion desorption energies, atom residence times, surface diffusion coefficients, and surface coverage as functions of substrate surface temperature and adsorbate arrival flux.

The experimental design and techniques used in this work are described in detail in the Final Report on Contract NAS 3-5249. A summary of the important features is included here. Figure 1 illustrates some features of the experiment. A plane parallel electrode geometry with superimposed electric and magnetic fields is used. The collector is fabricated from the same pure material as the emitter to ensure the correct surface characteristics during energetic cesium ion emission, which results in sputtering of the collector back onto the emitter surface.

TABLE I

Materials Under Experimental Study

Material	Studied Under NAS 3-5249	Studied Under NAS 3-6278 and Reported Herein	Not Yet Reported
beryllium		x	
titanium		x	
chromium	x	x	
iron	x		
nickel		x	
copper	x	x	
niobium			x
molybdenum	x		
tungsten			x
rhenium		x	
osmium			x
iridium		x	
platinum		x	
304 stainless steel		x	
tantalum boride	x		(x)
zirconium carbide			x
molybdenum carbide			x
molybdenum silicide	x		
tantalum silicide			x
tungsten silicide			x
aluminum oxide (sintered)	x		
aluminum oxide (Lucalox)		x	
oxygenated copper			x

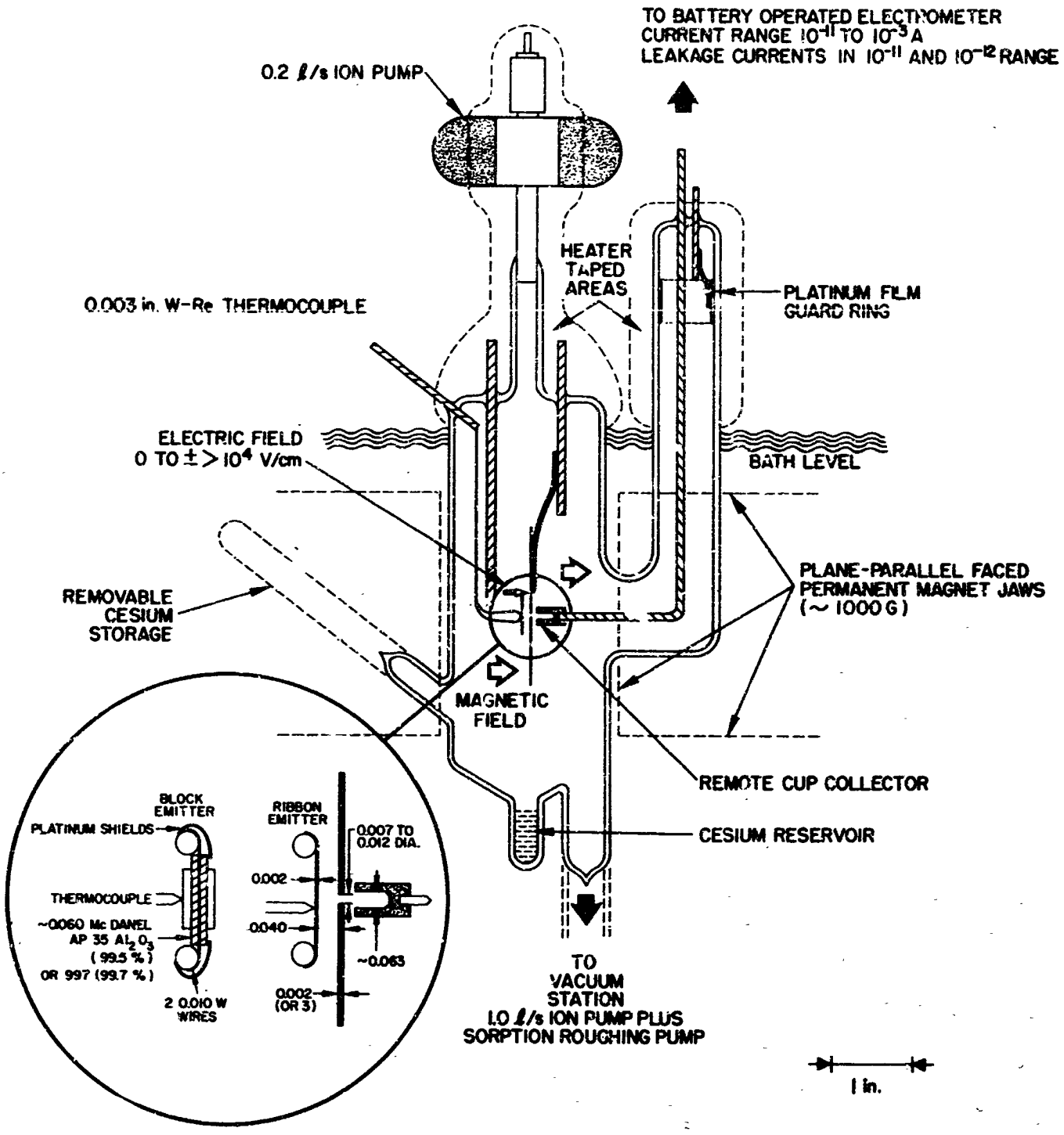

Fig. 1. Experimental tube geometry.

A dual collector system, one of which is a remotely mounted aperture-Faraday cup collector, is employed. Three-mil tungsten-rhenium thermocouples continuously monitor the emitter surface temperature. The cesium arrival flux is controlled and varied by a magnetic thermostat controlled temperature bath. A sorption roughed and ion pumped bakeable vacuum system produces pressures of 1×10^{-9} Torr, excluding cesium and emitter vapor (at high temperatures). Each experimental tube is pinched off from the main vacuum system, and is subsequently pumped by an appendage ion pump. Emission data are recorded automatically with continuous current and temperature calibration on an x-y recorder as emission current density versus thermocouple millivolts. The recorder traces are fed to a digital computer which subtracts the background currents, multiplies by an area factor to yield current density, and plots the answer on a logarithmic ordinate; the thermocouple millivolts are converted to degrees Kelvin by use of a reference table, and the reciprocal is plotted on the abscissa. Six cesium arrival fluxes between 10^{13} and 10^{17} atoms/cm^2-sec are studied for each surface. Six cesium electron emission S curves are obtained, and six cesium ionization critical temperatures allow an envelope to be drawn; the slope of this envelope determines the cesium ion desorption energy at the critical coverage, which is between 0.002 and 0.03.

II. THEORETICAL CALCULATIONS

Using equations already developed,[1] digital computer programs were generated to calculate and plot composite surface work functions and atom and ion desorption energies as functions of surface coverage. This program was used to calculate and plot these quantities for 21 adsorbates on each of nine substrates. The adsorbates include the desorbable elements studied experimentally under Contracts NAS 3-6278 and NAS 3-5249, five of the six metals being studied under Contract NAS 3-6273, several alkali and alkaline earth metals, and a few others. A total of 567 curves on 261 graphs (some for two values of the heat of sublimation) have been plotted. One hundred eighty-seven of these graphs (561 curves) have been reproduced and bound separately as a supplement to this report, entitled "Work Function and Desorption Energy Calculations." The nine substrates are tungsten, iridium, rhenium, rhodium, nickel, platinum, osmium, molybdenum, and tantalum. The 21 adsorbates are lithium, beryllium, carbon, sodium, aluminum, silicon, potassium, titanium, chromium, manganese, iron, nickel, copper, gallium, rubidium, indium, tin, cesium, barium, mercury, and lead. Curves for cesium on 27 substrates are included as an appendix to this report.

Also calculated, using a computer program but plotted by hand, are plots of composite surface work function and corresponding surface coverage as functions of the arrival flux of 27 adsorbates on the same nine substrates listed above. These calculations were made using the small coverage approximation. The results are accurate only to about 0.05 of a monolayer of surface coverage, which is probably too large a coverage to be tolerated in a cesium ion thrustor. These curves are plotted to $\theta = 0.1$ in Figs. 2 through 10. The calculations and curves cover the range of arrival flux from 10^{8} to 10^{21} atoms/cm^{2}-sec. The 27 adsorbates are lithium, beryllium, carbon, sodium, aluminum, silicon, potassium, calcium, titanium, chromium, manganese, iron, nickel,

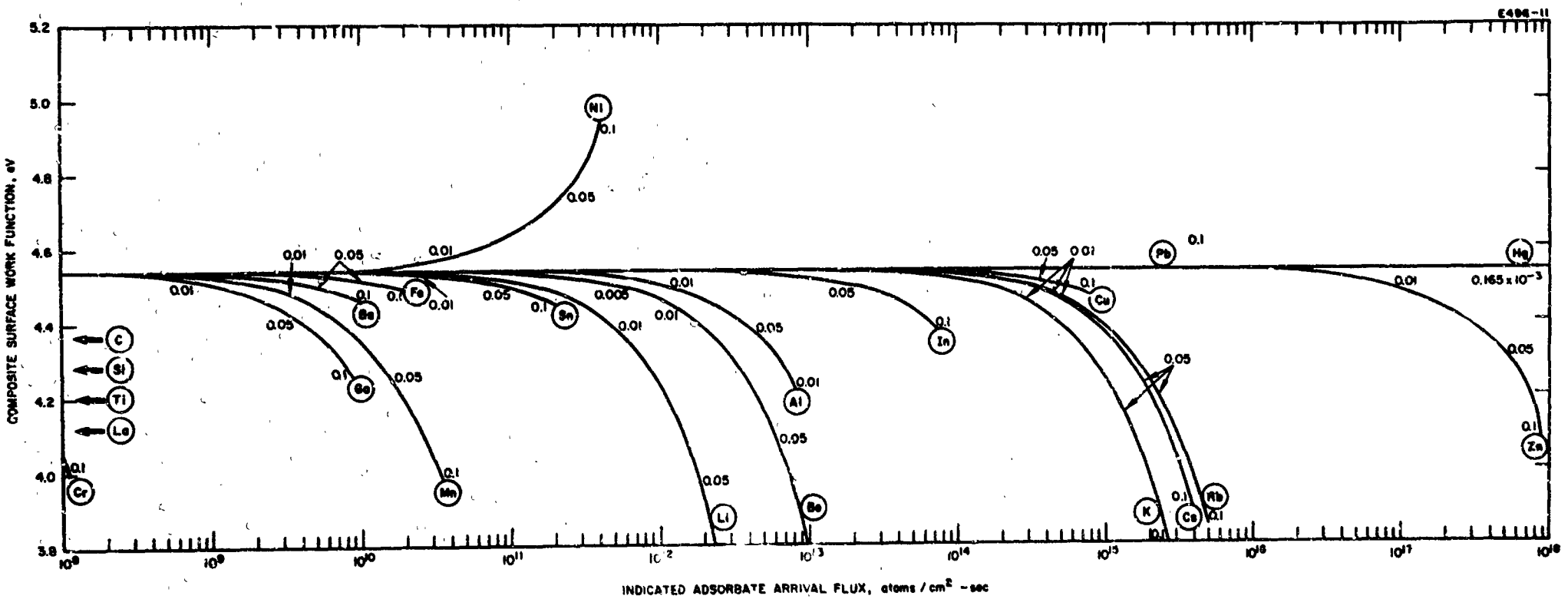

Fig. 2. Composite surface work function versus arrival flux for 27 adsorbate atoms on tungsten.

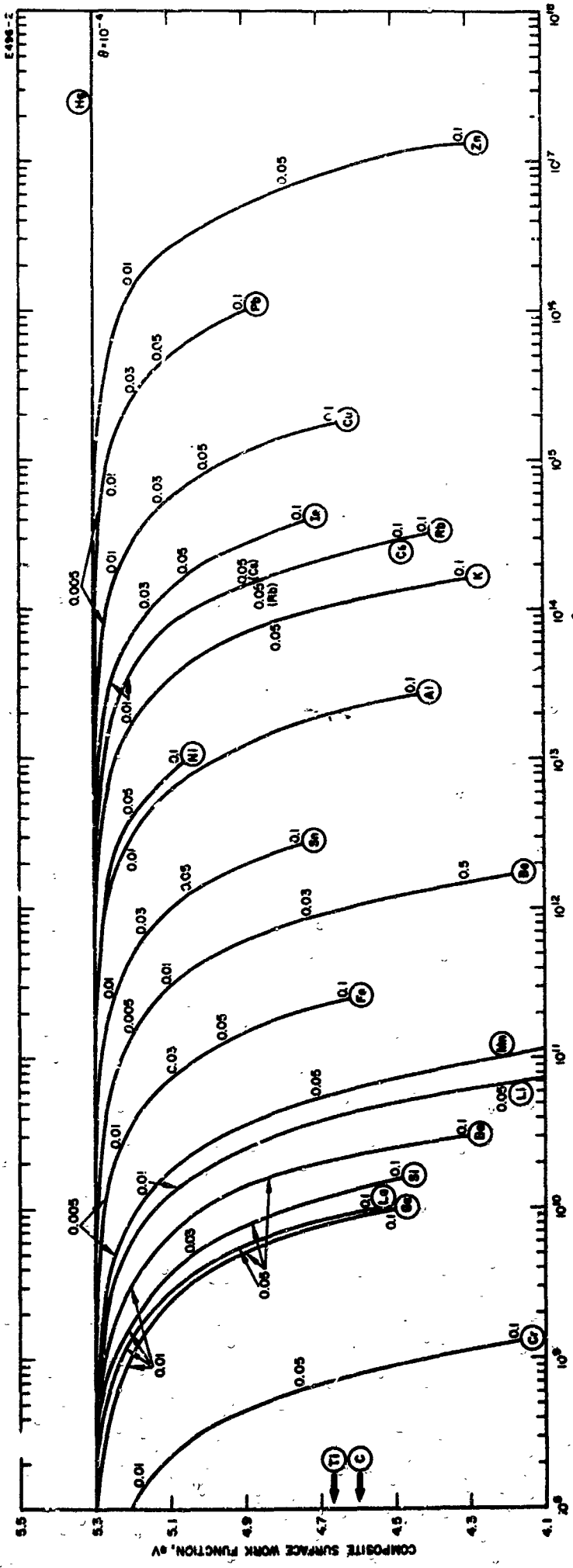

Fig. 3. Composite surface work function versus arrival flux for 27 adsorbate atoms on iridium.

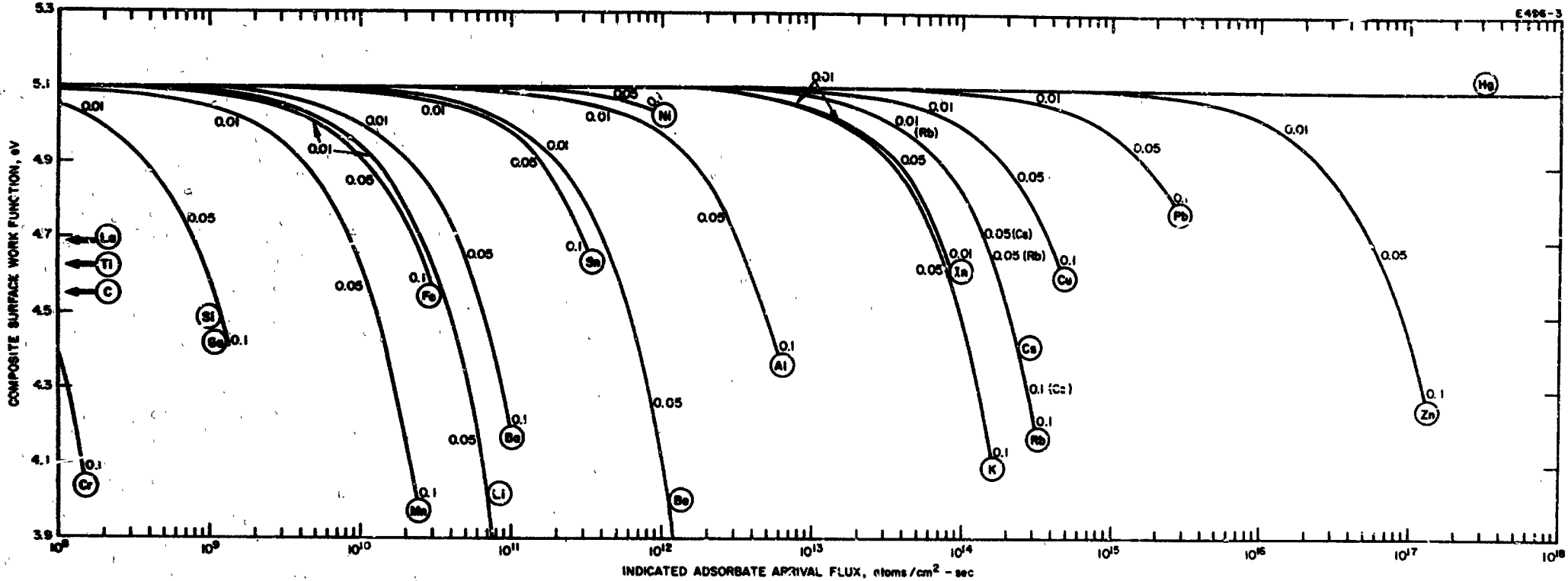

Fig. 4. Composite surface work function versus arrival flux for 27 adsorbate atoms on rhenium.

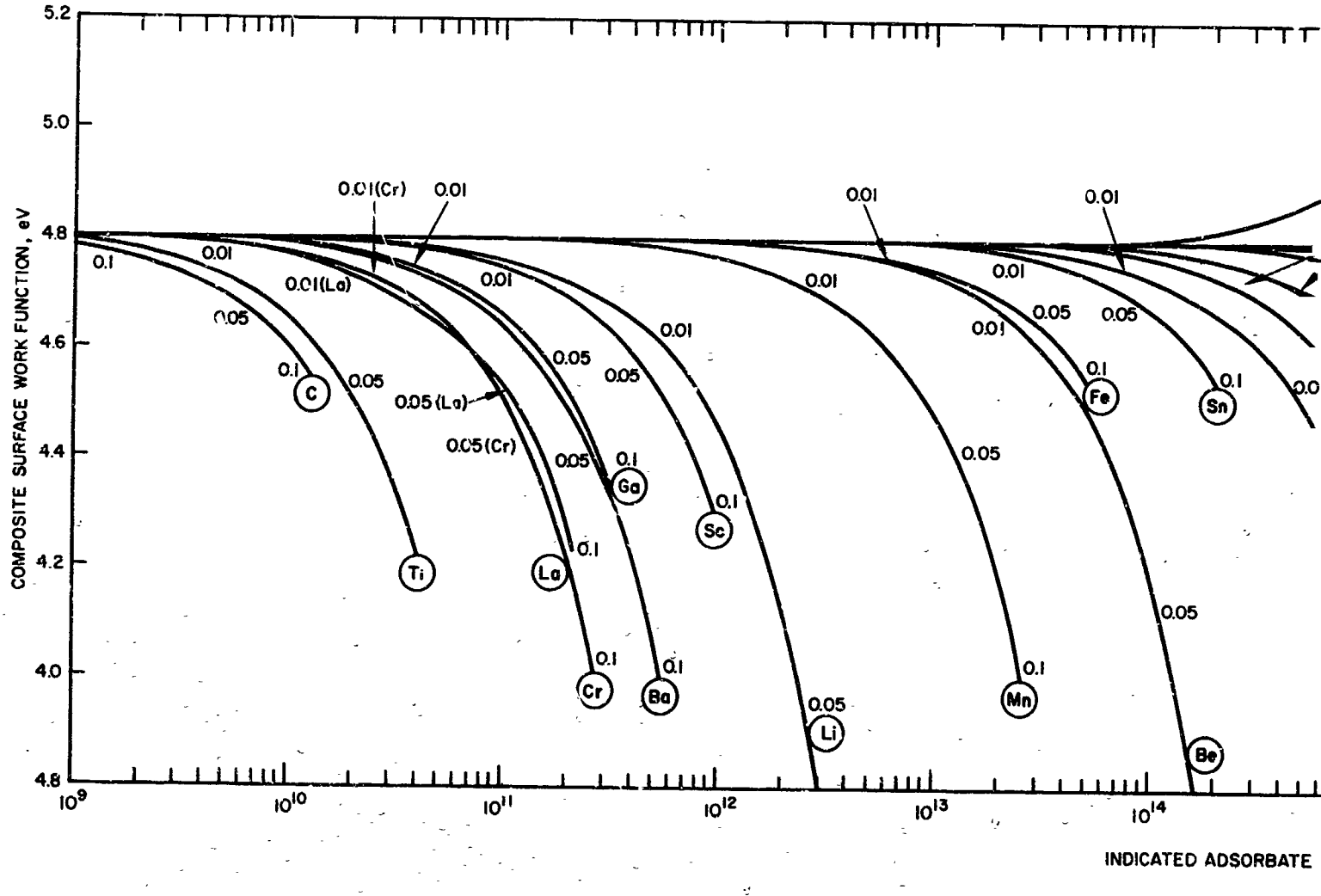

Fig. 5. Composite surface work function versu

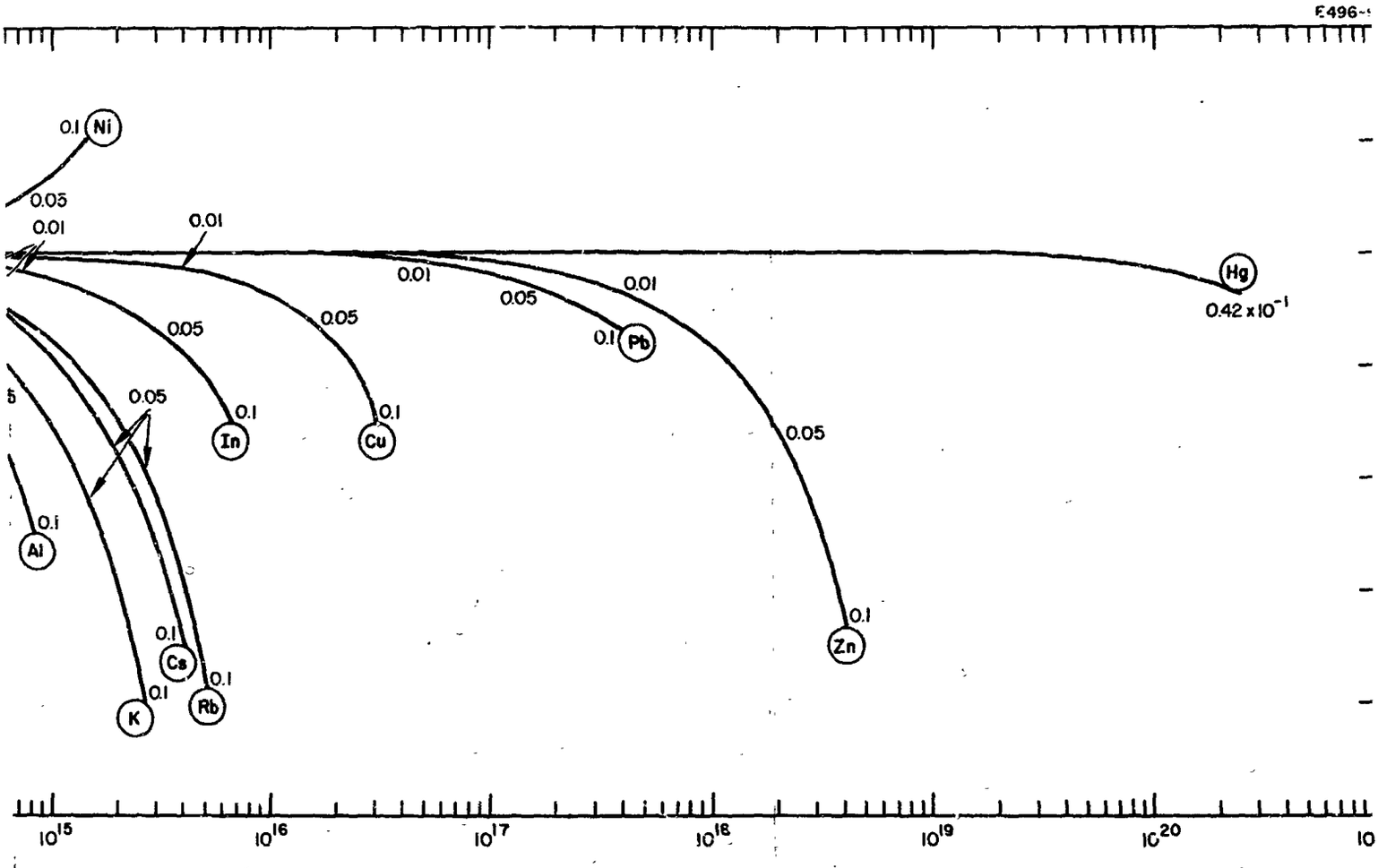

s arrival flux for 27 adsorbate atoms on rhodium.

(2)

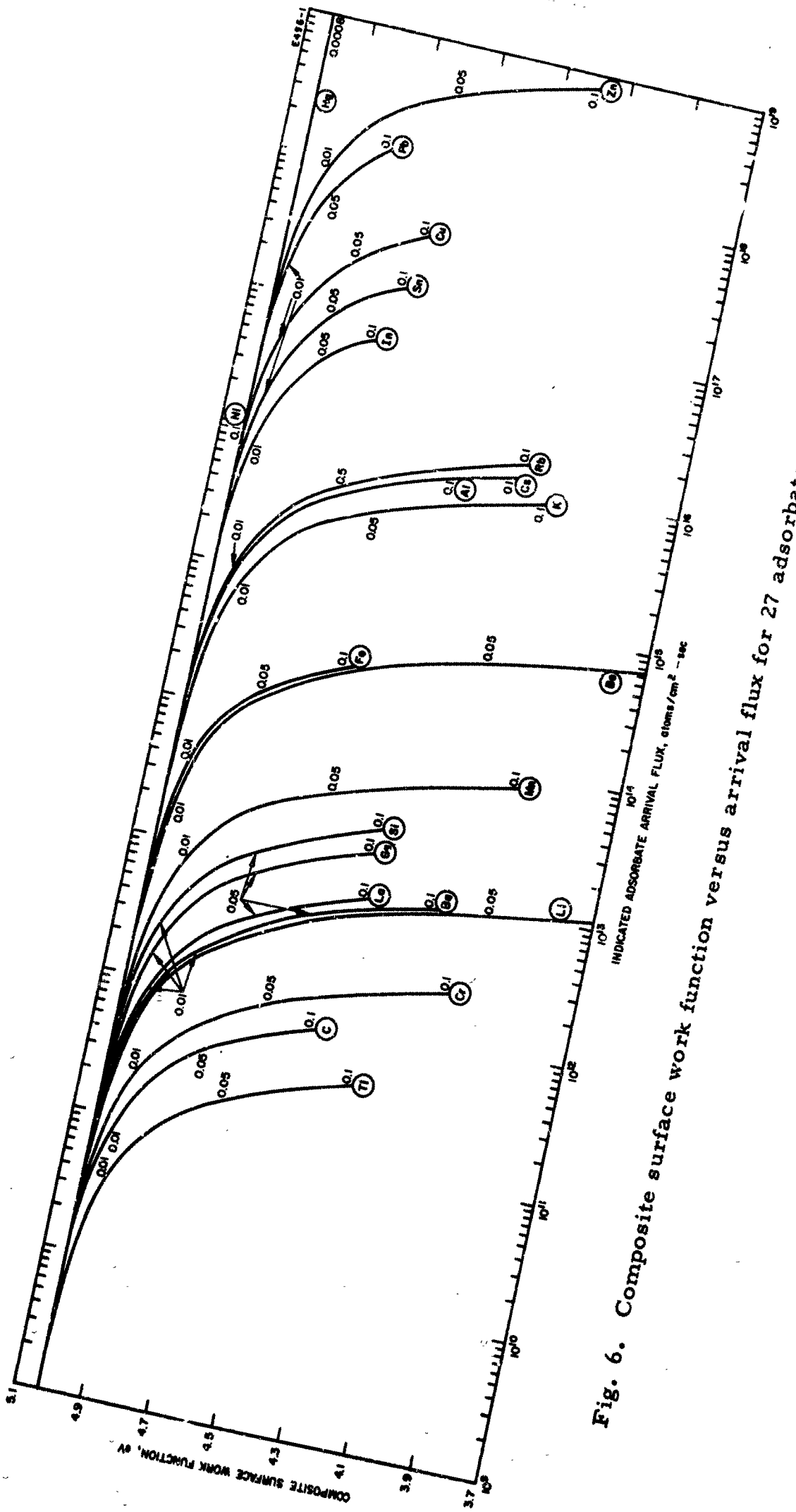

Fig. 6. Composite surface work function versus arrival flux for 27 adsorbate atoms on nickel.

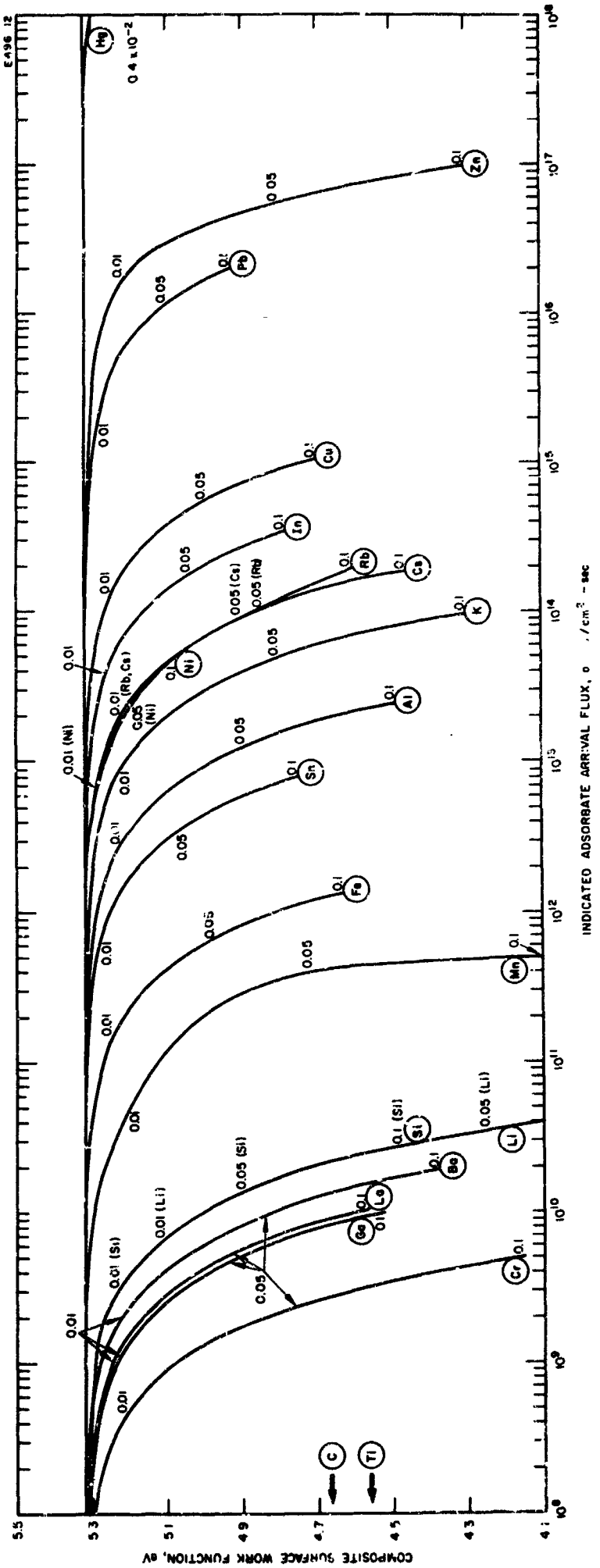

Fig. 7. Composite surface work function versus arrival flux for 27 adsorbate atoms on platinum.

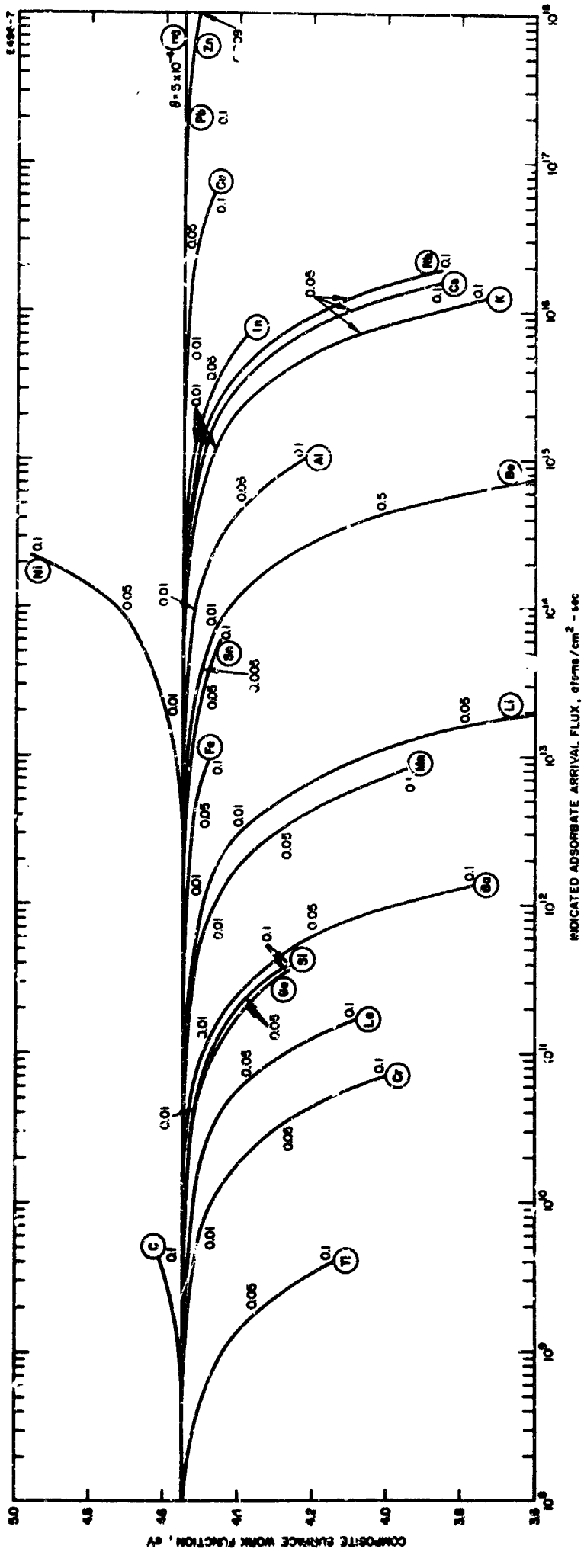

Fig. 8. Composite surface work function versus arrival flux for 27 adsorbate atoms or osmium.

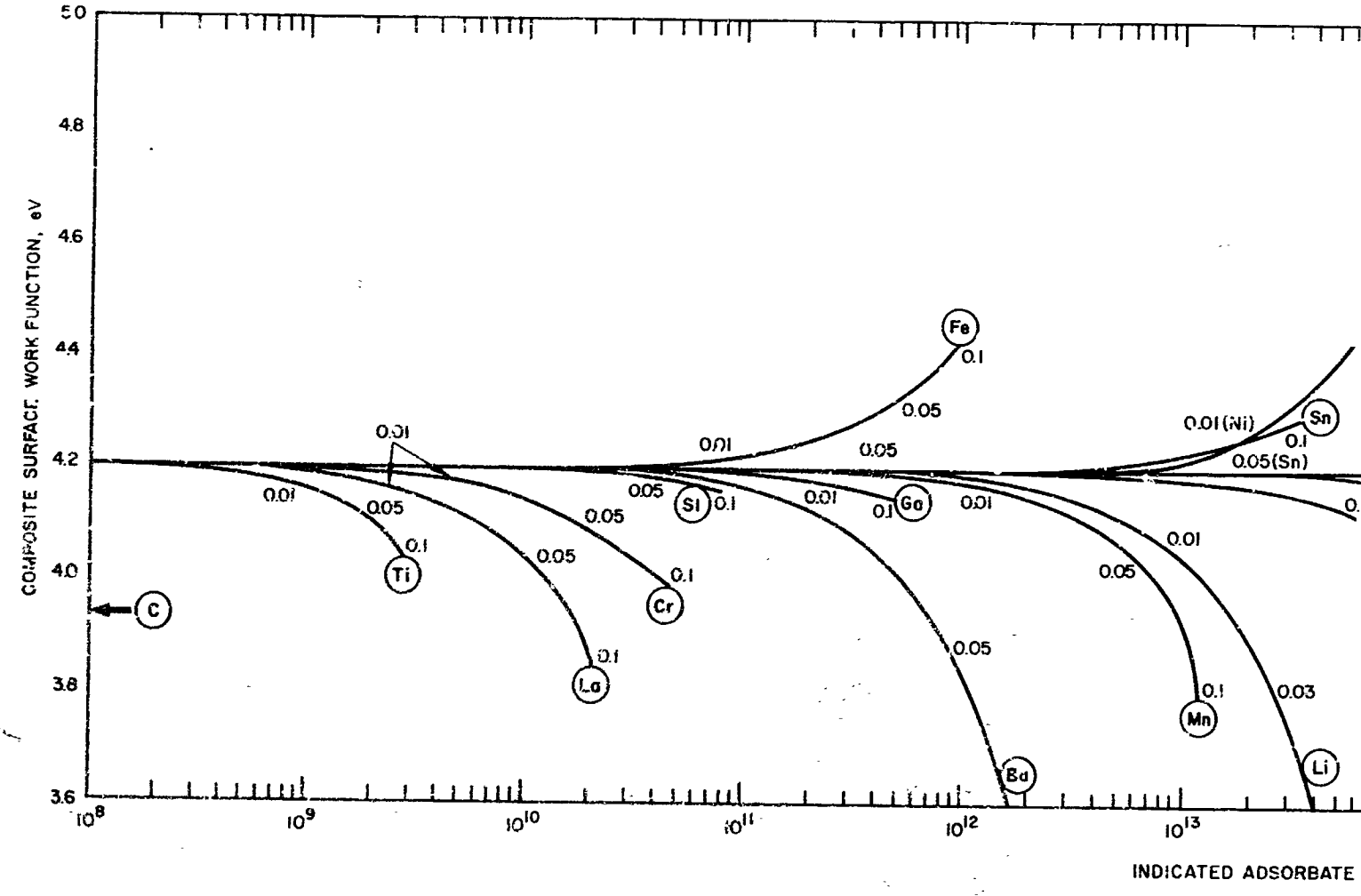

Fig. 9. Composite surface work function versus arr

PRECEDING PAGE BLANK NOT FILMED.

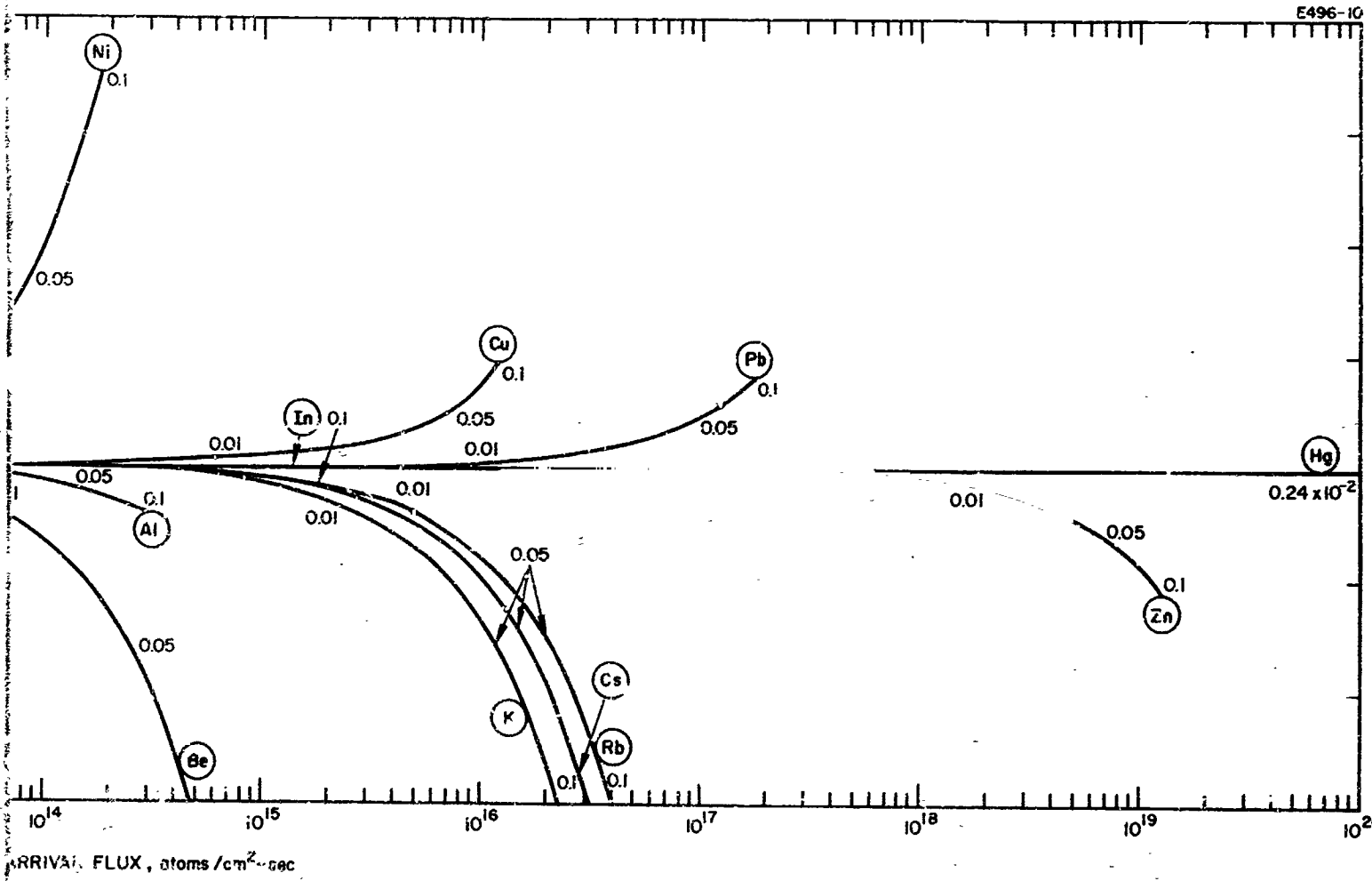

val flux for 27 adsorbate atoms on molybdenum.

BLANK PAGE

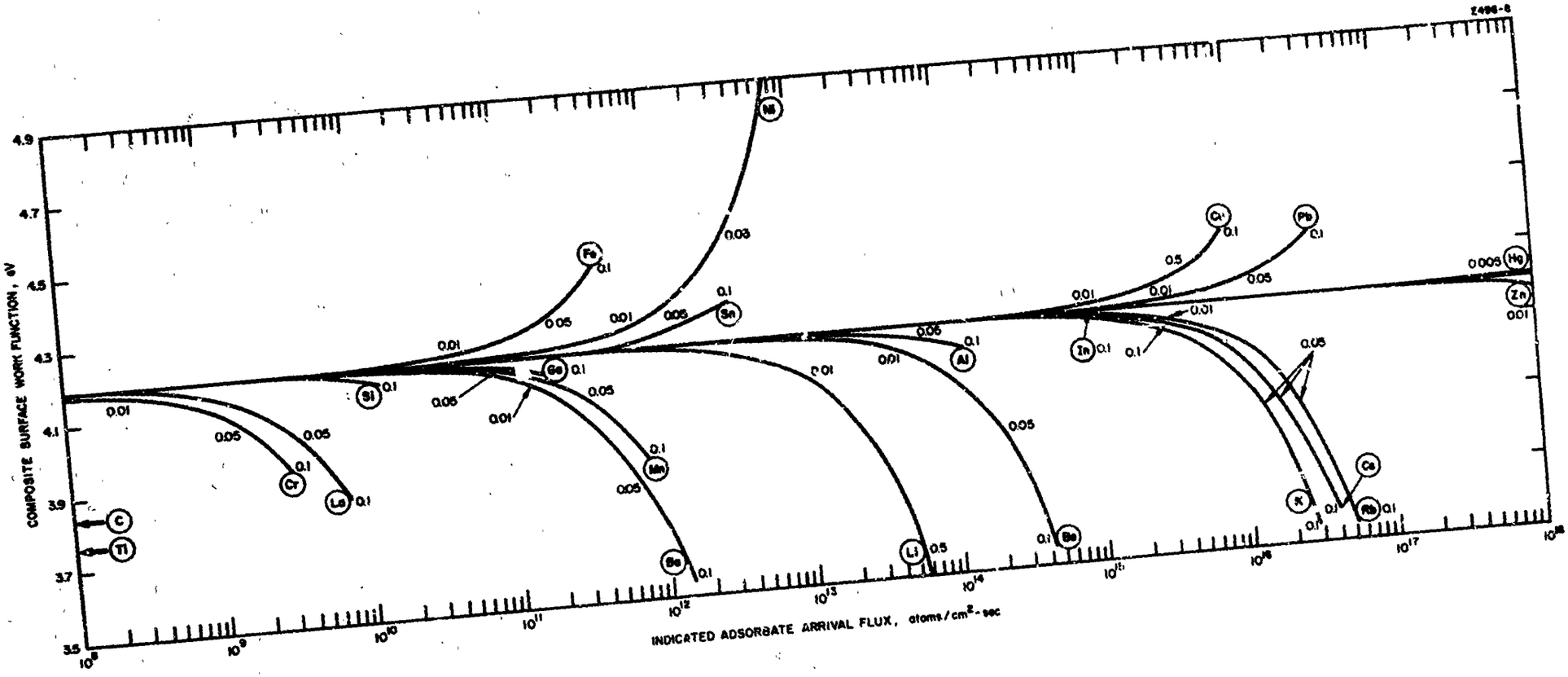

Fig. 10. Composite surface work function versus arrival flux for 27 adsorbate atoms on tantalum.

copper, zinc, gallium, rubidium, strontium, silver, cadmium, indium, tin, cesium, barium, lanthanum, mercury, and lead.

To show more clearly the variations among the nine substrates, three particular adsorbates with a wide range of work functions – beryllium (3.7 eV), copper (4.4 eV), and nickel (5.0 eV) – have been selected, and the composite surface work function versus arrival flux curves for the nine substrates have been plotted on separate graphs (Figs. 11 through 13). As before, these curves are for the small coverage approximation, and are plotted to $\theta = 0.1$. To show the influence of surface temperature, composite surface work function versus arrival flux curves for four adsorbates (aluminum, copper, iron, and nickel) on tungsten are plotted in Fig. 14 for surface temperatures of 1300, 1400, 1500, and 1600 K. These curves are also for the small coverage approximation.

A computer program was formulated for composite surface work function versus adsorbate arrival flux for several adsorbate metals on tungsten with the full θ dependence rather than with the small surface coverage approximations. Such calculations involve lengthy iterative processes to some chosen degree of accuracy, but result in full curves of $\phi[\theta(\mu)]$ versus μ. Calculations of this type were run for each of five adsorbates on each of three substrates throughout the arrival flux range from 10^8 to 10^{21} atoms/cm^2-sec. These curves are included as Figs. 15 through 17. The five adsorbates are beryllium, aluminum, iron, nickel, and copper, and the three substrates are tungsten, rhenium, and iridium. Additional curves of this type were not calculated because very long, expensive computer computation times would have been required.

Computer programs were written for two residence time calculations. One determines residence times versus (reciprocal) substrate surface temperature for the series of surface coverages: 0.00, 0.01, 0.05, 0.10, 0.25, 0.50, and 1.00. The second calculates and plots residence times versus adsorbate arrival flux for the series of surface temperatures, 1300 to 1900 K, by hundreds of degrees. These programs have been used to calculate residence times in the range from 10^{-5} to 10^{+5} sec

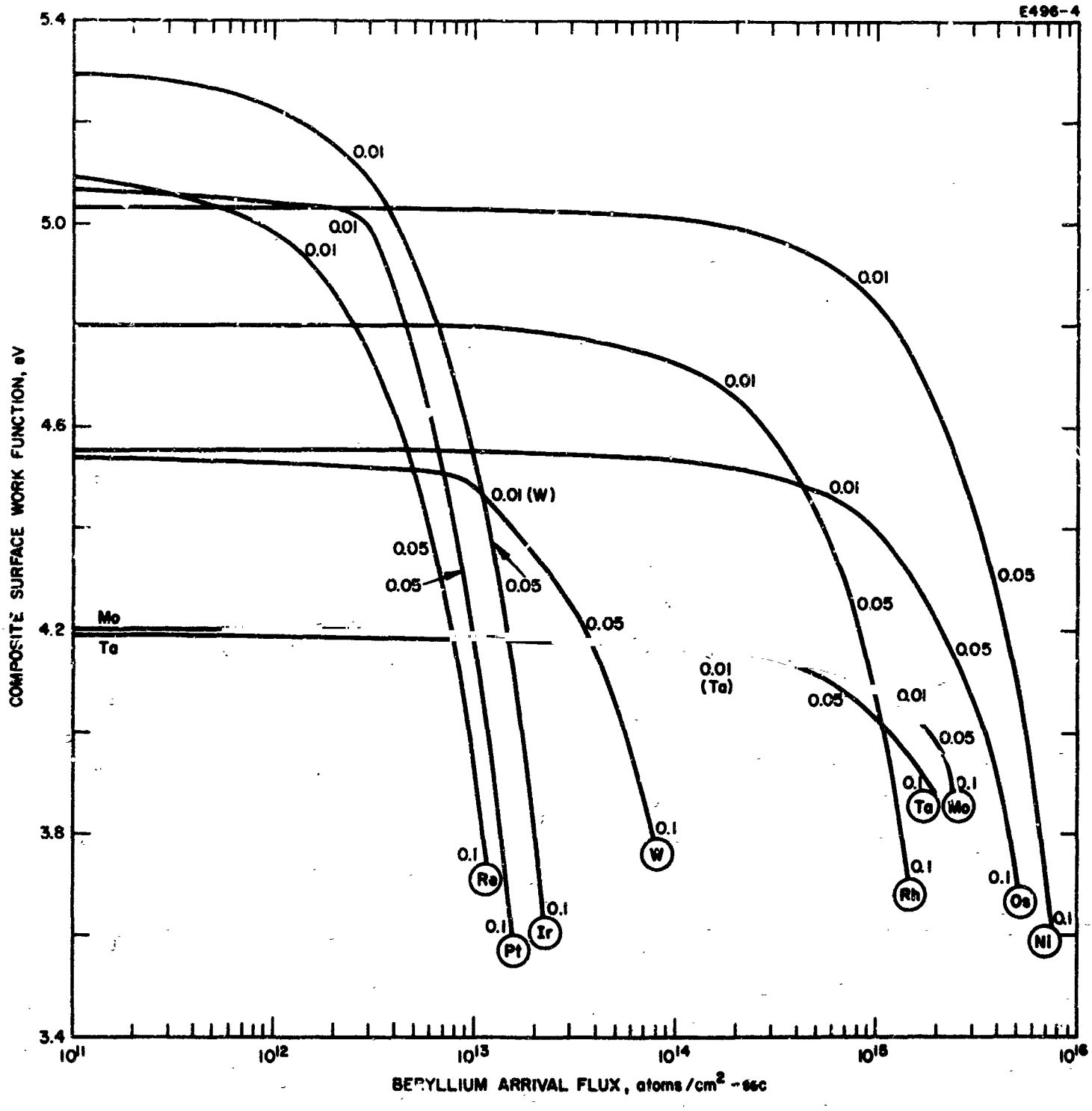

Fig. 11. Composite surface work function versus arrival flux for beryllium on nine substrate surfaces.

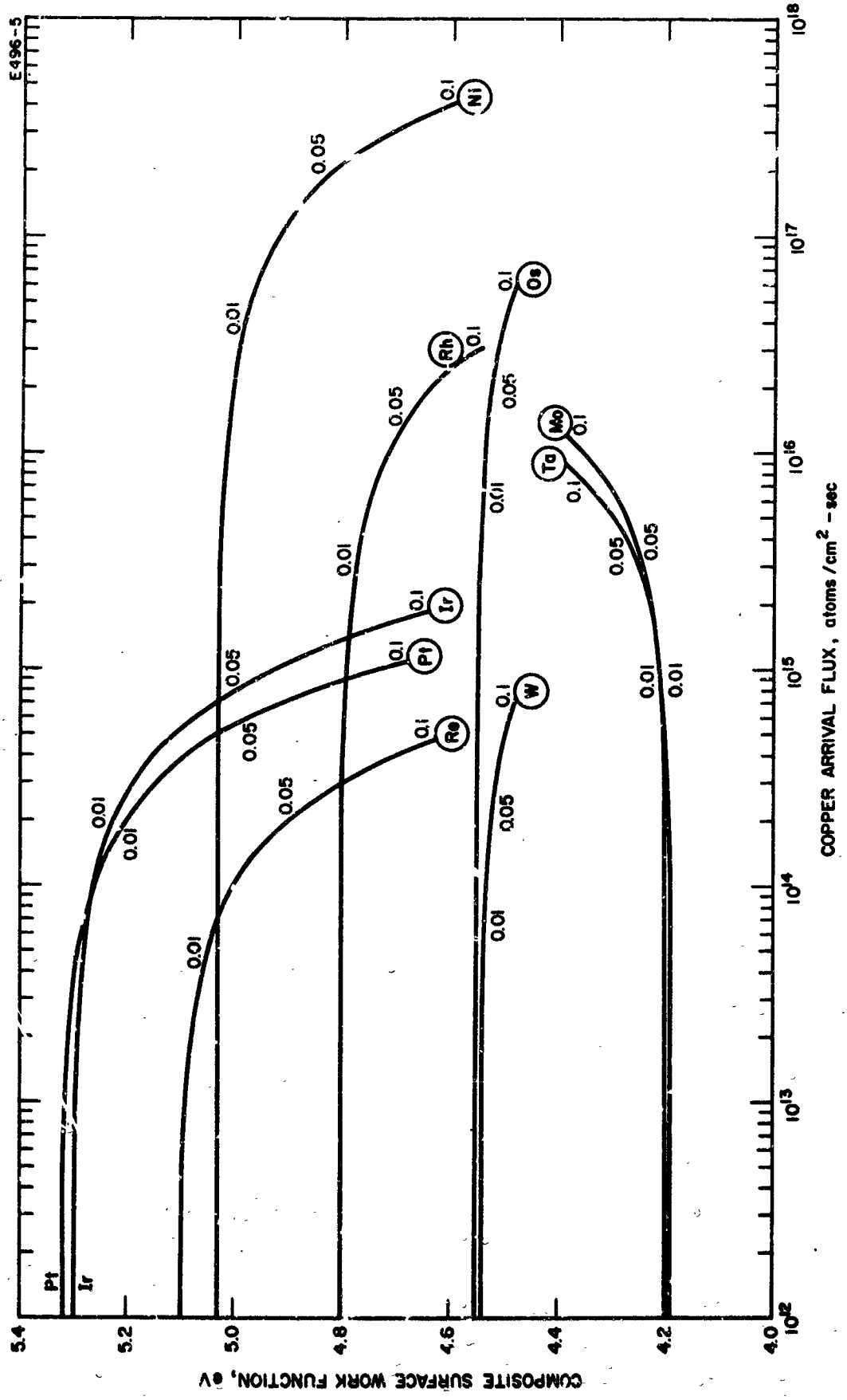

Fig. 12. Composite surface work function versus arrival flux for copper on nine substrate surfaces.

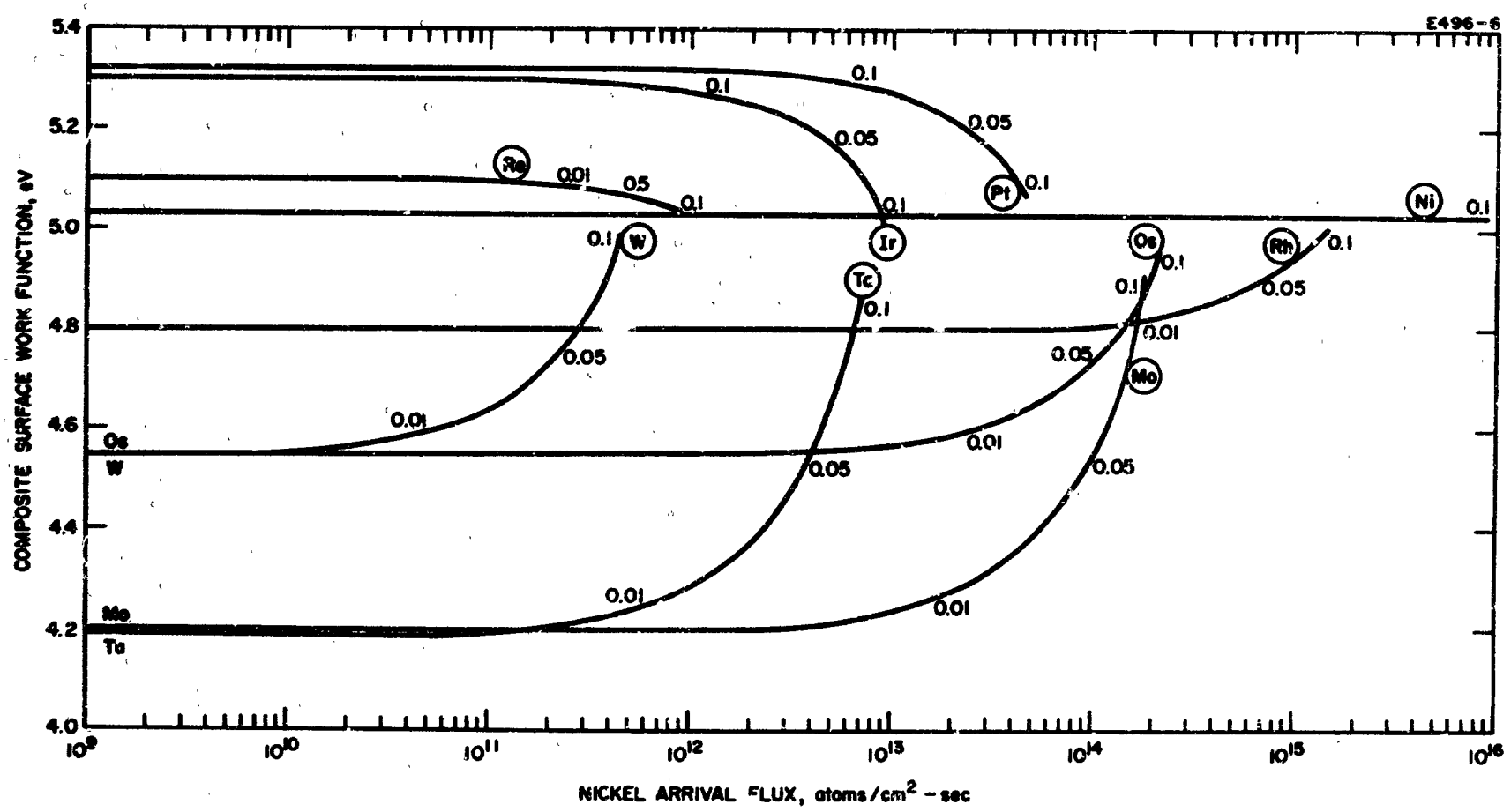

Fig. 13. Composite surface work function versus arrival flux for nickel on nine substrate surfaces.

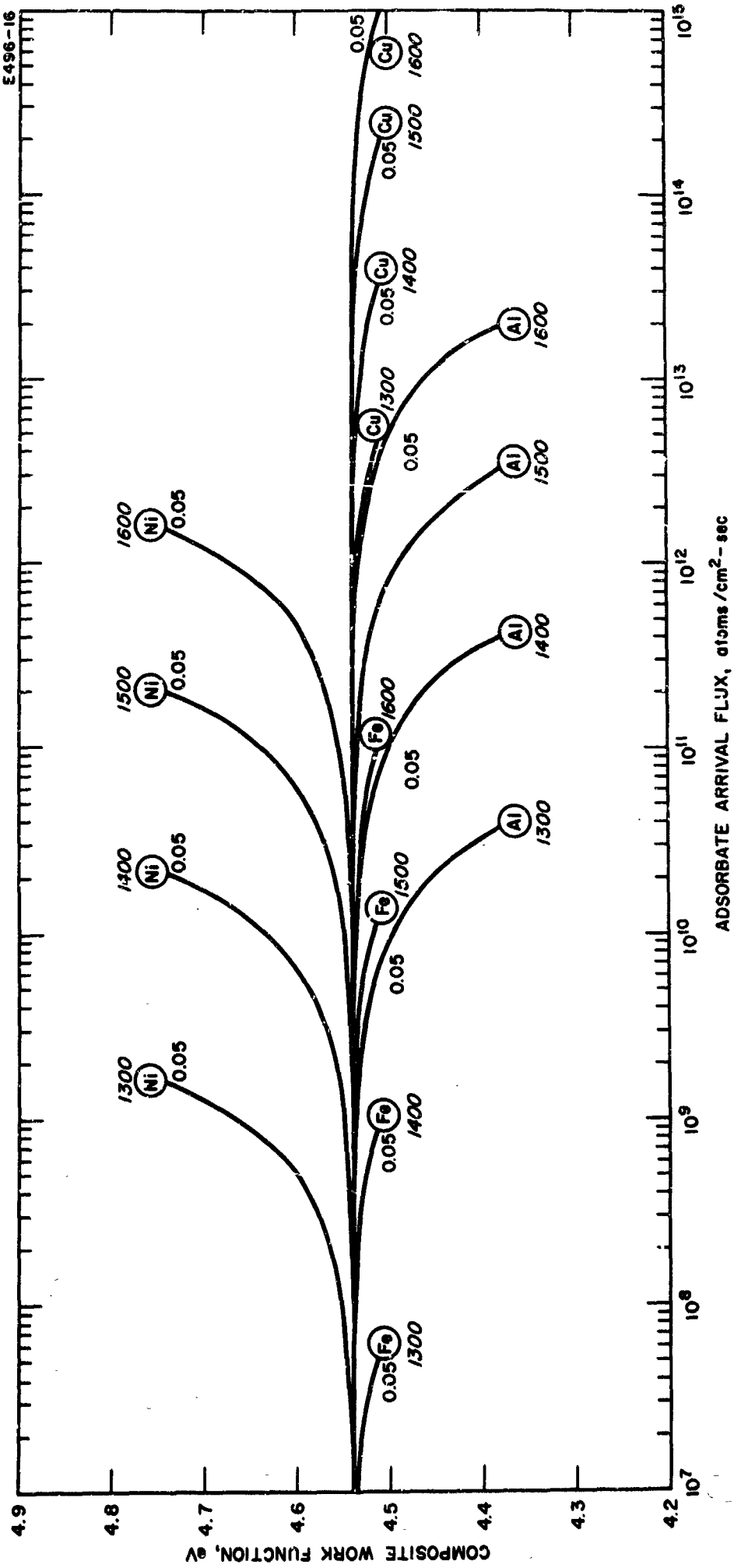

Fig. 14. Composite surface work function versus arrival flux for adsorbate atoms of aluminum, iron, copper, and nickel on tungsten surface at the four surface temperatures, 1300, 1400, 1500, and 1600 K.

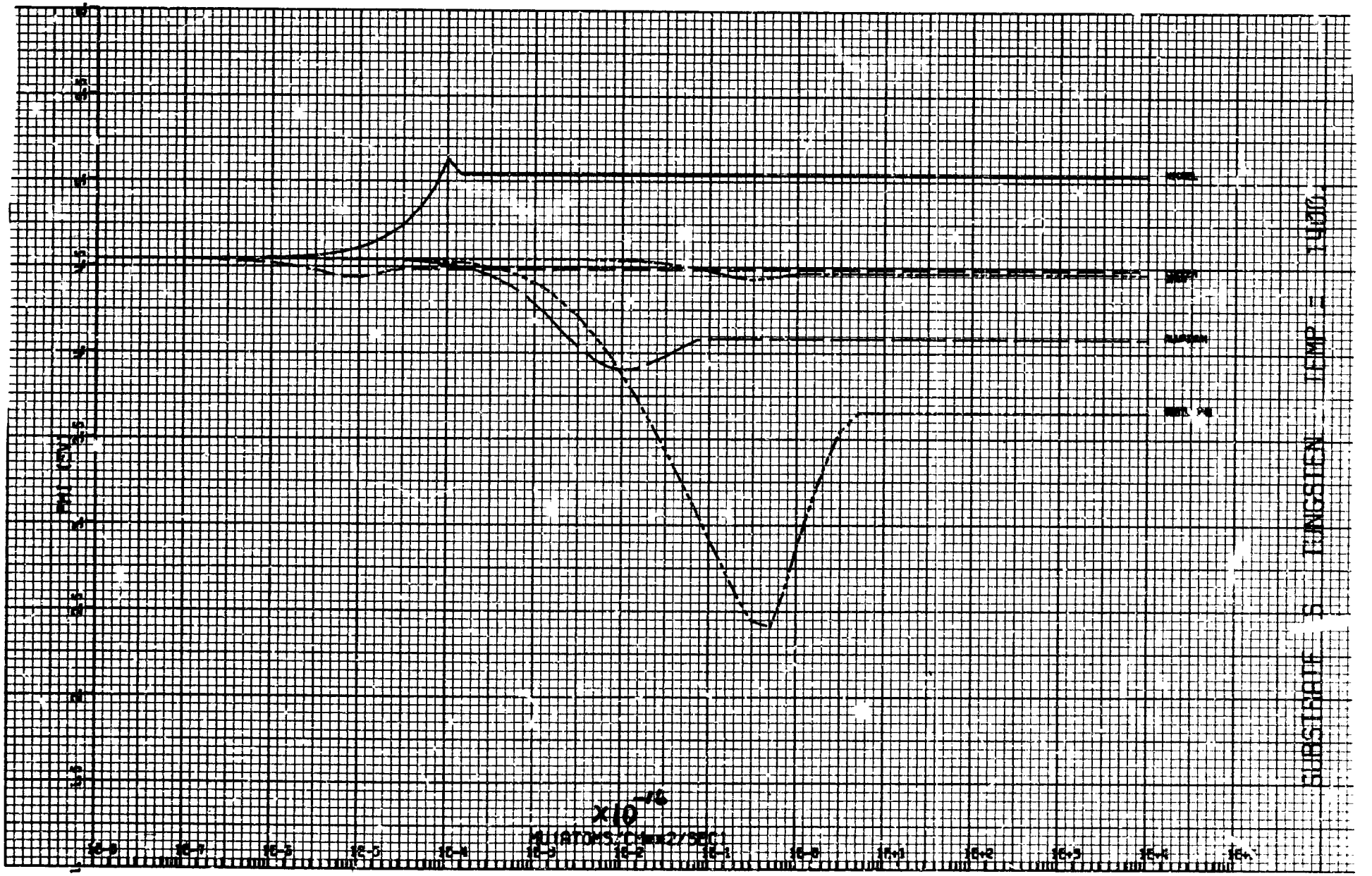

Fig. 15. Composite surface work function versus arrival flux for the five adsorbate atoms beryllium, aluminum, iron, nickel, and copper o . a tungsten surface (no surface coverage limitation).

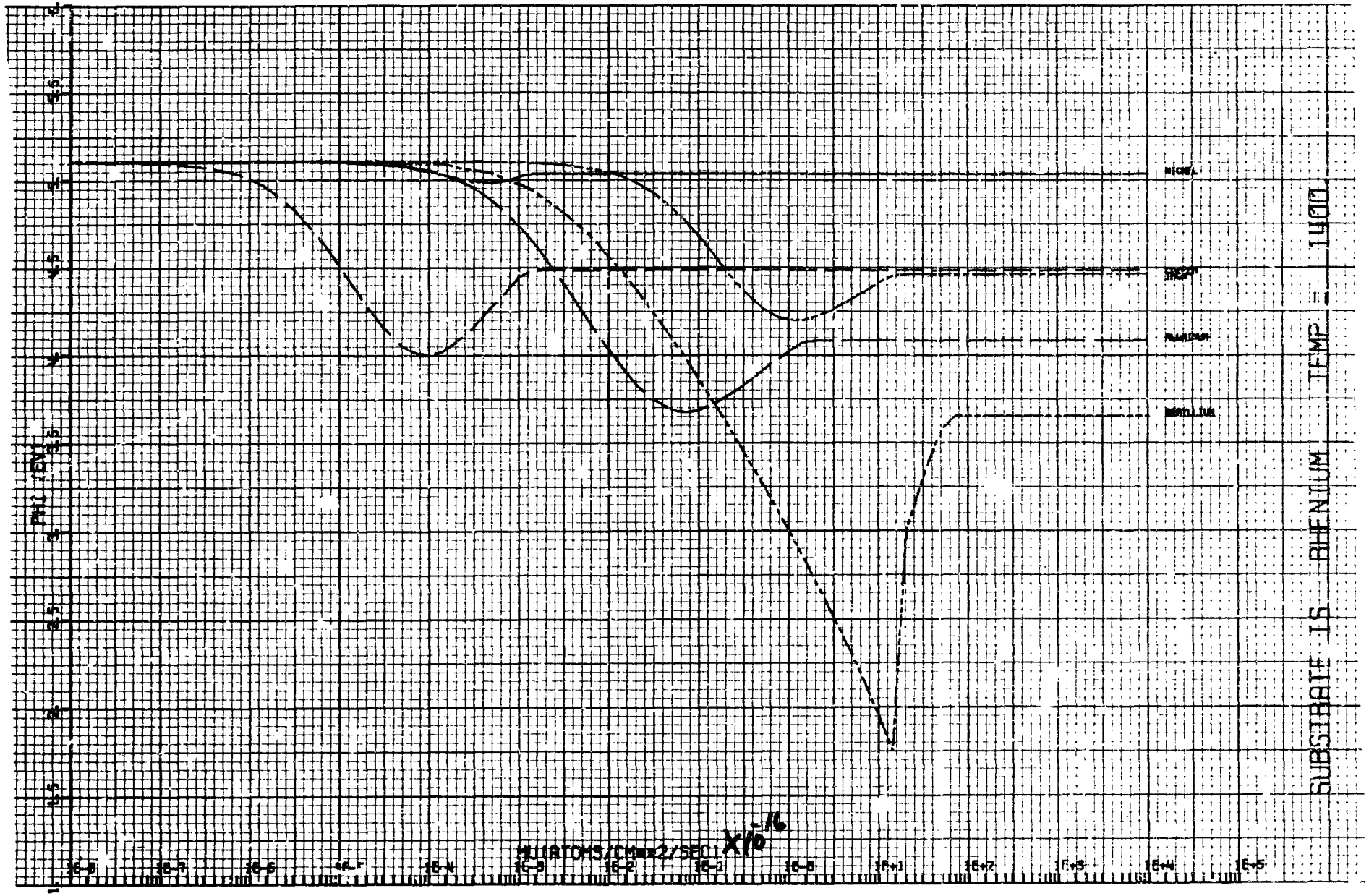

Fig. 16. Composite surface work function versus arrival flux for the five adsorbate atoms beryllium, aluminum, iron, nickel, and copper on a rhenium surface (no surface coverage limitation).

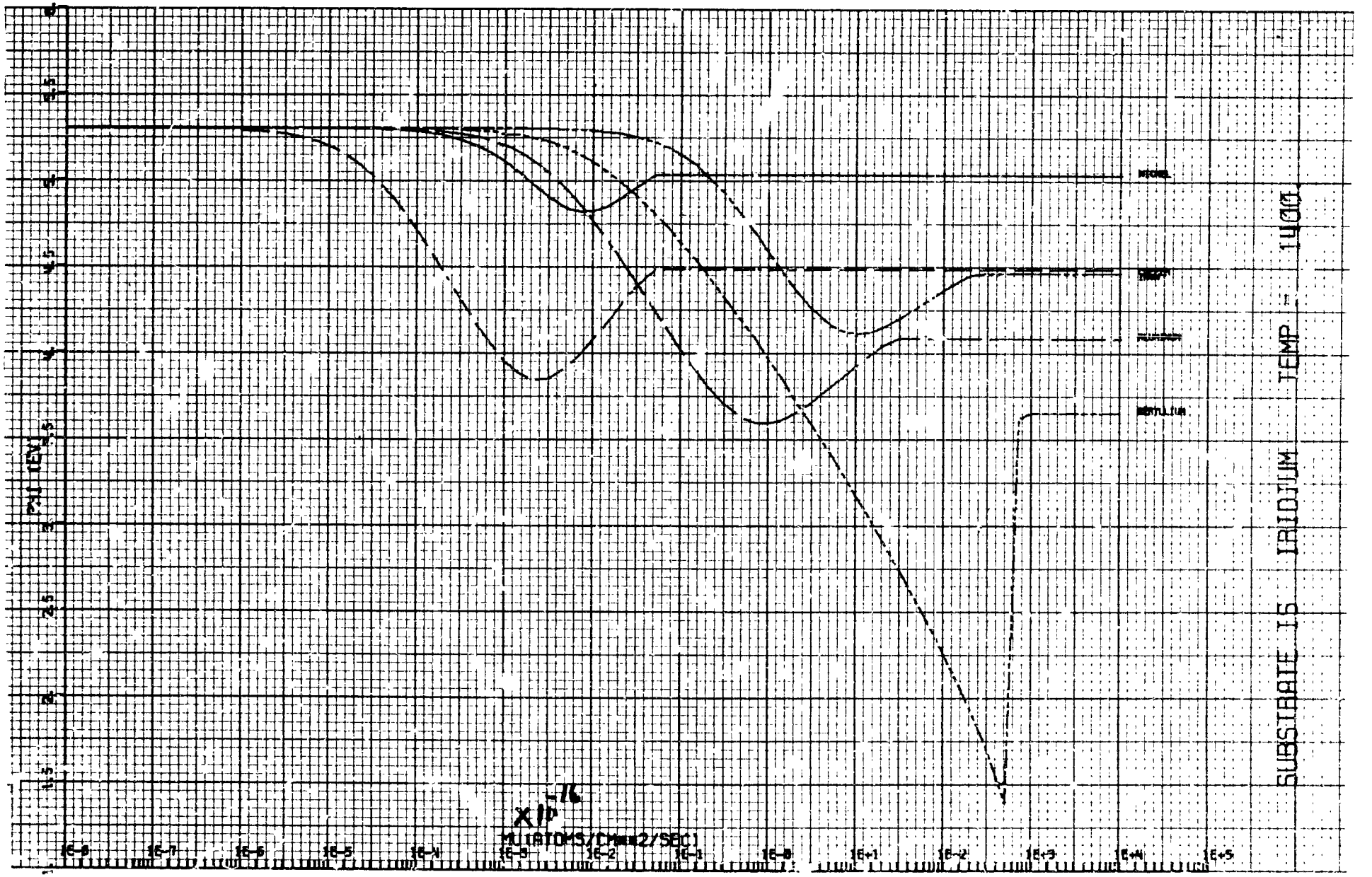

Fig. 17. Composite surface work function versus arrival flux for the five adsorbate atoms beryllium, aluminum, iron, nickel, and copper on an iridium surface (no surface coverage limitation).

for a wide range of surface temperature and for the six values of coverage with the first program, and for the range of arrival flux of 10^3 to 10^{21} atoms/cm^2-sec for the seven (or two of them) values of surface temperature with the second program, for eleven adsorbates (beryllium, carbon, aluminum, silicon, titanium, chromium, iron, nickel, copper, tin, and cesium) on nine substrates (tungsten, iridium, rhenium, rhodium, platinum, osmium, molybdenum, tantalum, and nickel). The resulting 198 graphs (812 curves) have been bound into a separate supplemental volume to this report, entitled "Residence Time Calculations."

Experimental work reported since these calculations has partially substantiated the results. Godwin and Lüscher[2] have measured the atomic desorption energies for copper and gold from a clean tungsten surface. Their values agree with these results. Shelton[3] has measured residence times for a number of atomic species from a tungsten surface. Some of his values agree very well with the calculations, while for some for which the surface conditions are questionable, the agreement, though still fairly good, is not excellent.

III. EXPERIMENTAL MEASUREMENTS

The experimental measurements and the results obtained in the first six months of this contract are divided into four areas for presentation: (1) vacuum work functions, (2) cesiated electron emission, (3) cesium ion emission, and (4) emitter fabrication.

A. Vacuum Work Functions

Before any cesiated emission measurements are made, vacuum work function data are obtained for each surface under study. The zero-field-extrapolated effective thermionic electron work functions of the polycrystalline surfaces studied in the first six months of this contract are summarized in Table II. The pertinent information regarding these polycrystalline surfaces is included in Table II: purity, number of data points, temperature range of measurements, and work function values. The following tables give the work function values and the specific measurement temperatures for each of the surfaces studied.

1. Beryllium

The vacuum work function of beryllium was measured at 11 temperatures between 900 and 1200 K. The results are shown in Table III for both of the collector systems. Combining these results, the measured value for the effective thermionic vacuum work function between 900 and 1200 K for a 99.7% pure polycrystalline beryllium surface is 3.67 ±0.03 eV. If the slight indication of a negative temperature coefficient in the diaphragm collector is included, the result is $\phi(T) = 3.75 - 8 \times 10^{-5} T$. The upper temperature limit of 1200 K was dictated by vaporization of the beryllium surface; the melting point is about 1550 K.

2. Titanium

Measurements made for a first 99.6% pure 2-mil polycrystalline titanium ribbon between 1100 and 1600 K indicated a negative temperature coefficient expressed by $\phi(T) = 5.14 - 6.9 \times 10^{-4} T$. The

TABLE II

Summary of Effective Thermionic Vacuum Work Function Data (Zero-Field Extrapolations)

Surface	Purity	Melting Temperature, K	Number of Temperatures	Total Number of Measurements	Temperature Range of Measurements, K	Work Function, eV (Including Temperature Dependence)	ϕ (1200 K)	ϕ (1500 K)	ϕ (1900 K)
Beryllium	0.997	1551	11	17	900-1200	3.665 ± 0.025	3.67	–	–
Titanium	0.996	1950	21	38	1100-1600	3.55 to 4.25 (see text)	(3.55 to 4.25)	–	–
Chromium	0.9999	2173	18	28	1050-1450	3.90 ± 0.05	3.90	3.90	–
Nickel	0.995	1728	20	20	1150-1500	4.41 ± 0.02 T < 1250 $6.27 - 1.0 \times 10^{-3}$ T > 1380 1250 < T < 1380 (see text)	4.41	4.77	–
Copper	OFHC	1356	7	7	1100-1250	4.415 ± 0.02	4.42	–	–
Rhenium	0.9999+	3453	10	18	1325-2250	4.96 ± 0.05	4.96	4.96	4.96
Iridium	0.999	2727	13	22	1300-2100	5.27 ± 0.05	5.27	5.27	5.27
Platinum	0.9995	2042	17	28	1600-1950	5.79 ± 0.09 or $5.03 + 4.2 \times 10^{-4}$ T	–	5.66	5.83
304 Stainless Steel	alloy	~1700	10	10	1050-1400	4.34 ± 0.02 T < 1200 T > 1200, ϕ decreases (see text)	4.32	(4.18)	--
Al_2O_3 (Lucalox)	0.999	~2315	6	6	1550-1750	5.19 ± 0.09	–	5.19	5.19

TABLE III

Vacuum Work Function of 99.7% Pure Polycrystalline Beryllium Surface

Surface Temperature, K	Effective Vacuum Work Function, eV	
	Diaphragm Collector	Aperture-Cup Collector
1180	3.65	3.65
1155	3.65	3.65
1133	3.66	3.66
1108	3.66	3.66
1083	3.68	3.67
1055	3.69	3.64
1032	3.70	Current $< 10^{-13}$ A
1005	3.69	
976	3.68	
957	3.70	
920	3.66	
Average	3.67	3.66

first titanium tube failed, and a replacement was fabricated. The first set of vacuum work function measurements for the replacement titanium ribbon emitter also indicated a negative temperature coefficient expressed by $\phi(T) = 5.09 - 7.4 \times 10^{-4}$ T for the diaphragm collector and $\phi(T) = 5.10 - 8.8 \times 10^{-4}$ T for the cup collector. Because of the difference between these data and those for the first surface, the vacuum work function was checked after the titanium ribbon had been outgassed at 1585 K for 10 min. A shift to lower work function was observed for both collector systems, which exhibited a negative temperature coefficient of $\phi(T) = 5.18 - 8.8 \times 10^{-4}$ T for the diaphragm collector and $\phi(T) = 6.14 - 1.91 \times 10^{-3}$ T for the cup collector. These measurements started at a maximum temperature and decreased to lower temperatures. A third set of measurements

for the vacuum work function was recorded on another day, starting at a minimum temperature and increasing to a maximum value, but without further degassing. The vacuum work function for both collector systems yielded the same results as those recorded for the decreasing temperature measurements made after outgassing. The previous drift toward a lower work function probably resulted from gettered substances and changes in the crystalline structure of the ribbon produced by processing at elevated temperatures, both characteristic of titanium. Titanium contains quantities of hydrogen and oxygen which change with the temperature and with the heat treatment history. The amounts decrease with increasing temperature in the thermionic emission temperature range, and degassing at 1585 K drives both impurities out. The data above indicate a reduction in work function by degassing. Therefore, it is implied that the presence of hydrogen and oxygen in titanium increases the work function; this is a logical conclusion because both are electronegative gases. It is concluded that the work function of titanium is at least as low as 3.6 to 3.8 eV, the actual work function of a titanium surface is dependent upon the amount of dissolved (and adsorbed) gases, the influence of these gases is to increase the work function, the work function will change with temperature and heat treatment history, and work function values of titanium above 3.9 eV are probably for contaminated surfaces. The upper temperature limit was imposed by vaporization; the melting point is about 1950 K. The results are presented in Table IV for both collector systems.

3. Chromium

Vacuum work function measurements for chromium were reported in the Final Report on Contract NAS 3-5249. The measurements made on the second chromium tube (for which the cesiated emission data reported herein were obtained) gave similar results, and, therefore, no new data are reported.

TABLE IV

Vacuum Work Function of a 99.6% Pure Polycrystalline Titanium Surface

Surface Temperature, K	Effective Vacuum Work Function, eV			
	Diaphragm Collector		Aperture-Cup Collector	
	New Data	Old Data	New Data	Old Data
1586	3.80		3.60	
1585		4.09		4.10
1545	3.78		3.50	
1535		4.12		4.12
1488		4.16		4.16
1445	3.93		3.69	
1442		4.18		4.17
1432	4.05		3.93	
1395		4.20		4.19
1347		4.22		4.21
1320	4.11		4.02	
1304	4.02		3.84	
1300		4.27		4.26
1270	4.16		4.08	
1253		4.30		4.30
1218	4.20		4.15	
1205		4.32		$<10^{-13}$ A
1165	4.15		4.06	
1160	4.23			
1156		4.36		$<10^{-13}$ A
1113	4.26			

4. Nickel

The vacuum work function of a well outgassed nickel ribbon was measured at 20 temperatures (at three different times and for increasing and decreasing temperatures) between 1150 and 1500 K. The upper temperature limit was imposed by vaporization; the melting temperature is about 1730 K. The results are given in Table V.

TABLE V

Vacuum Work Function of a 99.5% Pure Polycrystalline Nickel Surface

Surface Temperature, K			Effective Vacuum Work Function, eV	
Run No. 1	Run No. 2	Run No. 3	Diaphragm Collector	Aperture-Cup Collector
1490			4.80	4.79
	1487		[illegible]	4.77
	1462		4.80	4.79
1443			4.81	4.82
	1439		4.82	current
		1417	4.85	less than
	1415		4.86	10^{-13} A
1409			4.83	↓
		1392	4.85	
	1390		4.89	
		1370	4.73	
1358			4.80	
1319			4.75	
		1311	4.65	
		1272	4.54	
		1257	4.49	
		1222	4.40	
1217			4.42	
1178			4.41	
		1172	4.41	

Two distinct work function values were reproducibly observed:

$$\phi(T) = 6.27 - 1.0 \times 10^{-3}\, T \quad \text{for} \quad 1380 < T < (1500)$$

$$\phi(T) = 4.41 \pm 0.01 \quad \text{for} \quad (1170) < T < 1250.$$

Between 1250 and 1380 K, a very nearly constant emission current was observed. The constant current decreased slightly with each subsequent series of measurements. A maximum work function value of 4.9 eV occurs at about 1390 K unless the discontinuity can be driven to even lower temperatures, in which case a work function of 5.0 eV could be predicted at 1270 K.

5. Copper

The vacuum work function of an oxygen-free copper surface was measured at seven temperatures between 1100 and 1300 K, as seen in Table VI. The result was 4.42 ± 0.02 eV. The upper temperature limit was dictated by the melting point, 1356 K.

TABLE VI

Vacuum Work Function of an OFHC Copper Surface

Surface Temperature, K	Effective Vacuum Work Function, eV
1100	4.40
1123	4.40
1158	4.40
1180	4.40
1205	4.40
1230	4.42
1255	4.43

6. Rhenium

The vacuum work function of a 2-mil 99.99+% pure rhenium ribbon was measured at 10 temperatures between 1325 and 2250 K. The upper temperature limit was imposed by vaporization of the emitter support posts. The results are presented in Table VII for both of the collector systems. The measured value for the effective thermionic vacuum work function for a pure polycrystalline rhenium surface is 4.96 ± 0.05 eV when both diaphragm and cup collectors are considered. When treated individually, the diaphragm collector measures 4.98 ± 0.06 eV and the cup collector 4.93 ± 0.03 eV. The two lowest temperature values for the diaphragm collector are not weighted heavily.

TABLE VII

Vacuum Work Function of a 99.99+% Pure Polycrystalline Rhenium Surface

Surface Temperature, K	Effective Vacuum Work Function, eV	
	Diaphragm Collector	Aperture-Cup Collector
2225	4.92	4.92
2115	4.94	4.94
2009	4.99	4.96
1905	5.00	4.96
1803	5.00	4.95
1704	5.01	4.95
1606	4.99	4.90
1515	5.00	4.90
1430	5.05	Current $< 10^{-13}$ A
1348	5.10	

7. Iridium

The vacuum work function of a 2-mil 99.9% pure iridium ribbon was measured at 13 temperatures between 1300 and 2100 K. The results are tabulated in Table VIII for both of the collector systems. Combining these results, the measured value for the effective thermionic vacuum work function between 1300 and 2100 K for a 99.9% pure polycrystalline iridium surface is 5.27 ± 0.05 eV.

TABLE VIII

Vacuum Work Function of a 99.9% Pure Polycrystalline Iridium Surface

Surface Temperature, K	Effective Vacuum Work Function, eV	
	Diaphragm Collector	Aperture-Cup Collector
2076	5.27	5.27
2008	5.29	5.29
1941	5.32	5.31
1868	5.30	5.30
1802	5.31	5.31
1737	5.28	5.28
1667	5.25	5.23
1607	5.23	5.23
1545	5.25	5.23
1488	5.26	
1433	5.28	Current
1374	5.28	$< 10^{-13}$ A
1317	5.28	
Average	5.276	5.27

8. Platinum

The vacuum work function of a 99.95% pure platinum ribbon emitter was measured at 16 temperatures between 1600 and 1950 K. The melting point of platinum is approximately 2046 K. A necessary safety factor below this value established the upper temperature limit. The data obtained with the aperture-cup collector system are shown in Table IX as "new" data. The diaphragm currents yielded inconsistent and considerably different work function values, and were therefore discarded in favor of the more reliable cup data. The cup collector currents were below 10^{-13} A for temperatures below 1650 K.

For comparison, platinum vacuum work function measurements for both collector systems taken from earlier data for a different platinum emitter and tube and with a different vacuum system are included in Table IX as "old" data. The two sets of cup collector measurements are in good agreement. There is excellent correlation between the data point temperature for old and new data; this is worth noting because the former temperatures were obtained by corrected optical methods while the latter utilized a W(5% Re) - W(26% Re) thermocouple. When the 28 work function measurements of Table IX are averaged, independent of any temperature dependence, a value of 5.79 ± 0.09 eV is obtained for the effective vacuum thermionic work function of platinum. When the cup collector values are plotted and a straight line is drawn in the temperature range of the observations, the temperature dependent expression is $\phi(T) = 5.03 + 4.2 \times 10^{-4}\ T$ in electron volts.

9. 304 Stainless Steel

The effective vacuum work function of a machined 304 stainless steel surface was measured at 10 temperatures between 1050 and 1400 K. The results are given in Table X. The upper temperature limit was imposed by vaporization (primarily chromium); the melting point is about 1730 K.

TABLE IX

Vacuum Work Function of a 99.95% Pure Polycrystalline Platinum Surface

Surface Temperature, K	Effective Vacuum Work Function, eV		
	Aperture-Cup Collector		Diaphragm Collector
	New Data	Old Data	Old Data
1946		5.89	5.85
1913		5.85	5.80
1880		5.83	5.80
1850		5.80	5.80
1846	5.80		
1818		5.78	5.79
1813	5.82		
1783		5.78	5.83
1781	5.81		
1752		5.76	5.82
1748	5.81		
1717		5.73	5.81
1714	5.75		
1686		5.70	5.80
1650	5.70		
1654		5.70	5.80
1620		5.72	5.79

For 304 stainless steel, a value of 4.34 eV is exhibited at the lower temperatures. This value is in agreement with the lowest values previously obtained for pure iron under Contract NAS 3-5249, but is slightly lower than most of the iron data. Because the work function of chromium is 3.90 eV and because 304 stainless steel is nearly 20%

TABLE X

Vacuum Work Function of a Polycrystalline
304 Stainless Steel Surface

Temperature, K	Effective Work Function, eV
1395	4.22
1350	4.28
1321	4.30
1300	4.28
1274	4.29
1250	4.30
1212	4.32
1170	4.34
1127	4.34
1085	4.34

chromium, a somewhat lower work function would be predicted. The nearly 10% of nickel should not influence the effective polycrystalline thermionic work function because the effective work function of nickel was measured to be about 4.85 eV, greater than that of iron. The tendency for a decreased function at higher temperatures may be attributed to the higher vapor pressure of chromium. Chromium may be diffusing onto the surface and evaporating, resulting in a higher surface concentration of chromium than the approximately 18% in the bulk. Therefore, the data shown above may indicate a vacuum work function for 304 stainless steel of 4.34 eV at temperatures below 1200 K, which then decreases toward the work function of chromium (3.9 eV) as the temperature is raised above 1200 K.

10. Aluminum Oxide (Lucalox)

The vacuum work function of a well outgassed block of Lucalox was measured at 10 temperatures between 1300 and 1750 K. The upper temperature limit was dictated by the melting point of the alumina

insert containing the heater wire. The high electric fields applied between the emitter and the diaphragm collector, which are required to draw saturated electron emission from the Lucalox emitter, also draw electron emission from other sources (such as the Kovar supporting posts and the rhenium shielding, both of which were at thermionic emission temperatures). If the electric field penetrates deep enough, electrons could be pulled from the tungsten heater wires. These factors probably caused the diaphragm collector currents to be too high and the apparent work function to be too low. Therefore, only the cup collector data are tabulated in Table XI. The cup collector currents were below 10^{-13} A for temperatures below 1550 K. The measured value of the effective thermionic vacuum work function between 1550 and 1750 K for a 99.9% pure polycrystalline aluminum oxide (Lucalox) surface is 5.19 ± 0.09. When the possible temperature coefficient is included, the result is $\phi(T) = 3.83 + 8 \times 10^{-4}\ T$.

TABLE XI

Vacuum Work Function of 99.9% Pure Polycrystalline Aluminum Oxide (Lucalox) Surface

Surface Temperature, K	Effective Vacuum Work Function, eV
	Aperture-Cup Collector
1551	5.10
1600	5.13
1617	5.14
1666	5.20
1707	5.28
1743	5.26
Average	5.185

B. Cesiated Electron Emission

The electron emission current density versus surface temperature at six cesium arrival fluxes between 10^{13} and 10^{17} atoms/cm^2-sec for cesiated surfaces of beryllium, titanium, chromium, nickel, copper, rhenium, iridium, platinum, 304 stainless steel, and aluminum oxide (Lucalox) is plotted in Figs. 18 through 28. These curves correspond to essentially the zero-field extrapolated condition. The influence of applied field was reported in the Final Report on Contract NAS 3-5249, and no significant variations from the results of that work have been observed. It was concluded that the influence of applied field for a clean surface is just the Schottky effect. For contaminated surfaces, however, the field effect is greatly enhanced, so that at applied fields of the order of 10^5 V/cm, the minima in the S curves can be destroyed.

1. Beryllium

The emission levels from beryllium (Fig. 18) are the lowest measured so far. No minimum work function is observed in these curves; this is observed for other substrates, but it is especially vivid for beryllium. The final value of work function is 1.94 eV. This may mean that the vacuum work function of cesium is actually 1.94 eV rather than 1.85 eV. This is the first such measurement known to this author for cesium on a substrate which is an alkaline earth metal. Chemical interactions (covalent and ionic) between adsorbate and substrate, which may normally exist between the reactive alkali cesium and the transition metals (including all refractory metals) and the noble metals, etc., should account for this phenomenon; they may well be absent or very weak between an alkali and alkaline earth elements. Other substrates for which the minimum was absent are semiconductors and insulators, also differing in (or lacking) covalent and ionic bonding. Enough evidence has been gathered to indicate that the low vacuum work function of beryllium is not directly responsible. It is noted that a rather strong statement that the vacuum work function of cesium is not

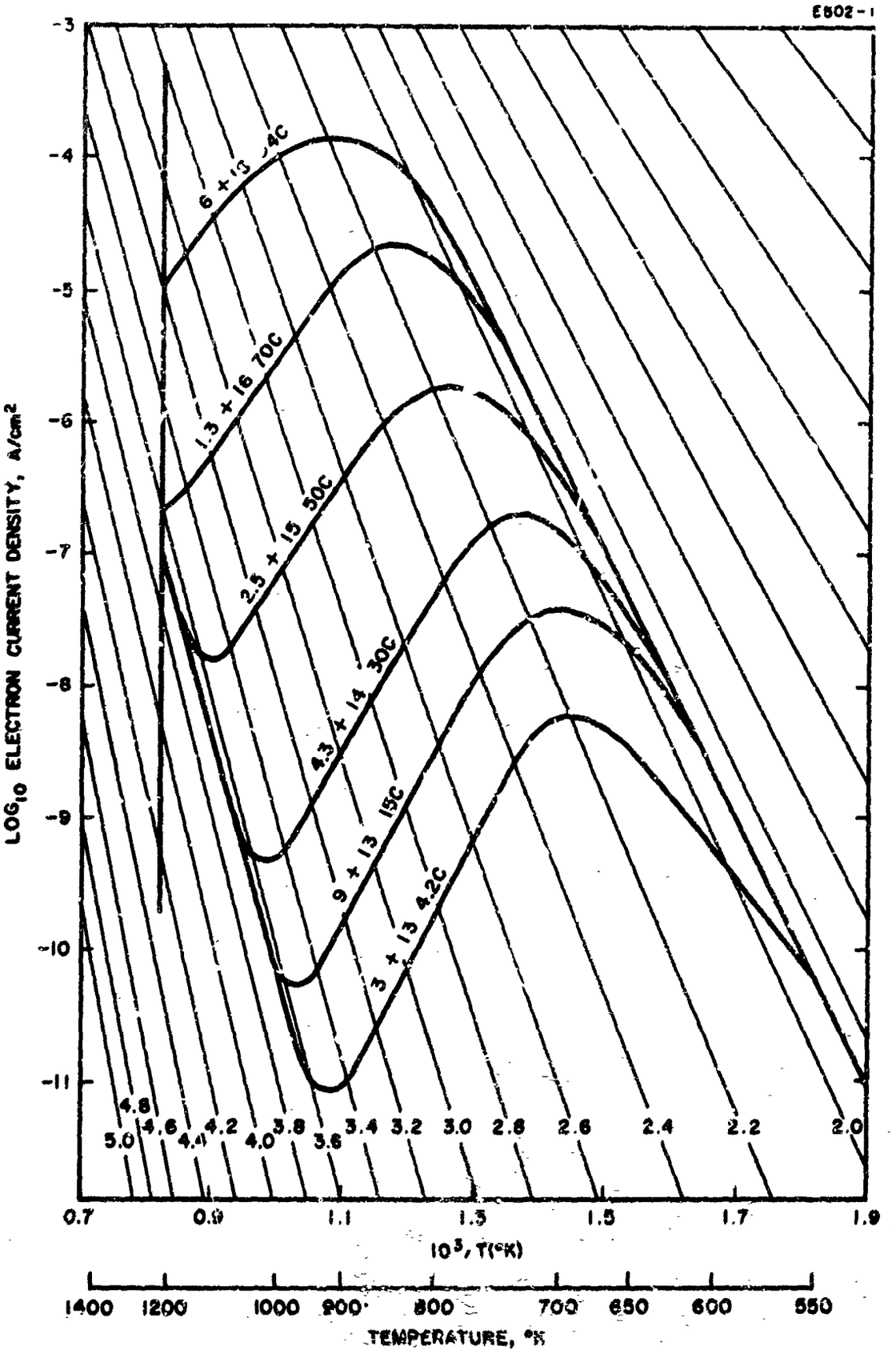

Fig. 18. Electron emission from cesiated beryllium.

1.81 eV, as is commonly used, but rather is 1.96 eV, as evidenced by measurements, was made in Paper No. 11 by Dresser (Franklin) at the 1964 Thermionic Energy Conversion Specialist Conference in Cleveland.

2. Titanium

The cesiated electron emission curves for titanium (Fig. 19) are notably different from the others. The emission peaks occur at lower temperatures and the associated work function is lower, although the emission levels are low. The data are sharp and uniform. The minimum work function is about 1.32 eV, and the heavily cesiated work function is about 1.44 eV. A heater failure terminated the cesiated emission measurements before the highest arrival fluxes were completed.

3. Chromium

The curves for chromium (Fig. 20) are similar to those for tungsten for lower temperatures. A minimum work function of about 1.7 eV is observed. The lower vacuum work function of chromium causes differences at higher temperatures. The "clean" cesiated work function for chromium is seen to be about 3.55 eV, whereas its vacuum work function is about 3.9 eV.

4. Nickel

The data for nickel (Fig. 21) exhibit several interesting characteristics. The heavily cesiated work functions are relatively high for increasing temperature runs (2.0 to 1.75 eV), and they increase with increasing cesium arrival flux, an unusual observation. A phenomenon which has the characteristics of a contamination is exhibited at higher temperatures. For the increasing temperature curves, a tendency for the emission to follow a work function of 3.6 eV is consistently exhibited, but with an eventual wandering over to higher work function. The net result is very shallow minima in the S curves. It is not known whether these characteristics are caused by some impurity gas adsorbed in the nickel which gradually diffuses to the surface, or by some fundamental

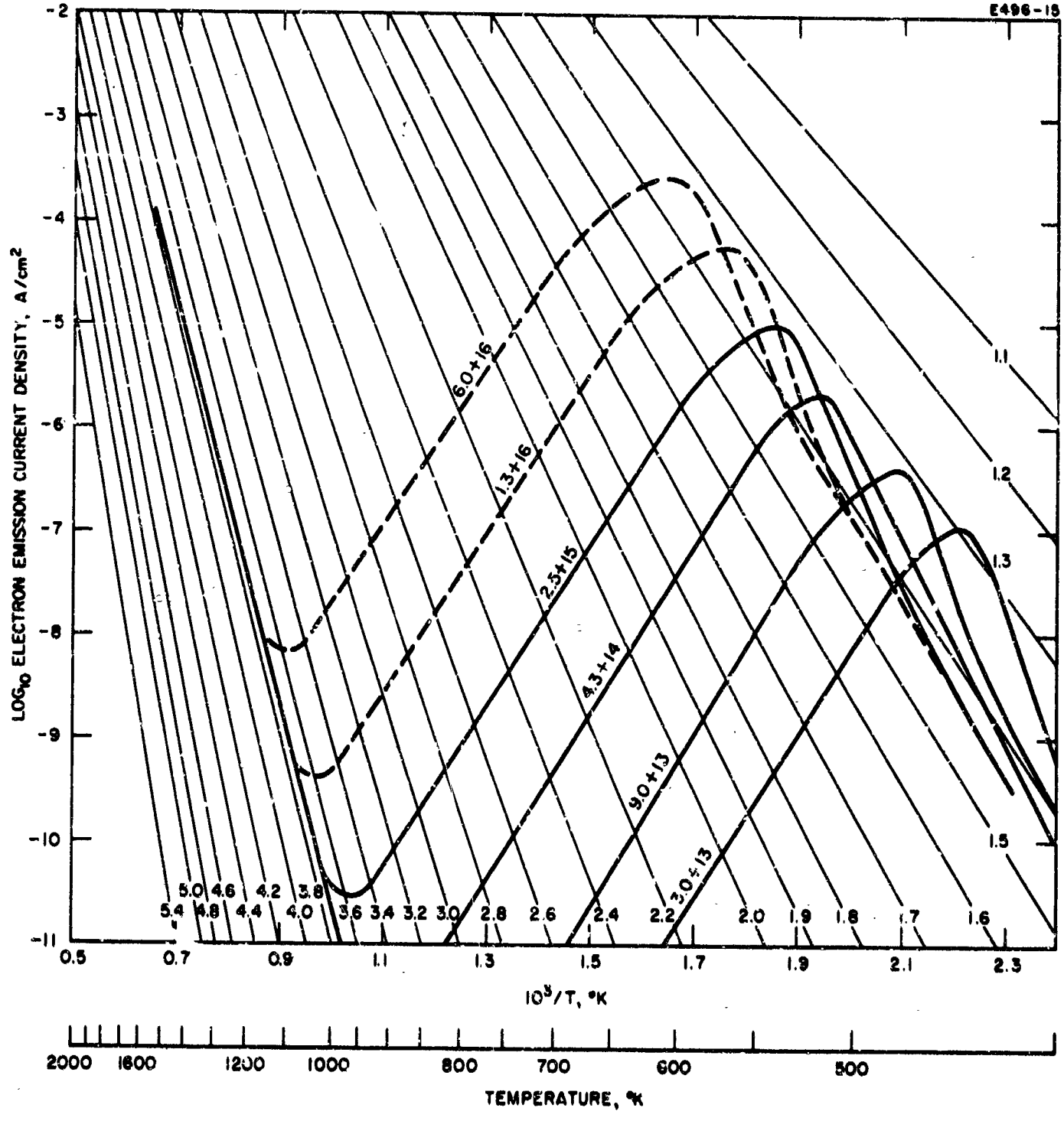

Fig. 19. Electron emission from cesiated titanium.

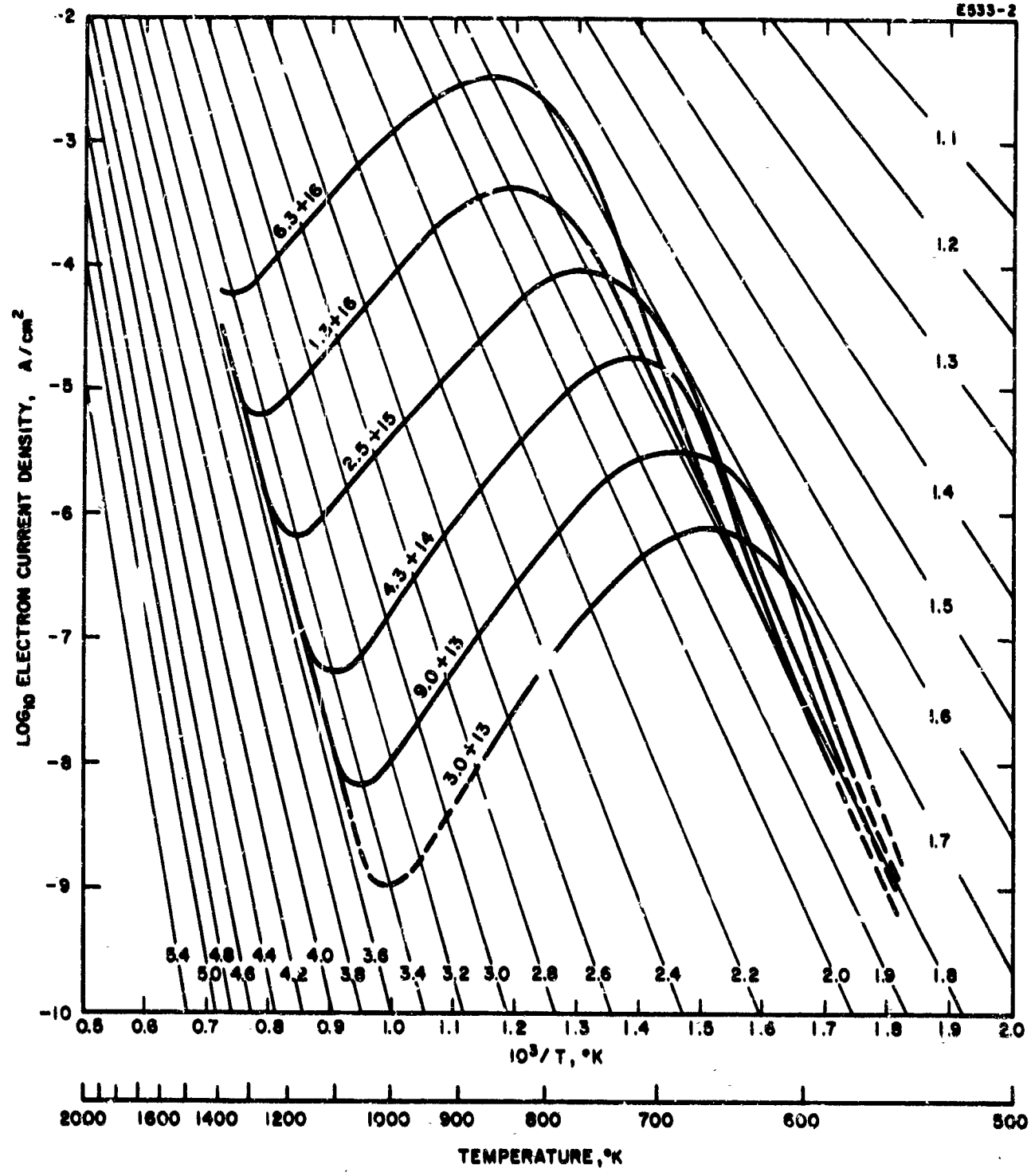

Fig. 20. Electron emission from cesiated chromium.

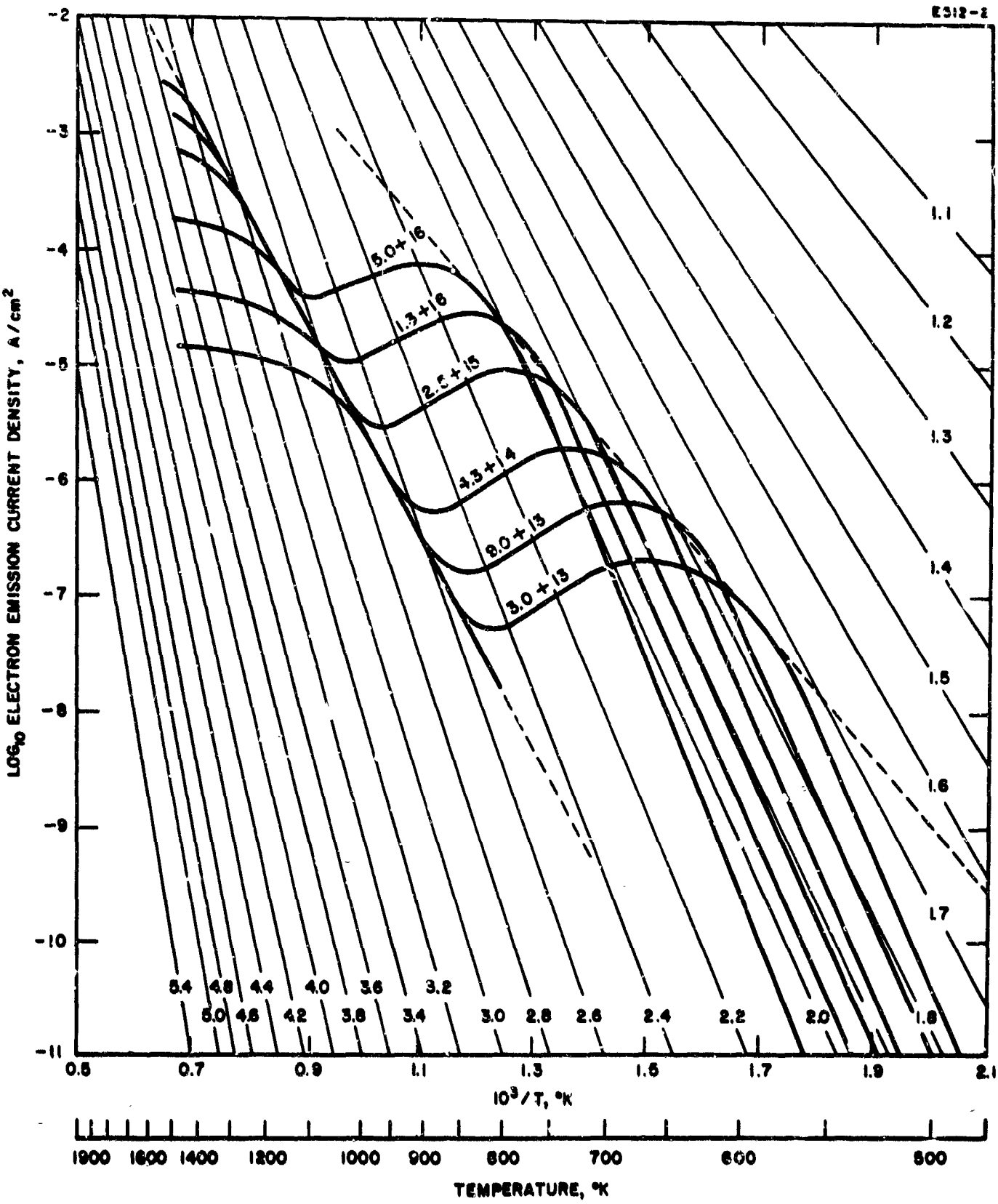

Fig. 21. Electron emission from cesiated nickel.

work function variation in the nickel surface. Two facts are known: the vacuum work function of the nickel surface exhibited two distinct work functions which were reversible with temperature change; if a contamination is responsible, it cannot be removed by lengthy processing at temperatures at which nickel is noticeably vaporizing.

5. Copper

The curves for copper (Fig. 22) show slight dissimilarity with those reported under Contract NAS 3-5249. The cesiated work functions are higher and the minima are deeper, indicating a cleaner surface. The emission maxima agree fairly well.

6. Rhenium

For rhenium (Fig. 23) the minimum work function (large θ) is about 1.53 eV. The curves are well spread out on the current density axis, resulting in relatively high emission at high arrival flux and relatively low emission at low flux. The "clean" work function for rhenium is about 4.8 eV, which is close to the 4.9 to 5.0 eV value measured for the vacuum work function. The emission peaks are relatively broad, broader than those for tungsten, but narrower than that for iridium.

7. Platinum

Platinum (Fig. 24) exhibits the broadest emission peak of all surfaces studied so far, and has a low minimum work function, 1.59 eV. The emission maxima are moderate.

8. Iridium

The emission levels for iridium (Fig. 25) are comparatively high in the medium temperature range. The minimum work function (large θ) is about 1.8 eV and coincides with a number of others. The "clean" cesiated function agrees with the vacuum work function (5.1 to 5.3 eV). The emission peak is very broad.

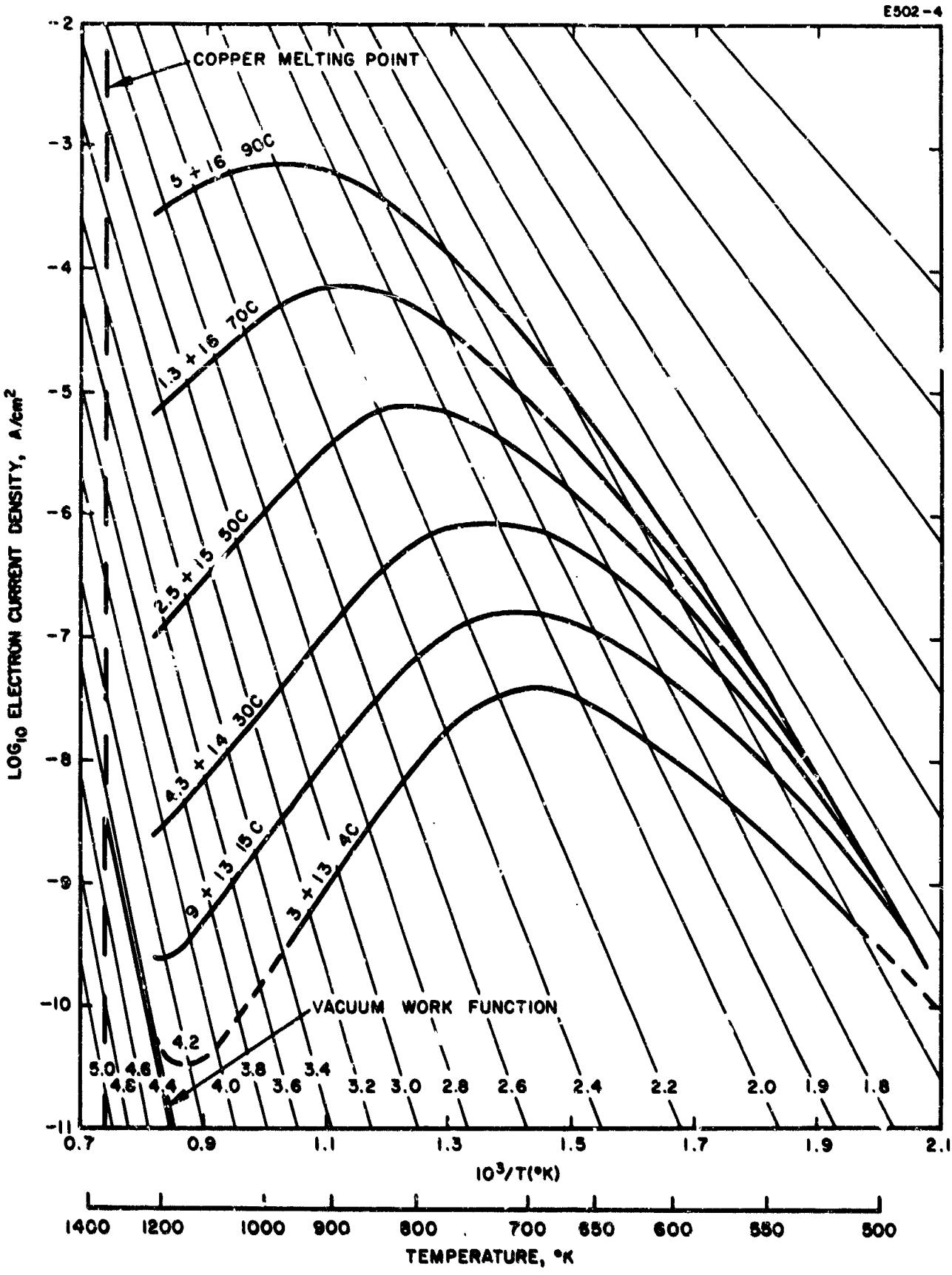

Fig. 22. Electron emission from cesiated copper.

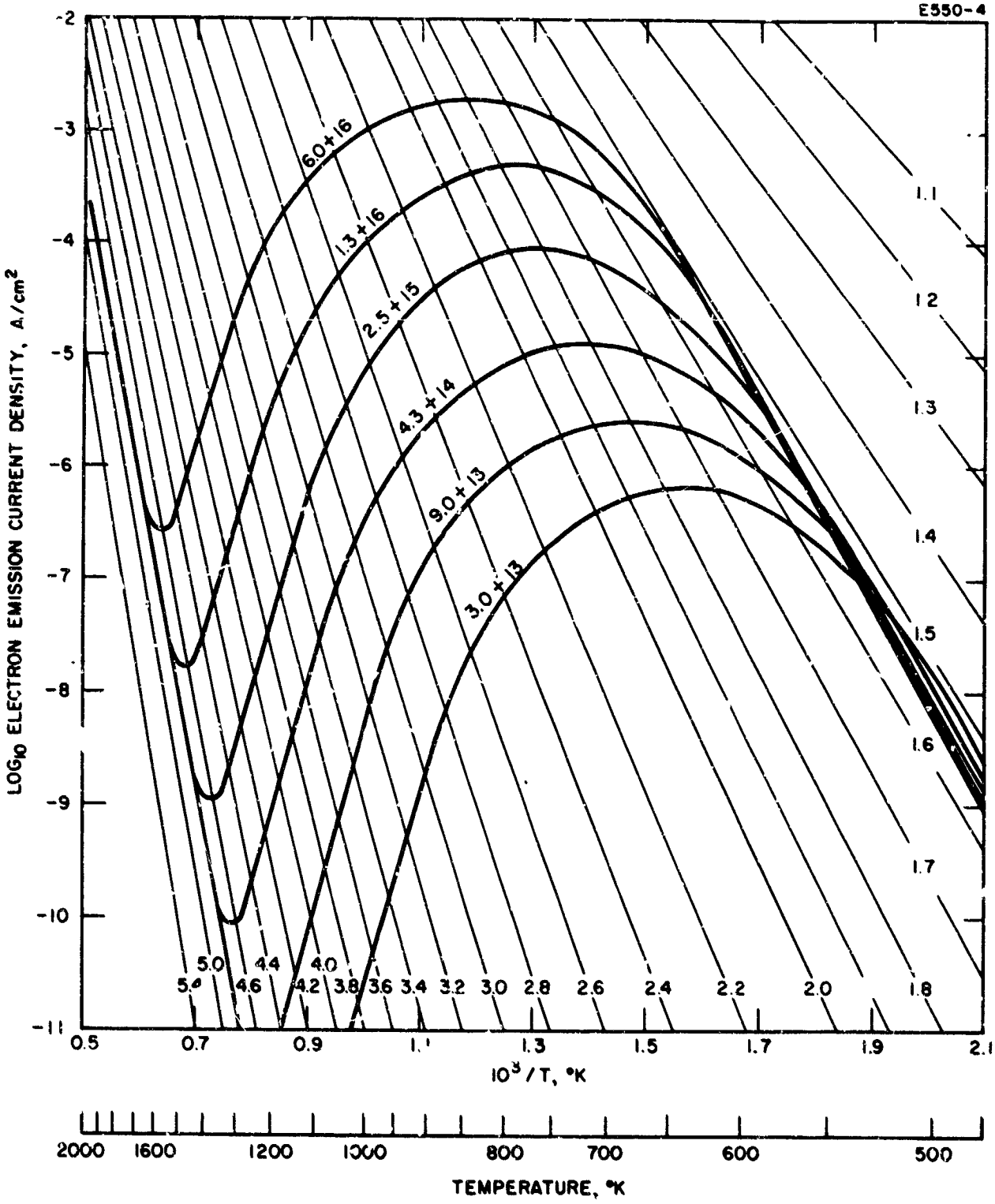

Fig. 23. Electron emission from cesiated rhenium.

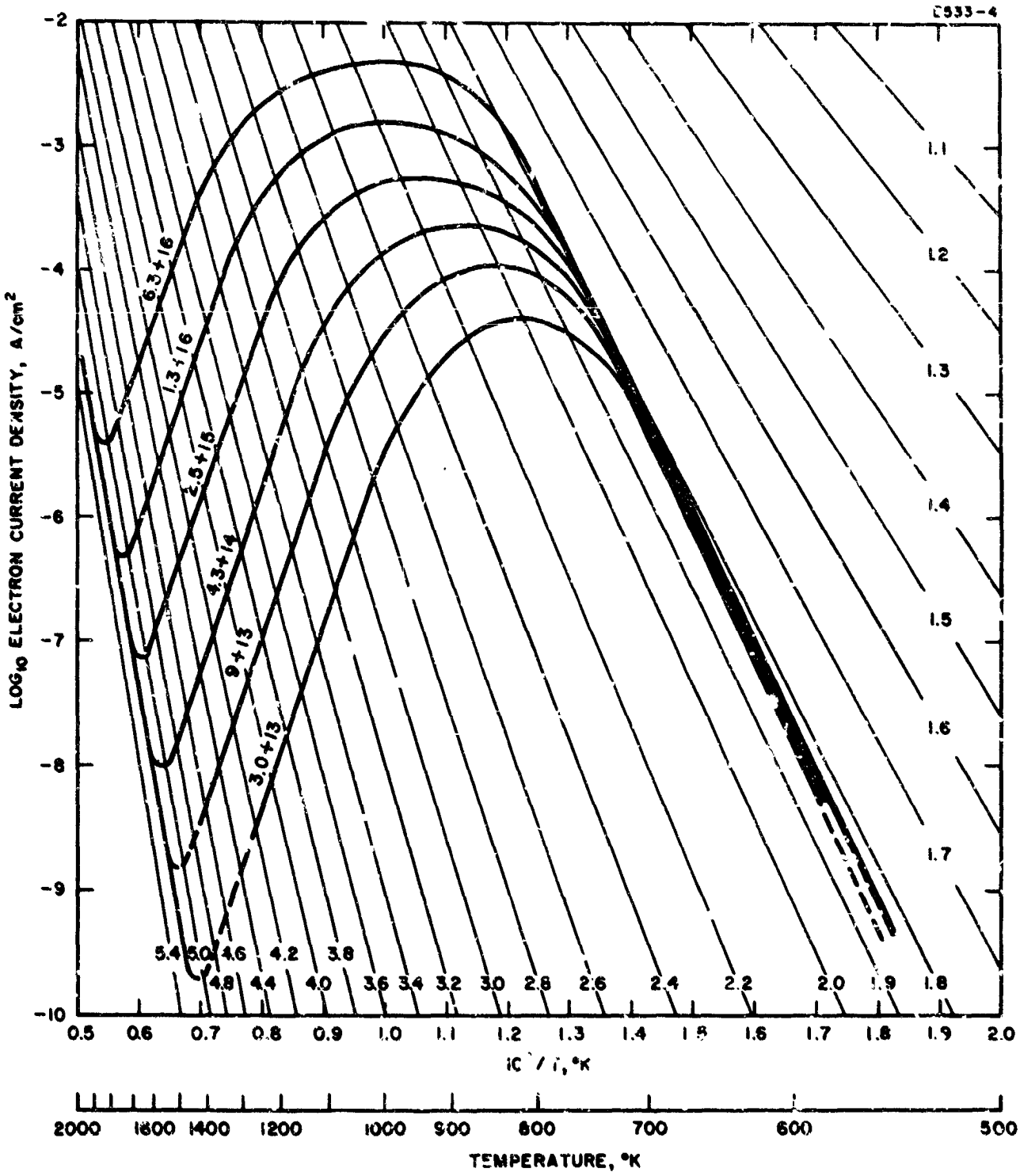

Fig. 24. Electron emission from cesiated iridium.

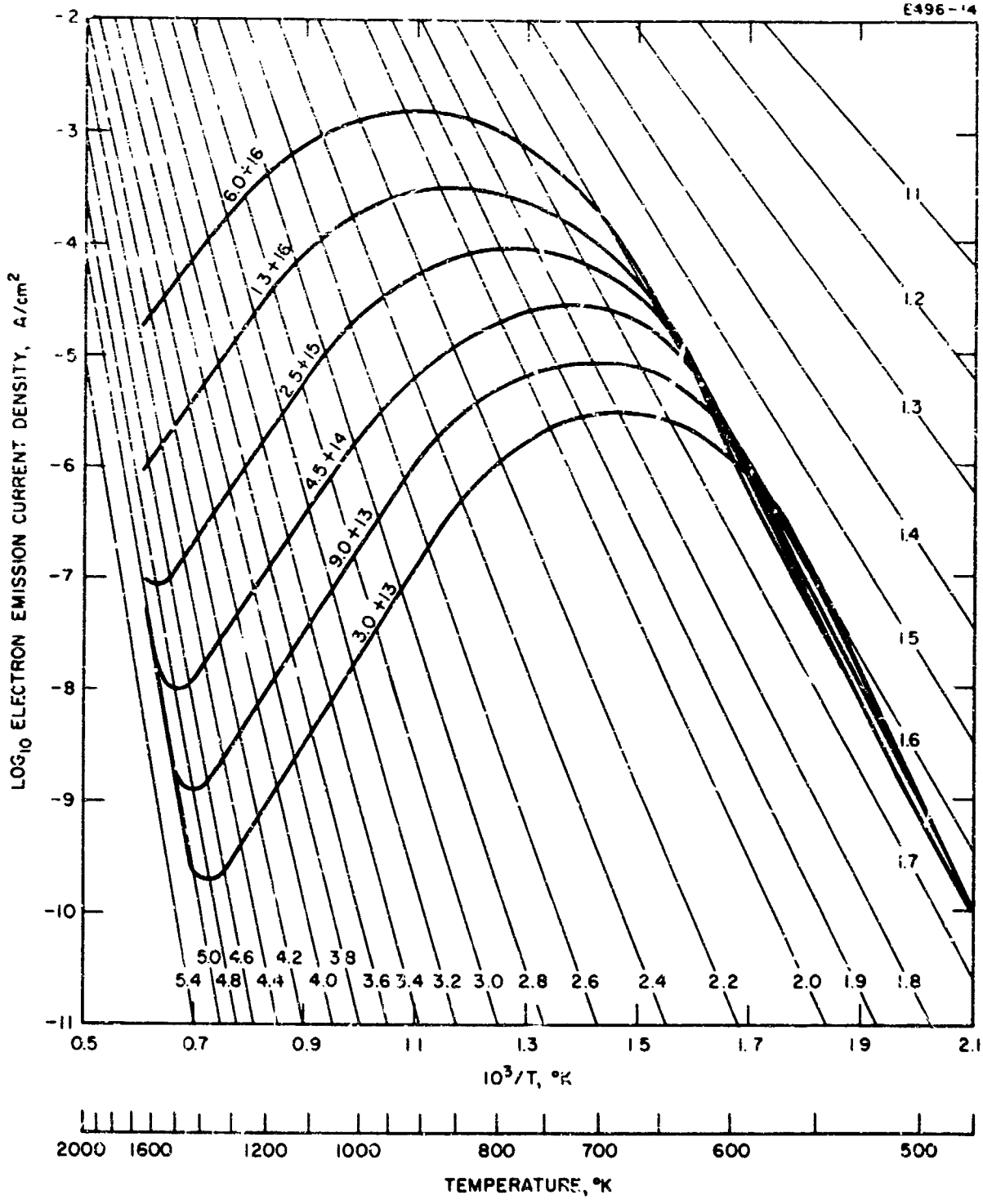

Fig. 25. Electron emission from cesiated platinum.

9. Stainless Steel

The emission levels for stainless steel (Fig. 26) are relatively high with low heavily cesiated work functions (1.52 eV).

10. Aluminum Oxide

The curves for Lucalox aluminum oxide (shown in Figs. 27 and 28) are somewhat anomalous, irregular, inconsistent, and nonreproducible. Figure 27 is a representative full set of matching data obtained by starting from maximum temperature. A resemblance to a normal set of S curves is seen, with some exceptions. The "clean" work function varied with arrival flux from about 4.0 to about 3.5 eV, whereas the vacuum work function was about 5.0 eV. The curves for various arrival flux are spread out rather strangely. The values of heavily cesiated work function or minimum work function vary widely and anomalously between 1.75 and 1.35 eV. The corresponding set of electron emission curves obtained by increasing the temperature from room temperature at each flux is shown in Fig. 28. They are seen to be completely anomalous, exhibiting no emission maxima, but having regions of nearly constant emission and some surface-ionization-like discontinuities. The results for Lucalox alumina were nonreproducible in detail, but were reproducible in general shape and characteristics. One fundamental problem in the experimental design of the alumina tube, or any other insulator surface, should be recalled when these data are interpreted: a conductor (in this case copper foil) must be used as the collector to oppose the insulator surface. It is expected, however, that any copper sputtered onto the emitter is vaporized off when the emitter is flashed to high temperature before each new descending temperature run is started. These curves are significantly different from those for a porous and relatively impure alumina insulator surface reported under Contract NAS 3-5249. The anomalies may also be attributed to the fact that this emitter is an insulator, which allows several possible arguments and explanations.

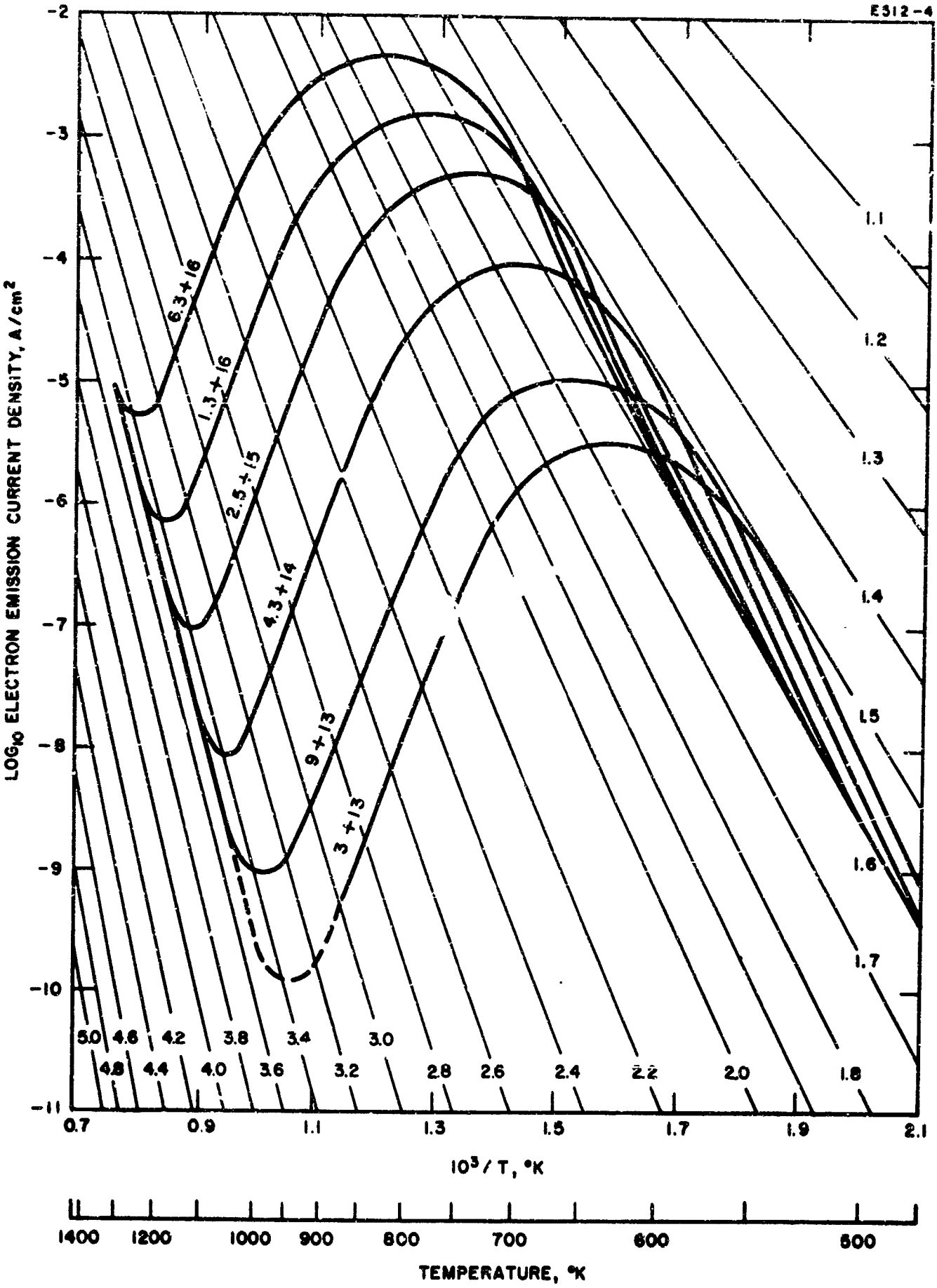

Fig. 26. Electron emission from cesiated 304 stainless steel.

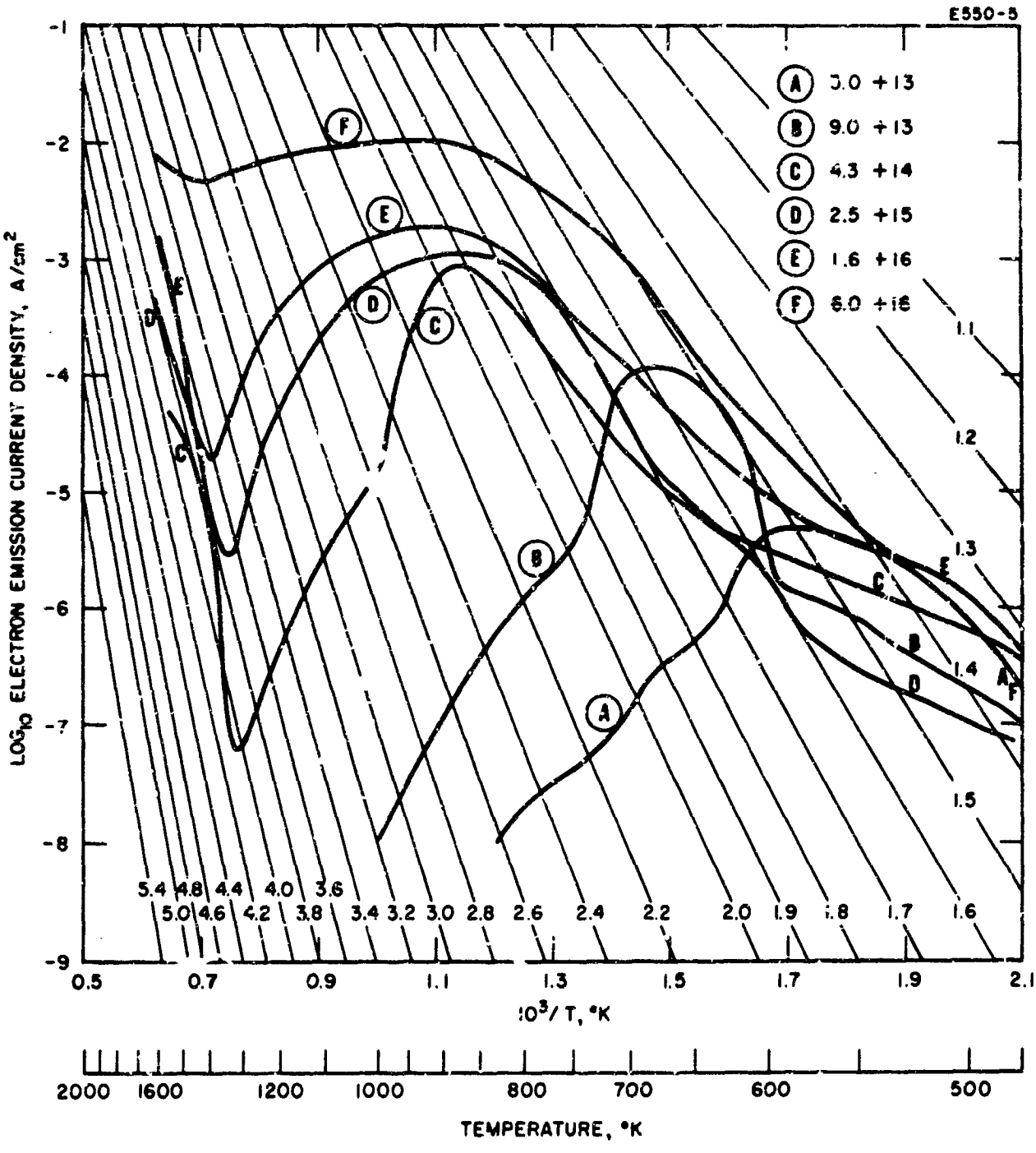

Fig. 27. Electron emission from cesiated Lucalox aluminum oxide (decreasing temperature).

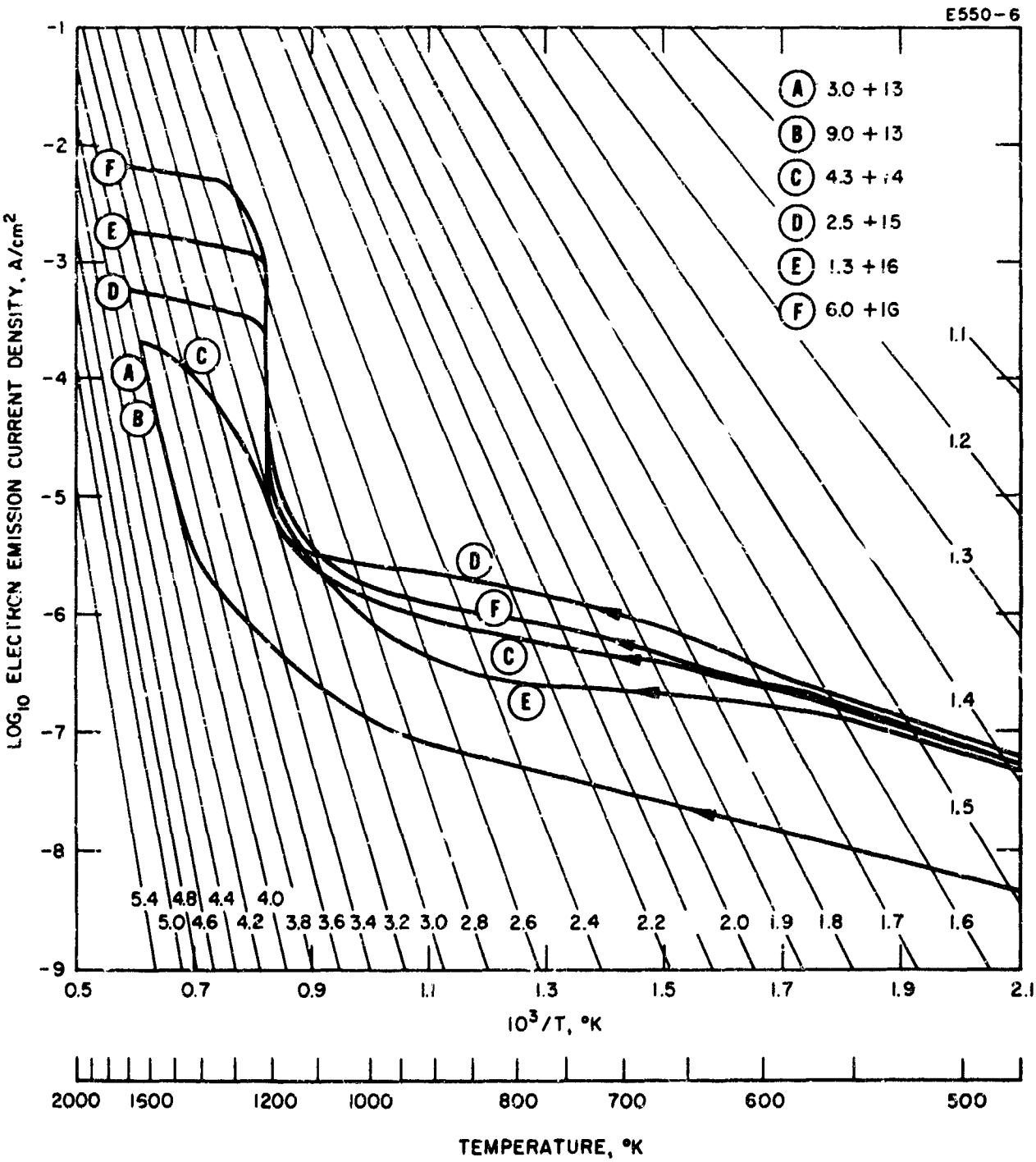

Fig. 28. Electron emission from cesiated Lucalox aluminum oxide (increasing temperature.

C. Cesium Ion Emission

The cesium ion emission current density versus surface temperature at six cesium arrival fluxes between 10^{13} and 10^{17} atoms/cm^2-sec for surfaces of beryllium, titanium, chromium, nickel, copper, rhenium, iridium, platinum, 304 stainless steel, and aluminum oxide (Lucalox) is plotted in Figs. 29 through 39.

1. Beryllium

For beryllium (Fig. 29), all of the increasing temperature curves fall on the same line, which corresponds to low emission levels and low ionization efficiencies at higher arrival fluxes, compatible with the low vacuum work function measured for beryllium (3.67 eV). The decreasing temperature curves exhibit an irregular and large hysteresis effect which increases with increasing arrival flux. This type of structure has also been observed for chromium. The two metals have one important common characteristic -- low work function -- and it may be speculated that curves of this shape may be characteristic of low work function surfaces. A critical temperature envelope cannot clearly be drawn for beryllium, but the slope of the straight line in Fig. 29 yields 3.06 eV for a desorption energy for cesium from beryllium at low coverage.

2. Titanium

The cesium ion emission curves for titanium (Fig. 30) are uniform and sharp. Small temperature hysteresis occurs at low arrival fluxes and disappears below 10^{-3} A/cm^2. The critical temperature envelope for titanium is the lowest observed for all of the materials studied to date or known to have been studied elsewhere. At 10 mA/cm^2, the critical temperature for titanium is 170 K lower than that for tungsten. A heater failure terminated the cesiated emission measurements before the highest cesium arrival fluxes were completed.

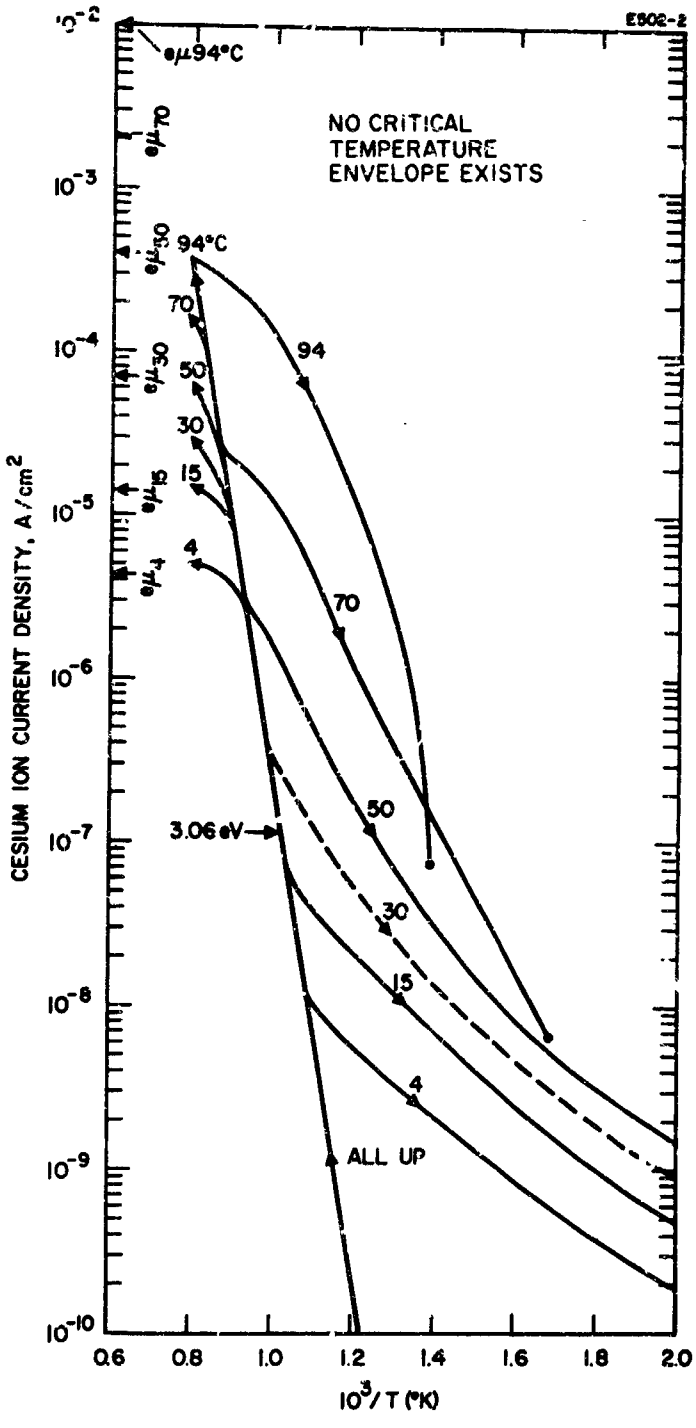

Fig. 29. Cesium ion emission from beryllium.

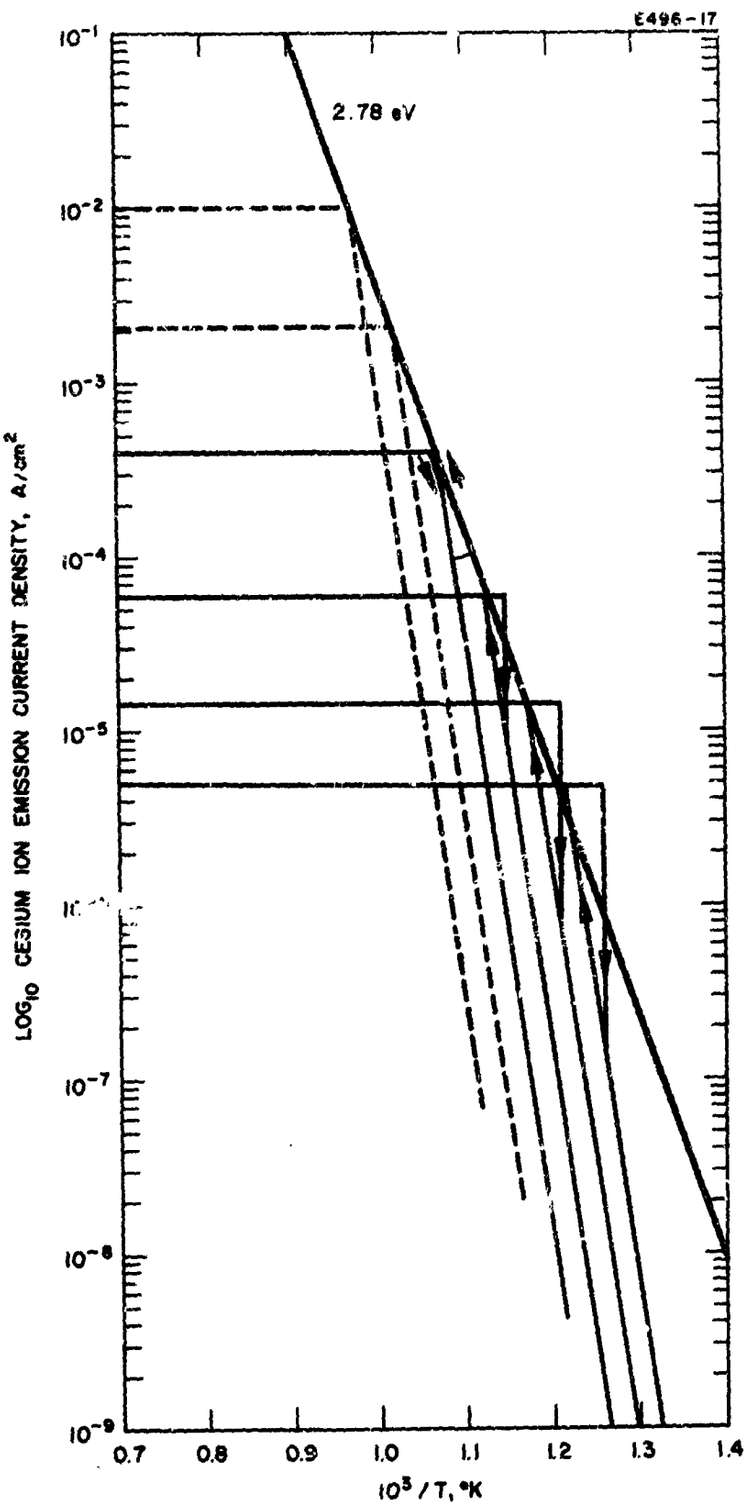

Fig. 30.
Cesium ion emission from titanium.

3. Chromium

Cesium ion emission data for chromium were previously reported in the Final Report on NAS 3-5249. Some anomalies, including very large hysteresis and two kinds of saturated ion emission, led to the statement that those data were questionable and therefore tentative and subject to remeasurement. The anomalies were attributed to a high pressure in the experimental tube. The measurements for chromium have been repeated (Fig. 31) under suitable pressure conditions, and the curves are not anomalous. Previously only two curves with a well defined critical temperature were observed. These two curves are included in Fig. 31. Although an extremely large anomalous temperature hysteresis effect was measured previously, only small conventional ones occurred during these measurements. However, an indication of the same high ion current emission at lower temperatures appears at a very low level in Fig. 31, and it increases with increasing cesium pressure. The subtractions of the two kinds of curves are shown. The two previously measured "normal" critical temperatures are seen to be in reasonable agreement with the new envelope. The ion desorption energy obtained from the chromium critical temperature envelope is 3.28 eV.

4. Nickel

The cesium ion emission data for nickel (Fig. 32) result in the second lowest critical temperature envelope observed to date, considerably lower than the third lowest. The curves are sharp and distinct. The ion and electron emission data for nickel when considered together may be indicative of an unusually wide range of work function distribution for nickel. The slope of the critical temperature envelope gives a value of 2.26 eV for the cesium ion desorption energy at critical coverage for nickel.

5. Copper

The curves for copper (Fig. 33) are normal. A more usual form of temperature hysteresis is observed. The effect decreases

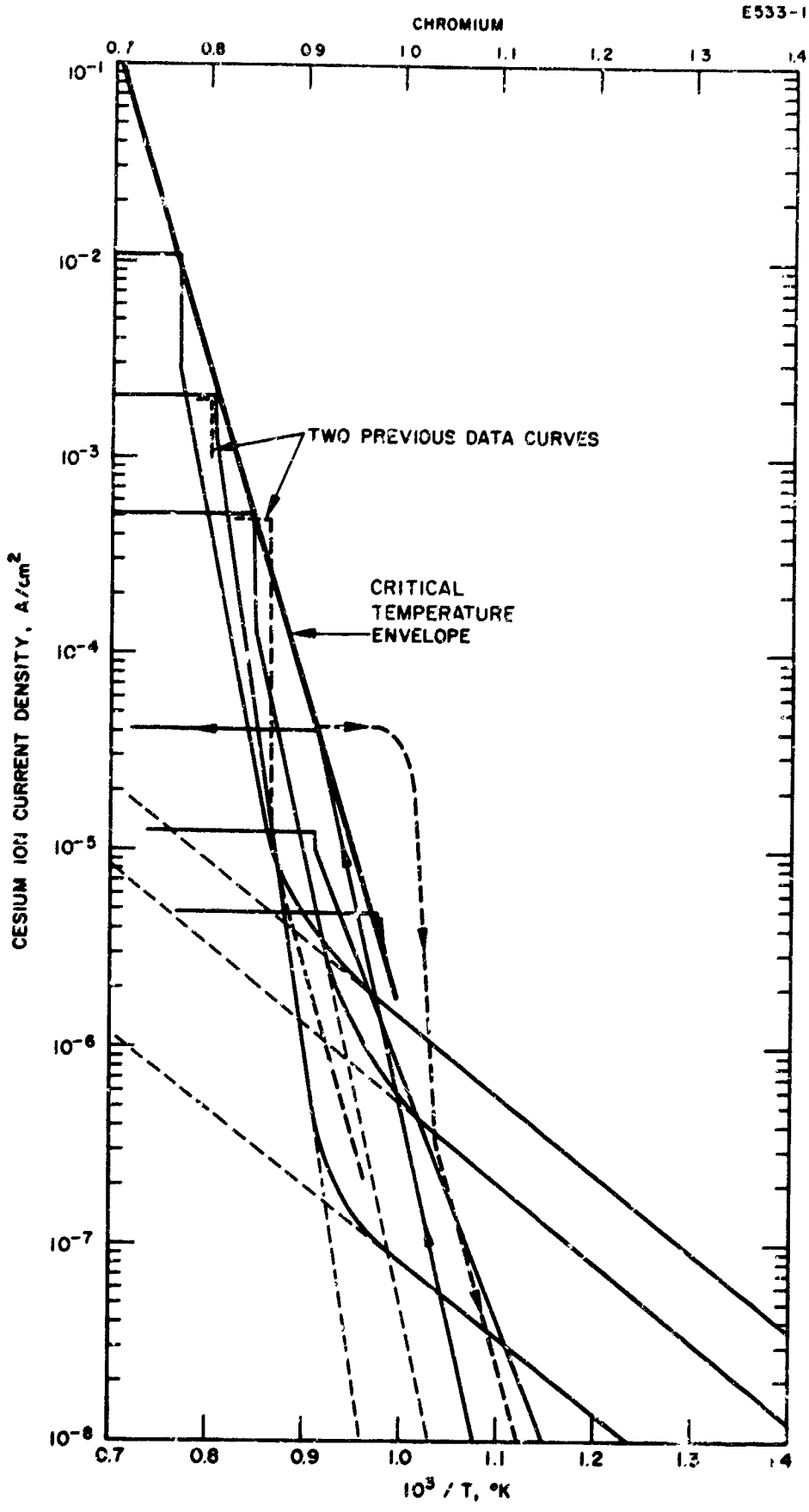

Fig. 31. Cesium ion emission from chromium.

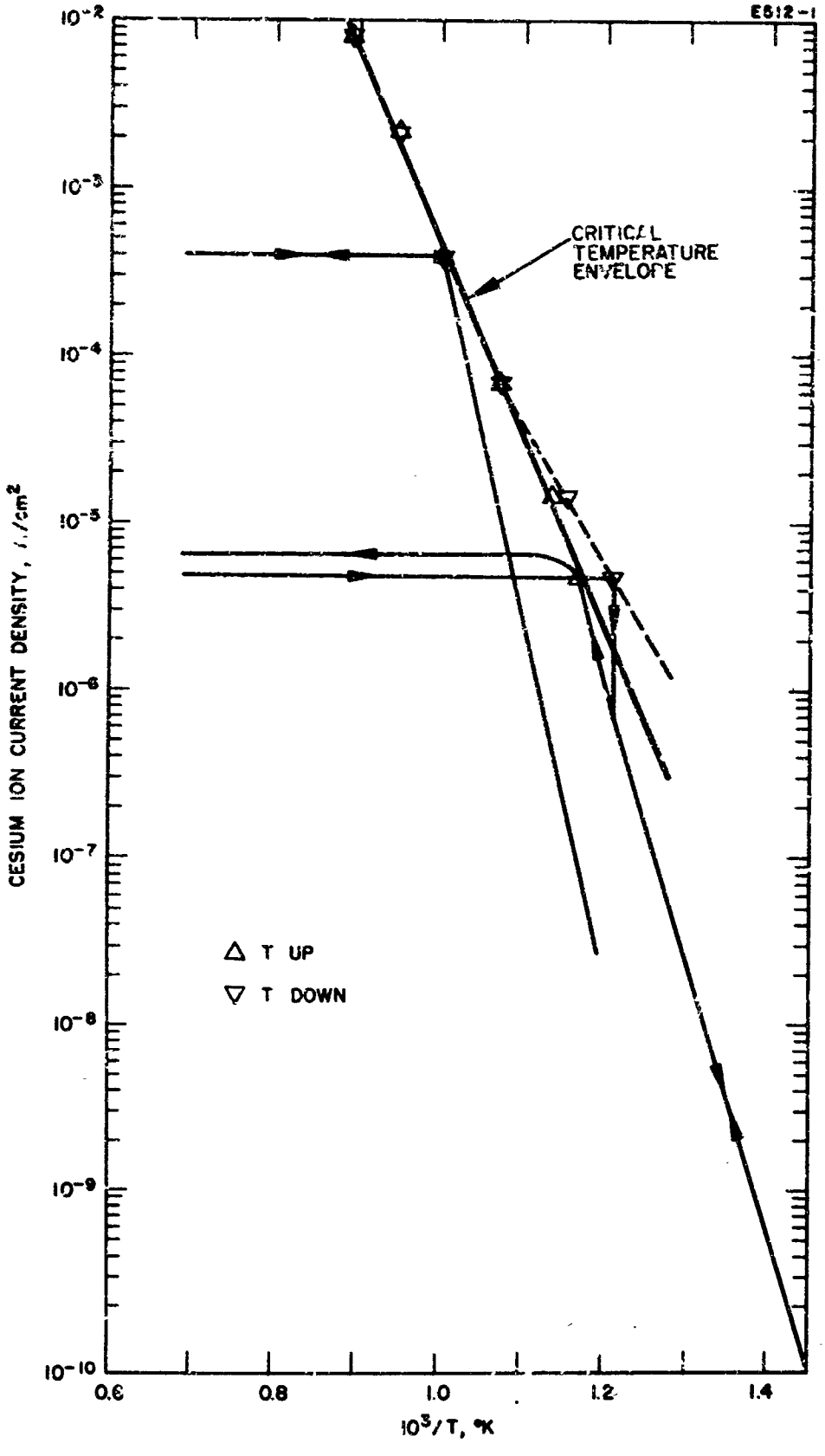

Fig. 32. Cesium ion emission from nickel.

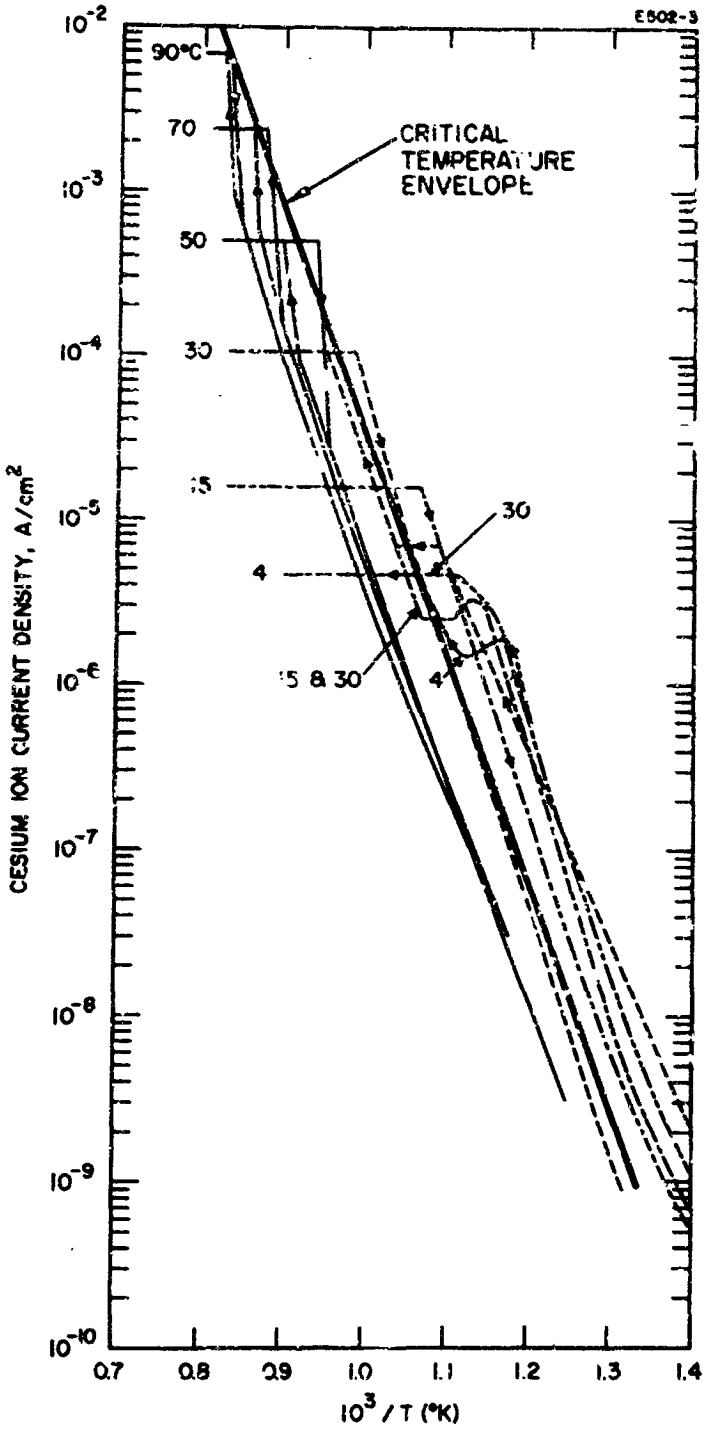

Fig. 33. Cesium ion emission from copper. The experimental data curves for cesium temperatures of 4, 15, and 30 C are done in different symbols because of overlapping.

with increasing cesium arrival flux, as usual, probably disappearing just above 10 mA/cm^2 of cesium ions. The same S-shaped curve (reported in the Final Report on NAS 3-5249) in the nonsaturated region for increasing temperature at low arrival fluxes was observed this time. A very good critical temperature envelope can be drawn for the copper data. Its slope yields the value 2.85 eV for the desorption energy of cesium from copper at low coverage.

6. Rhenium

The ion emission curves for rhenium (Fig. 34) are sharp and normal and are similar to those for tungsten. The increasing temperature critical temperature envelope is just slightly higher than that for tungsten, about 20 K. A relatively small temperature hysteresis effect is exhibited which disappears at about 10 mA/cm^2. The slope of the critical temperature envelope yields a value of 2.75 eV for the desorption energy of cesium ions from rhenium at low critical coverage.

7. Iridium

For iridium (Fig. 35), data from two sets of increasing temperature runs are included. A very large temperature hysteresis effect is observed for iridium. The critical temperatures exhibit rather large current discontinuities and are therefore clearly defined. The slope of the increasing temperature critical temperature envelope for iridium yields a value of 4.83 eV for the low coverage cesium ion desorption energy. The difference between the critical temperature of iridium and tungsten (iridium always greater) as a function of cesium ion current density is summarized in Table XII.

8. Platinum

Platinum (Fig. 36) exhibits the highest (normal) cesium ion critical temperatures of all materials studied to date. The saturation discontinuities are comparatively large at high current density. The slope of the envelope yields 3.61 eV for the desorption energy for cesium ions.

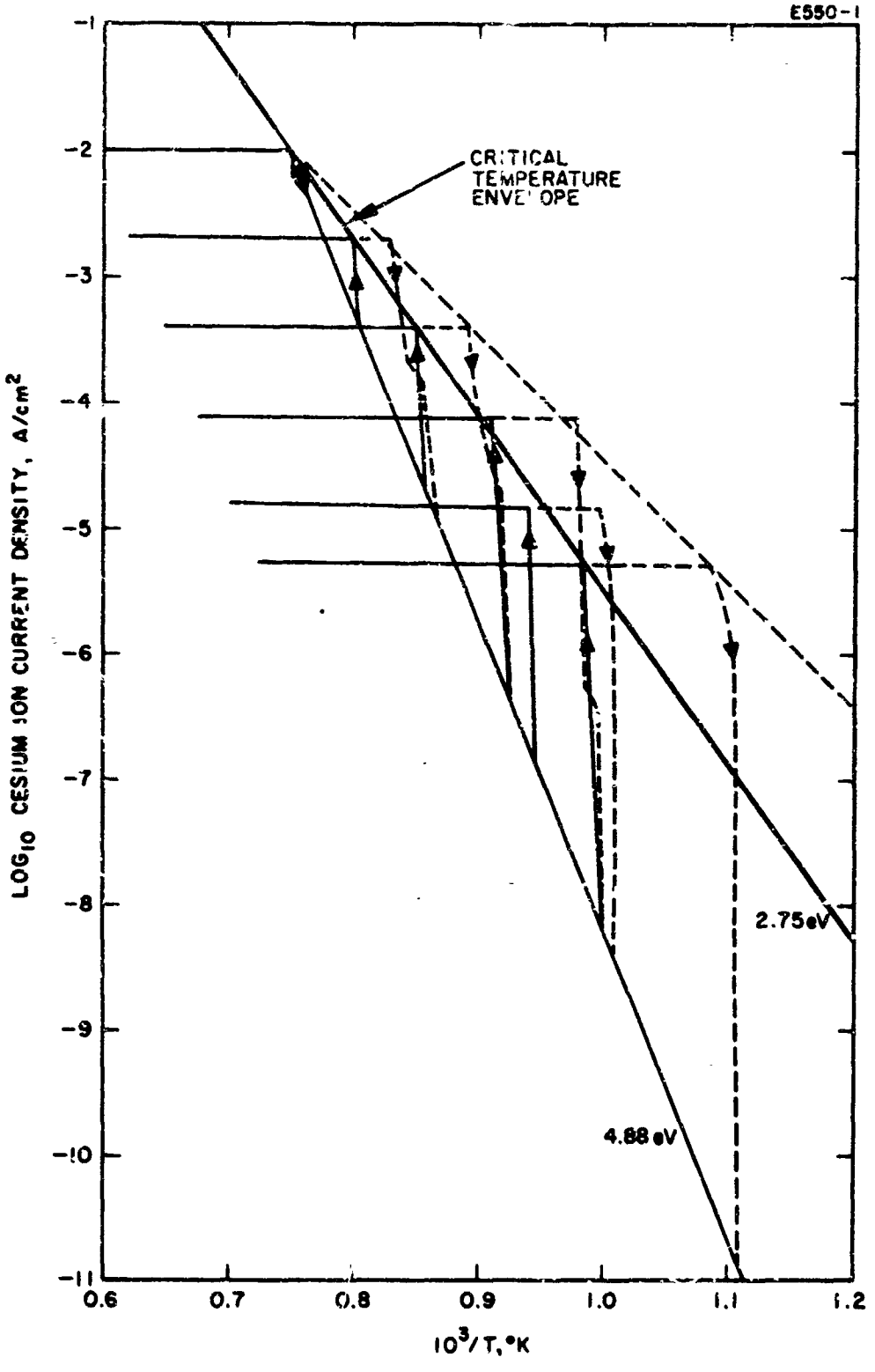

Fig. 34. Cesium ion emission from rhenium.

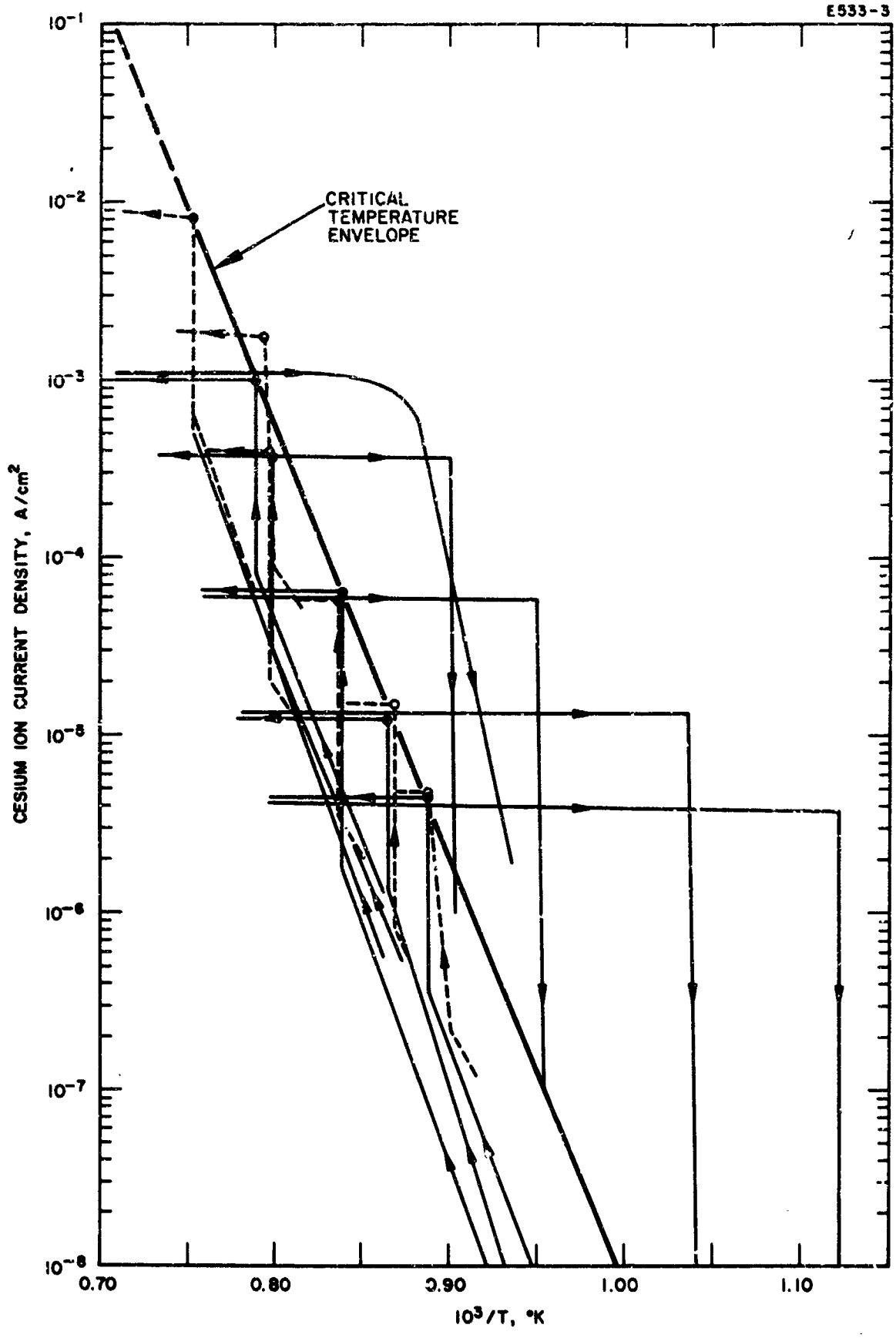

Fig. 35. Cesium ion emission from iridium.

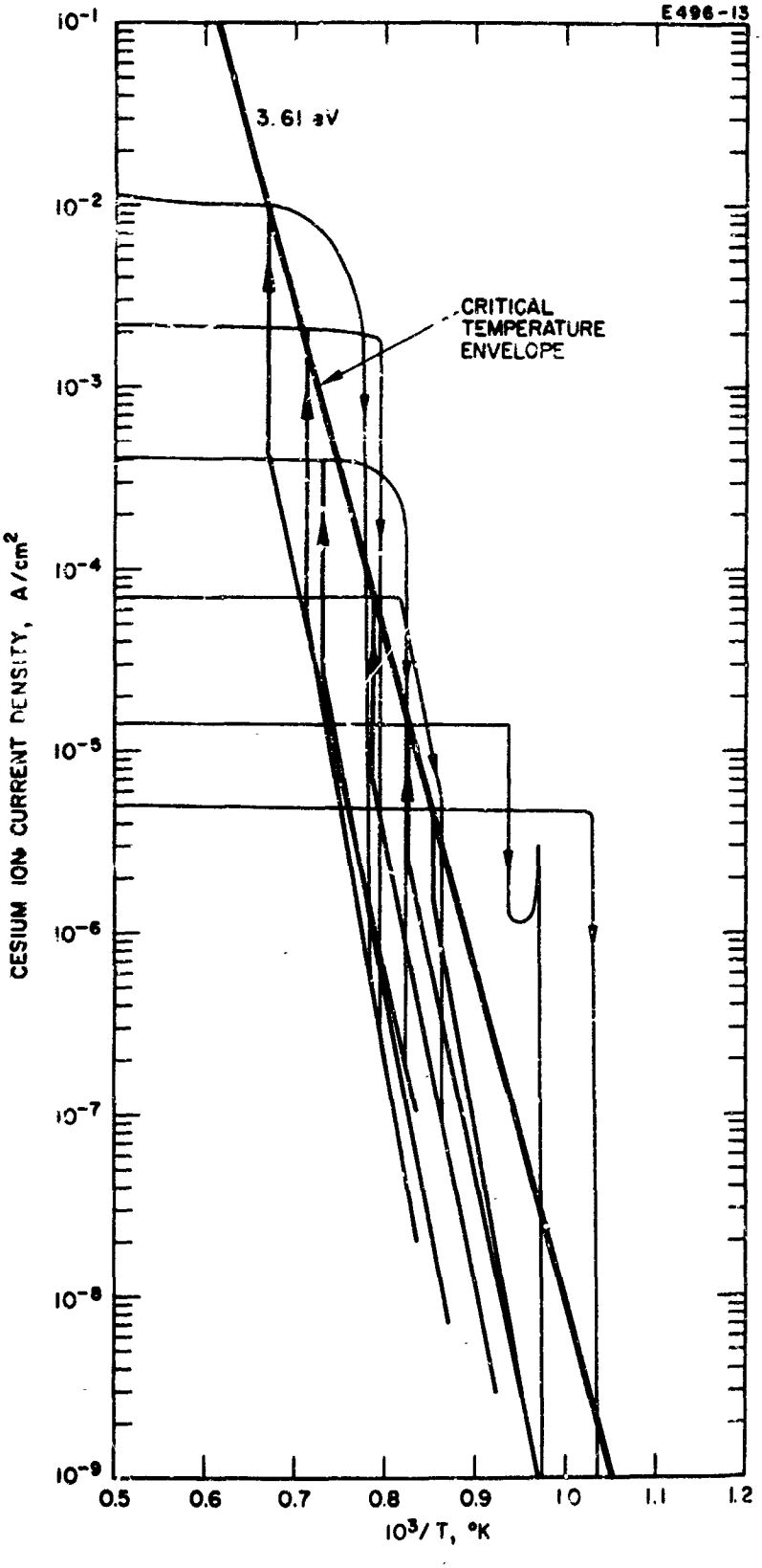

Fig. 36. Cesium ion emission from platinum.

TABLE XII

Difference Between the Critical Temperatures of Iridium and Tungsten

J_+, A/cm^2	T_c, K
10^{-2}	32
10^{-3}	75
10^{-4}	105
10^{-5}	123
10^{-6}	146
10^{-7}	158
10^{-8}	171

9. Stainless Steel

The cesium ion emission from 304 stainless steel (Fig. 37) is conventional. It shows rather large temperature hysteresis, probably disappearing just above 10 mA/cm^2. The increasing temperature critical temperature envelope falls slightly above that for tungsten, among many others. Its slope yields a value of 3.15 eV for the cesium ion desorption energy at critical coverage.

10 Aluminum Oxide

The ion emission data for aluminum oxide are plotted in Fig. 38 as recorded with slow time variation along the temperature axis. The curves are seen to be somewhat anomalous, inconsistent, and are non-reproducible in detail. Two facts are pointed out, as mentioned earlier. First, the collector cannot be an insulator, so copper is used. At lower emitter temperatures, therefore, there is the possibility that the emitter is covered with more copper atoms sputtered back from the

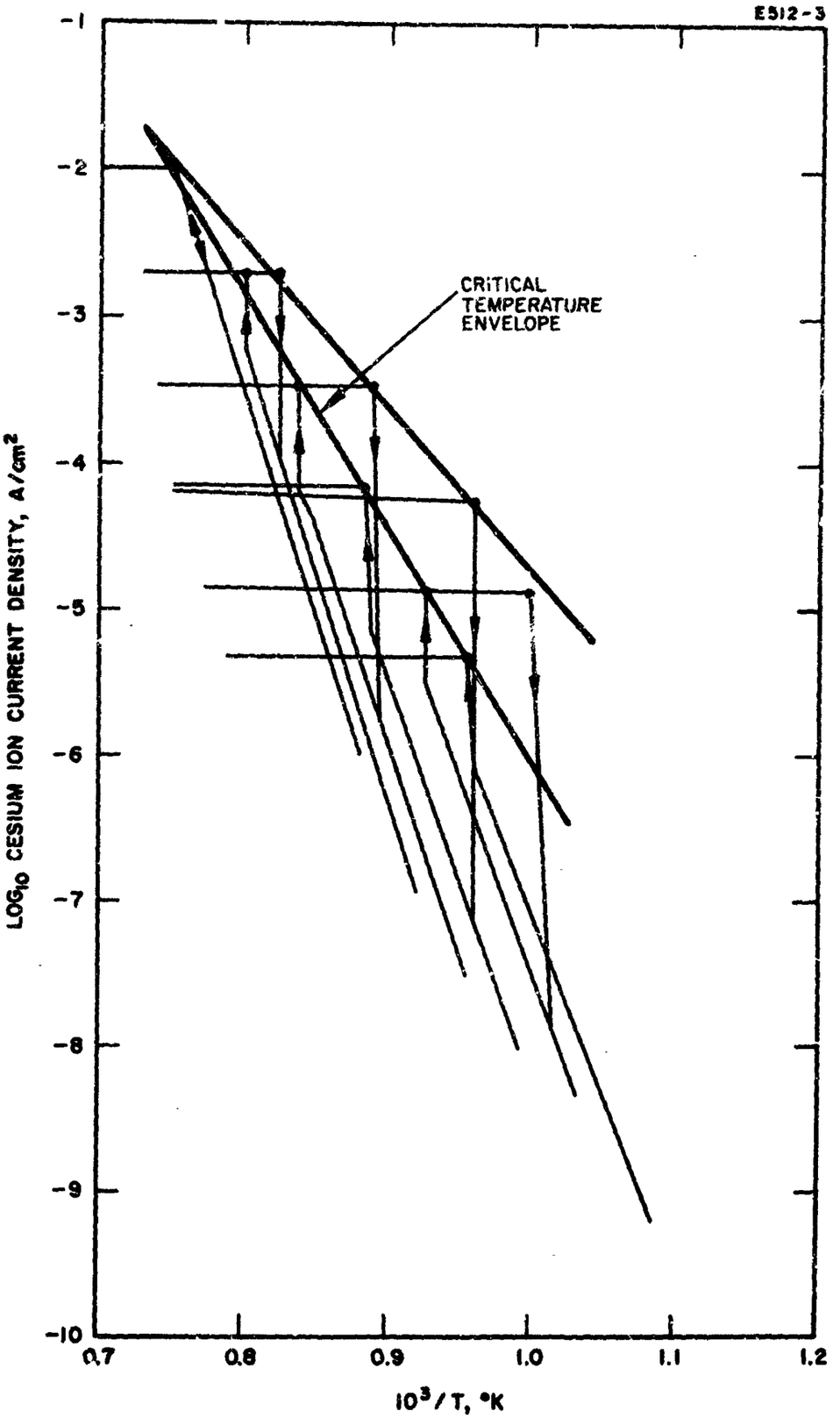

Fig. 37. Cesium ion emission from 304 stainless steel.

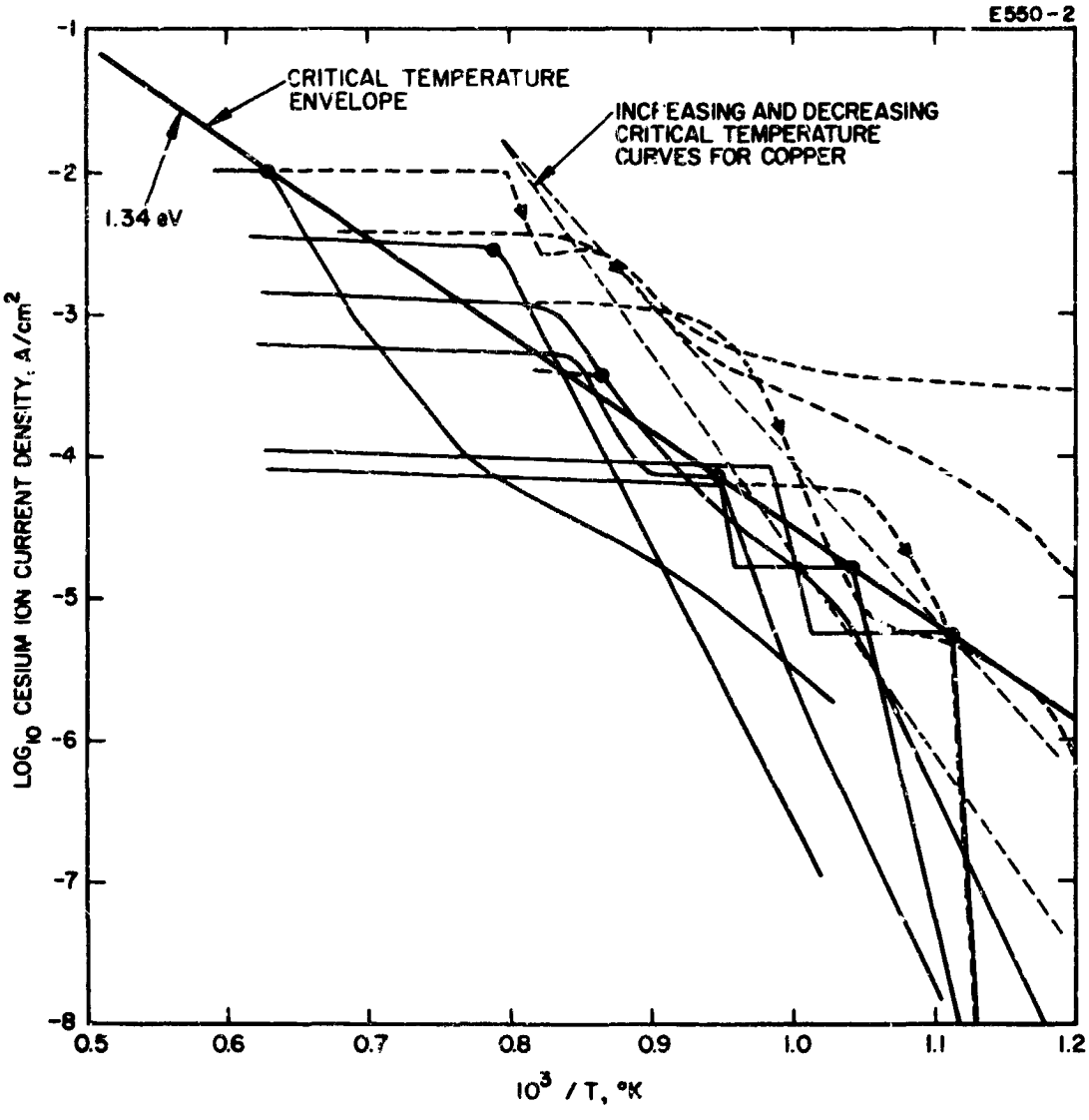

Fig. 38. Cesium ion emission from Lucalox aluminum oxide (actual data).

collector by the cesium ions than for hotter surface temperature. Second (and very important), the emitter is an insulator, much more pure than in the previous case of porous sintered alumina. The possibility therefore exists for charge buildup effects and long equilibration times. Surface charging and other insulator effects may account for the inconsistency and nonreproducibility effects. The curves shown in Fig. 38 are representative for Lucalox, but are not unique. A number of curves were recorded at different rates of temperature change, and some reproducibility checks were made at the same time rate of temperature change. Detailed reproducibility was not possible, and significant variations with rate of temperature change were observed. In Fig. 39, a set of curves is shown which has been made self consistent and made to fit most of the data for Lucalox. The value of the cesium ion desorption energy obtained from the slope of the increasing temperature envelope is about 1.34 eV, much lower than for any metals. This is not surprising because although alumina exhibits an electron work function similar to that of metals, it is an insulator and the bonding mechanisms for adsorbed cesium may be different. For example, ionic and covalent bonding may be impossible because of the lack of available electrons for this process in the substrate, leaving only an image charge force to comprise the bond However, the substrate is an insulator and the concept of an image charge is probably invalid. Thus, the bonding mechanism is probably different, and it is not surprising that the binding energy is less.

D. Emitter Fabrication

During this six month period, numerous experimental tubes were fabricated. In many cases, a variety of failures required a number of extra tubes to be built. In many cases, the failures were routine; in others, success could be achieved only by design modifications. These modifications and the nonroutine materials problems are described below as information for this technology.

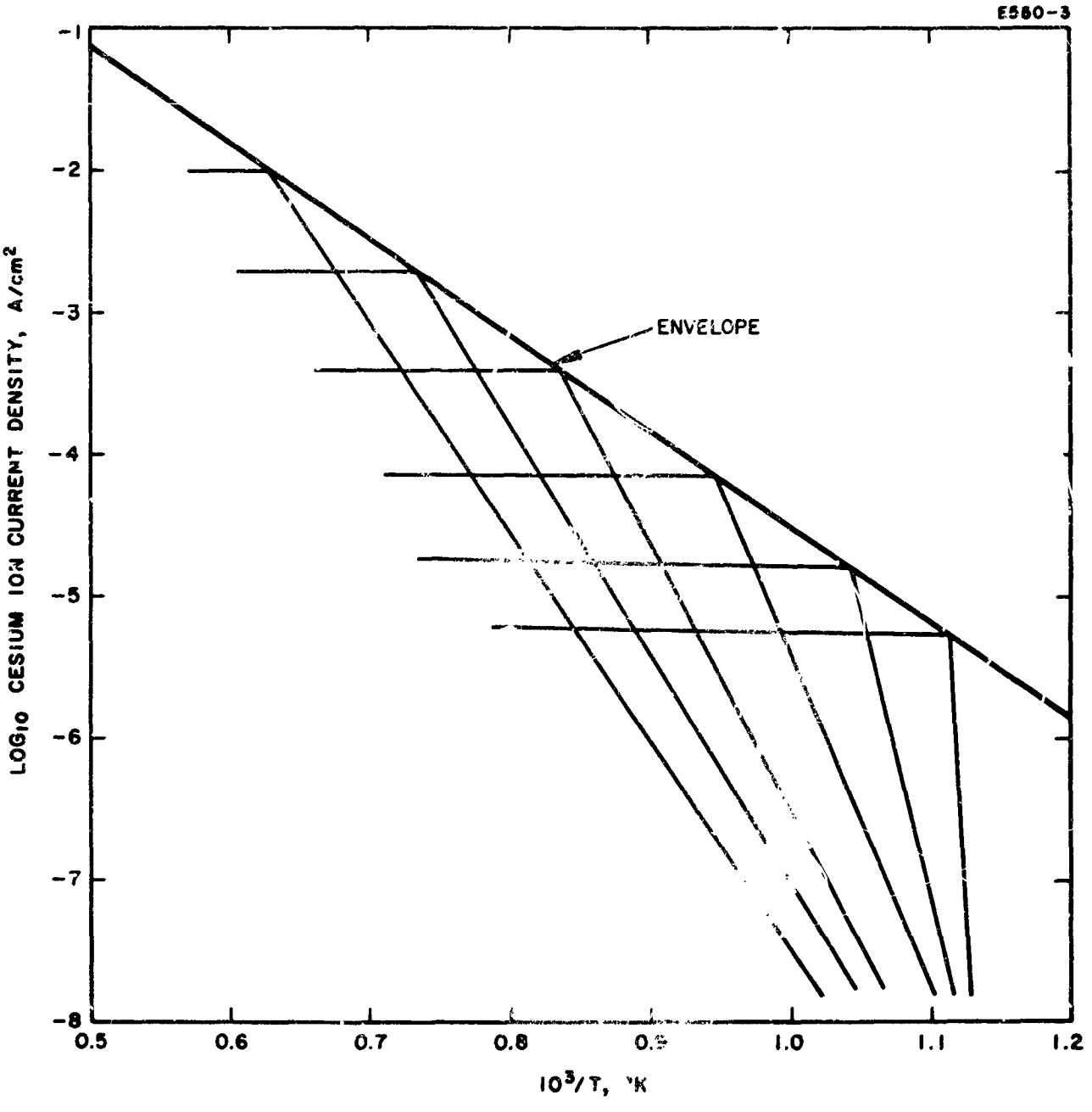

Fig. 39. Cesium ion emission from Lucalox aluminum oxide (smoothed-out data).

The materials for which the standard ribbon emitter design was tried are beryllium, titanium, nickel, rhenium, iridium, and platinum. For beryllium and titanium, ribbons proved to be unsatisfactory and solid block emitters had to be employed. The other four, nickel, rhenium, iridium, and platinum, were satisfactory as ribbons. The total list for which block emitters were used is beryllium, titanium, chromium, copper 304 stainless steel, and Al_2O_3 (Lucalox).

For iridium, a thermocouple welding problem occurred. The weldability of the W(5% Re) and W(26% Re) thermocouple wires to the iridium was very poor; five attempts yielded five failures. The primary problem was thermocouple weld rupture during temperature cycling. The final technique used to attach the thermocouple wires to the 99.9% pure iridium ribbon was the incorporation into the weld of a small "patch" of iridium foil. Since iridium does weld extremely well to itself, this "patch" served to fuse the thermocouple with the emitter surface and eliminated failures of the junction. Applying this new technique, a sixth iridium tube was fabricated, processed, and served satisfactorily for all experimental measurements.

Lucalox tube fabrication also proved difficult. Thermocouple failure during temperature cycling was a major obstacle. After several attempts, a Lucalox tube was completed and successfully passed preliminary temperature cycling tests. The tube was processed in the usual manner. Failure occurred during emitter outgassing because of partial shorting of the heater wire running through the center of the Lucalox block emitter. Following this failure, it was decided to redesign the emitter structure such that the failure modes would be minimized, if not eliminated. The new design incorporated four 0.010-in. tungsten heater wires instead of a single wire. These heater wires were contained in a 0.060-in. diameter Al 997 alumina rod with four parallel holes running through its length. This rod was placed inside a square machined Lucalox emitter and was grooved on the outside (5 mils) to receive the thermocouple wires laid parallel to the emitter. This allowed the thermocouple junction to be pressed against the inside

surface of the Lucalox emitter, midway between the ends and facing toward the collector just 0.018 in. from the portion of the emitter facing the collector aperture. It is assumed that this method yielded accurate thermocouple measurements, which are required in view of the impossibility of using optical measuring procedures on a translucent material, such as Lucalox, which transmits about 95% of visible light and for which no reliable emissivity data are available. Optical temperature measurements were compared with the thermocouple readings and found to be high by hundreds of degrees. The thermocouple indicates the maximum emitter temperature for this design. The too high optical pyrometer temperatures (obtained using standard alumina emissivity curves) are attributed to the translucency of the Lucalox.

Problems were encountered with the original use of a titanium ribbon emitter. Emitter burnout occurred during initial cesiated emission measurements. Failure appeared to be the result of grain growth which weakened the titanium structure, leading to distortion, thinning, and eventual failure. A thicker ribbon was tried, but yielded the same results. Rather extreme distortion caused by expansion of the ribbon resulted in a very wavy profile for both thicknesses of ribbon (1 and 10 mils). It was decided to abandon the ribbon type of construction in favor of a block emitter. Such an indirectly heated titanium emitter proved to be quite satisfactory.

A second vacuum system, identical to that built and operated under NAS 3-5249, was assembled and put into operation. Two vacuum stations allow experimental tubes to be tested and processed and vacuum work function measurements to be made at twice the previous rate. This and a second set of electronic test equipment are allowing measurements to be made on an efficient and productive time schedule.

REFERENCES

1. R. G. Wilson, "Electrode Surface Physics Research," Final Report (Appendix A) on Contract NAS 3-5249, December 1964.

2. R. P. Godwin and E. Lüscher, "Desorption energies of gold and copper deposited on a clean tungsten surface," Surface Sci. 3, 42-48 (1964).

3. H. Shelton, "Program of Analytical and Experimental Study of Porous Metal Ionizers," Reports on Contract NAS 3-5254, 1964-65.

APPENDIX — Calculations for Cesium on Various Substrates

Curves of composite surface work function (———), cesium atom desorption energy (— — — —), and cesium ion desorption energy (— — — —) versus surface coverage (θ) for cesium adsorbed on 27 substrates under the cesium ion thrustor surface conditions of 1400 K and $\sim 10^5$ V/cm comprise the 27 figures of the Appendix. The adsorbates are beryllium, aluminum, titanium, vanadium, chromium, manganese, iron, cobalt, nickel, copper, gallium, zirconium, niobium, molybdenum, ruthenium, rhodium, palladium, indium, tin, hafnium, tantalum, tungsten, rhenium, osmium, iridium, platinum, and lead.

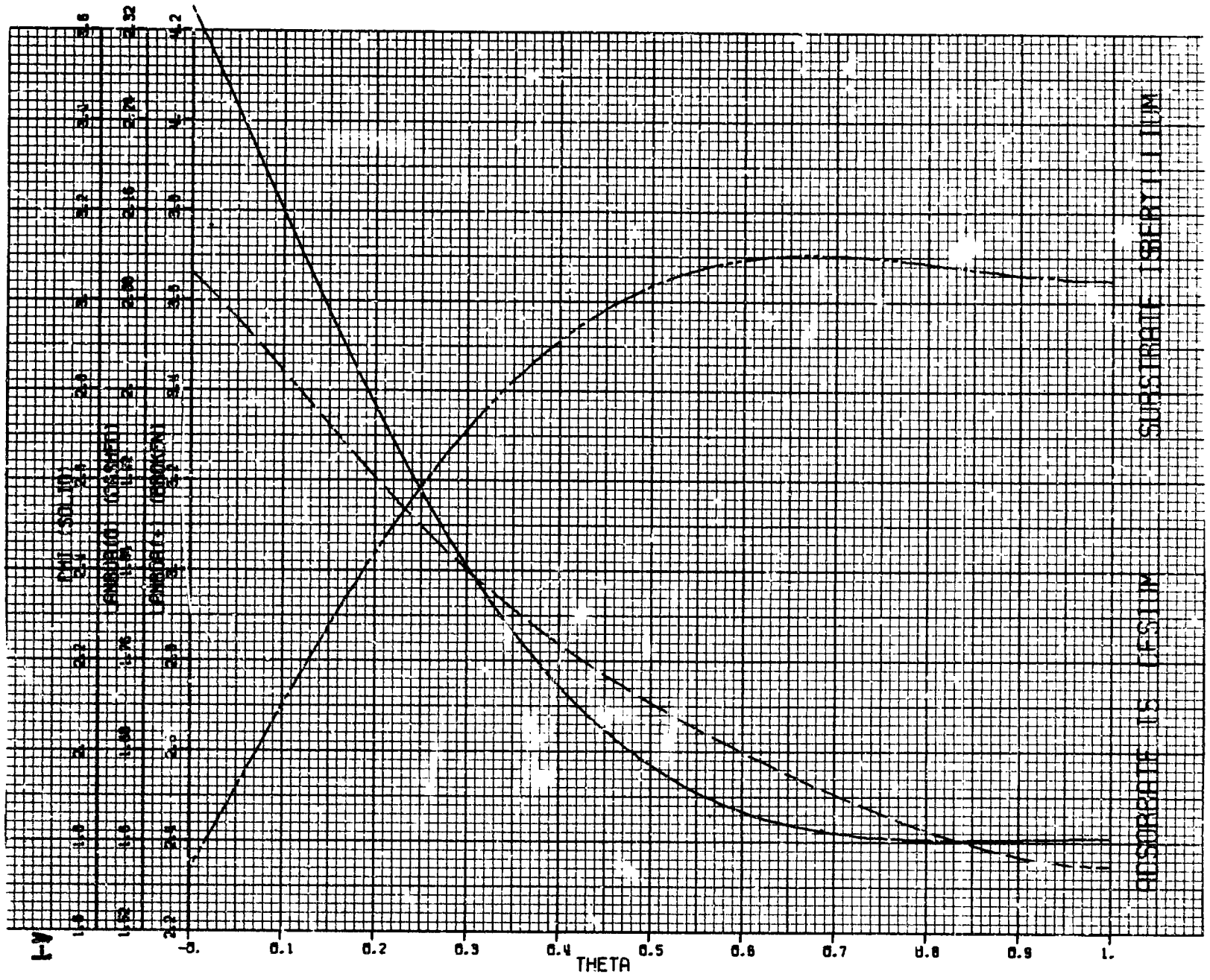
ADSORBATE IS LEAD ON SUBSTRATE LIBERTI LITHIUM
THETA
0.1
0.2
0.3
0.4
0.5
0.6
0.7
0.8
0.9
1.

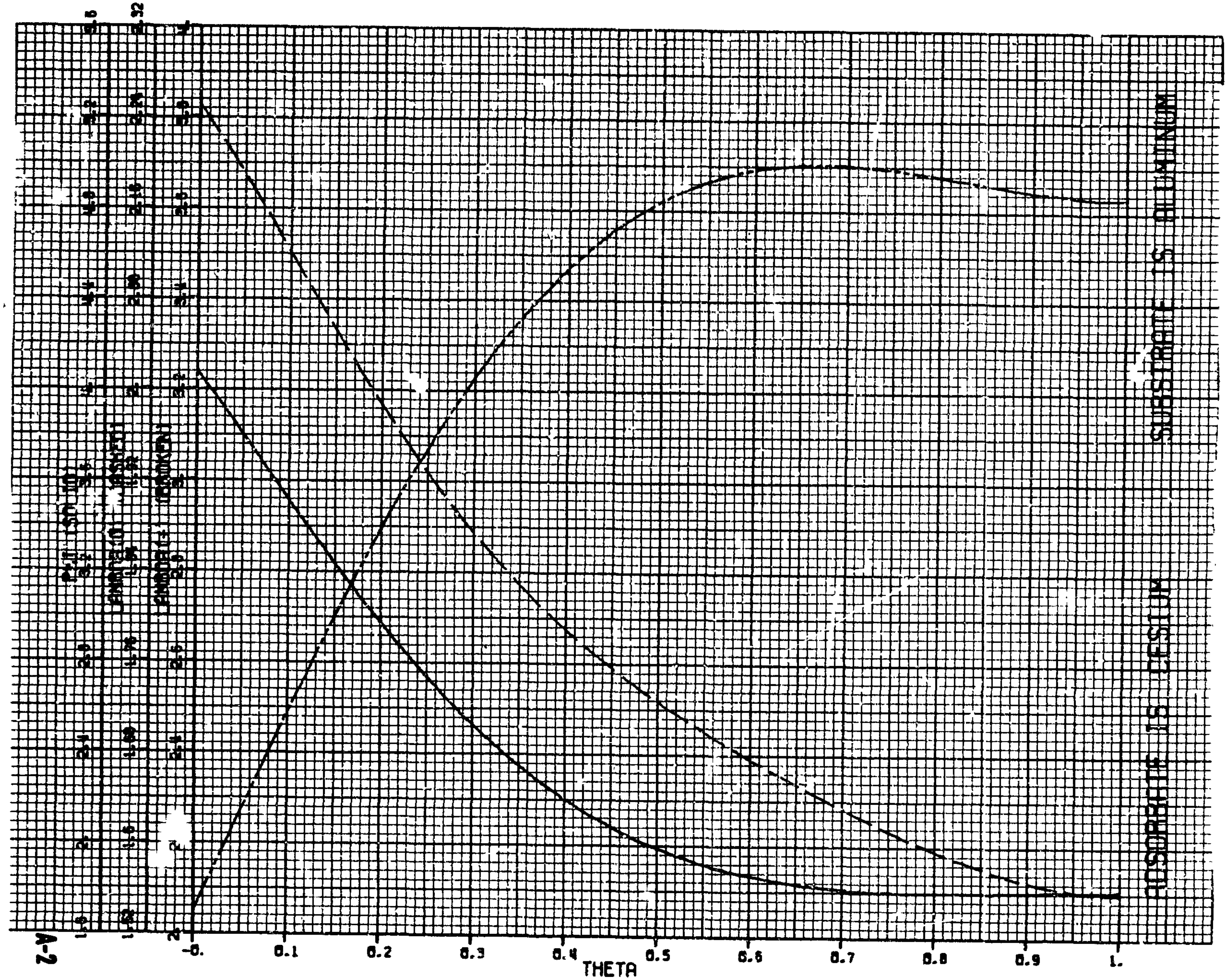

ADSORBATE IS CESIUM
SUBSTRATE IS ALUMINUM
THETA
-0.
0.1
0.2
0.3
0.5
0.6
0.7
0.8
0.9
1.

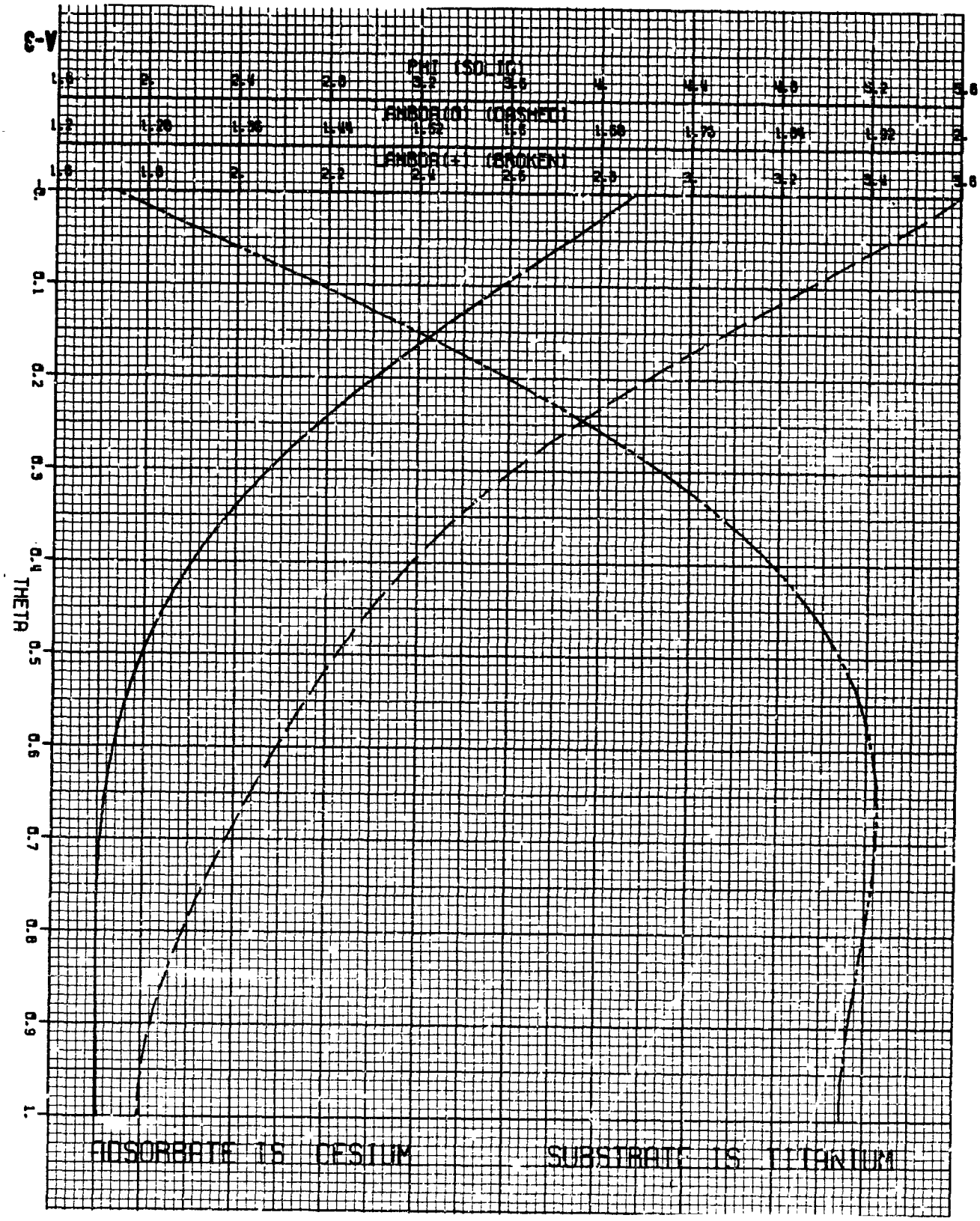
PHI (SOLID)
ANSOR(0) (DASHED)
ANSOR(+1) (BROKEN)
THETA
ADSORBATE IS CESIUM
SUBSTRATE IS TITANIUM

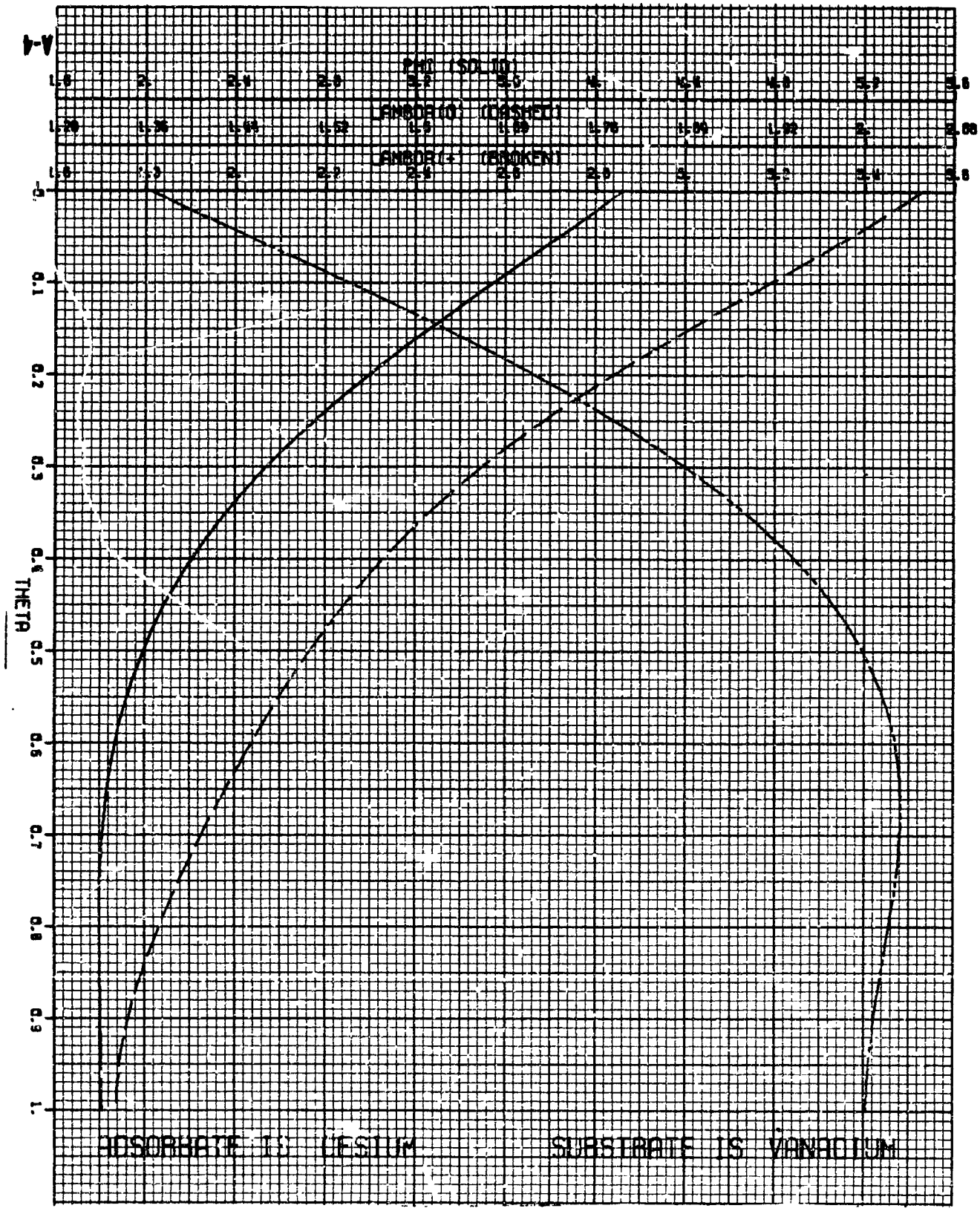
A-4
PHI (SOLID)
ANSOR(0) (DASHED)
ANSOR(+) (BROKEN)
THETA
ADSORBATE IS CESIUM
SUBSTRATE IS VANADIUM

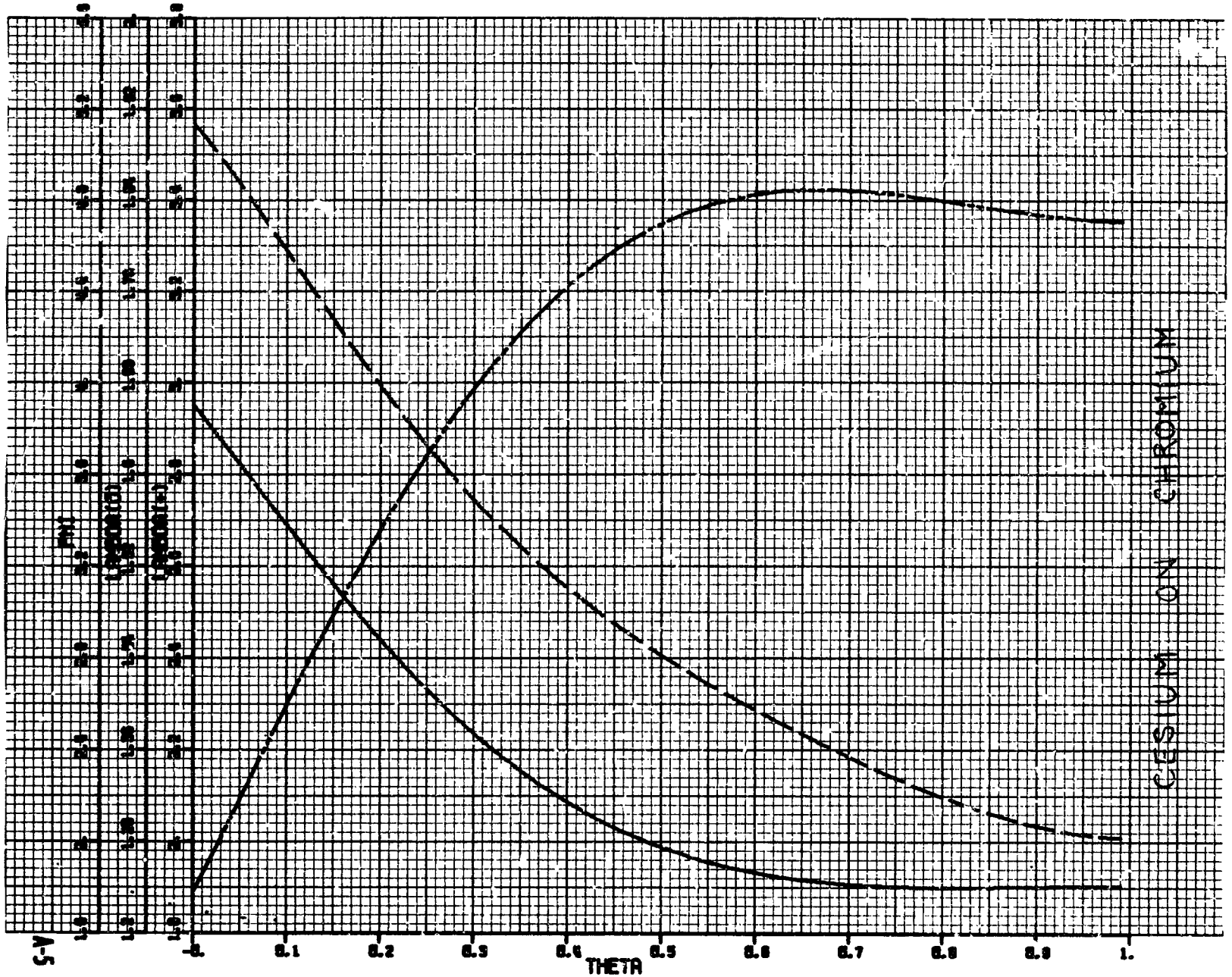
CHROMIUM
CESIUM
THETA
0.
0.1
0.2
0.3
0.4
0.5
0.6
0.7
0.8
0.9
1.

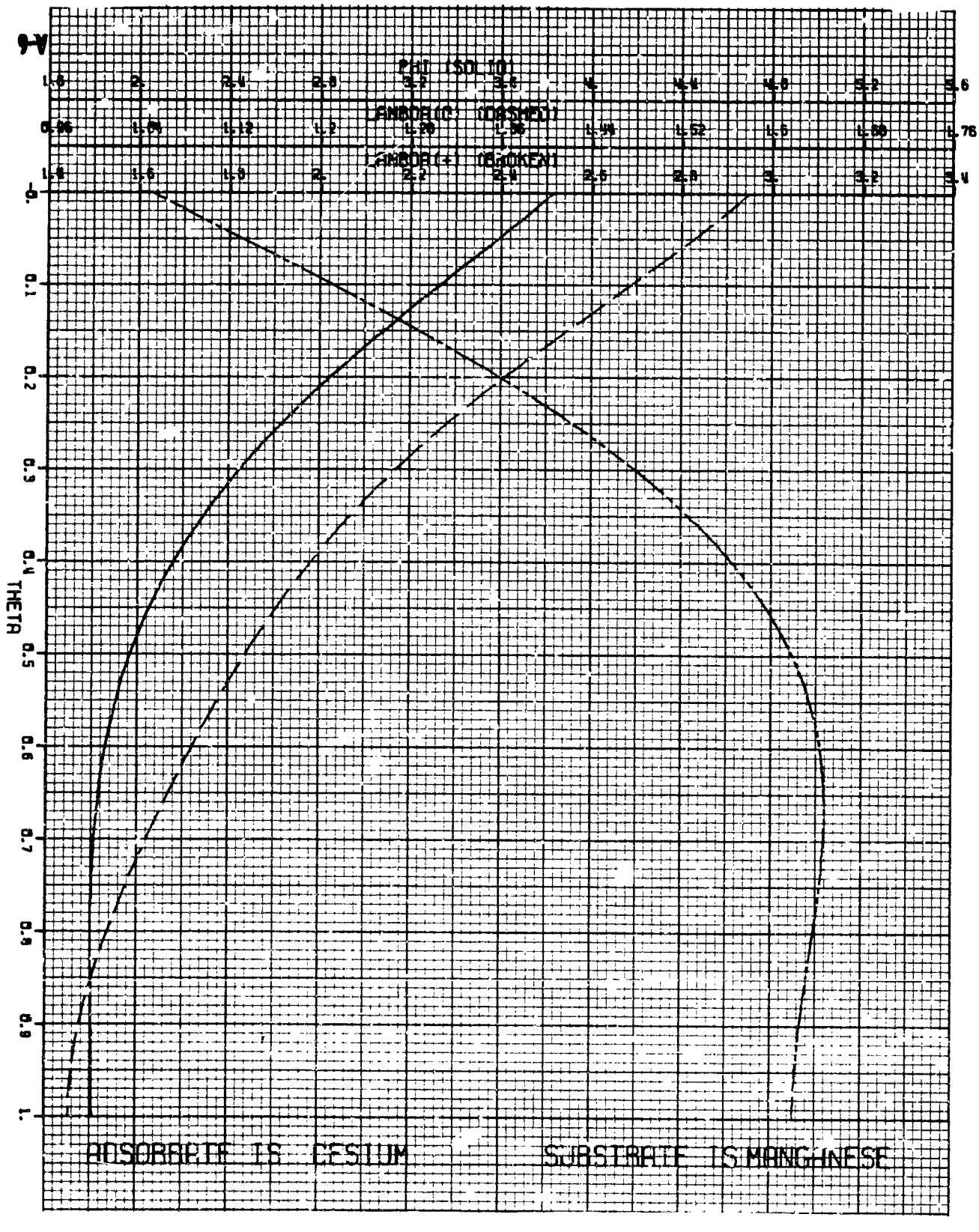
PHI (SOLID)
ANODE(C) (DASHED)
ANODE(+) (BROKEN)
THETA
ADSORBATE IS CESIUM
SUBSTRATE IS MANGANESE

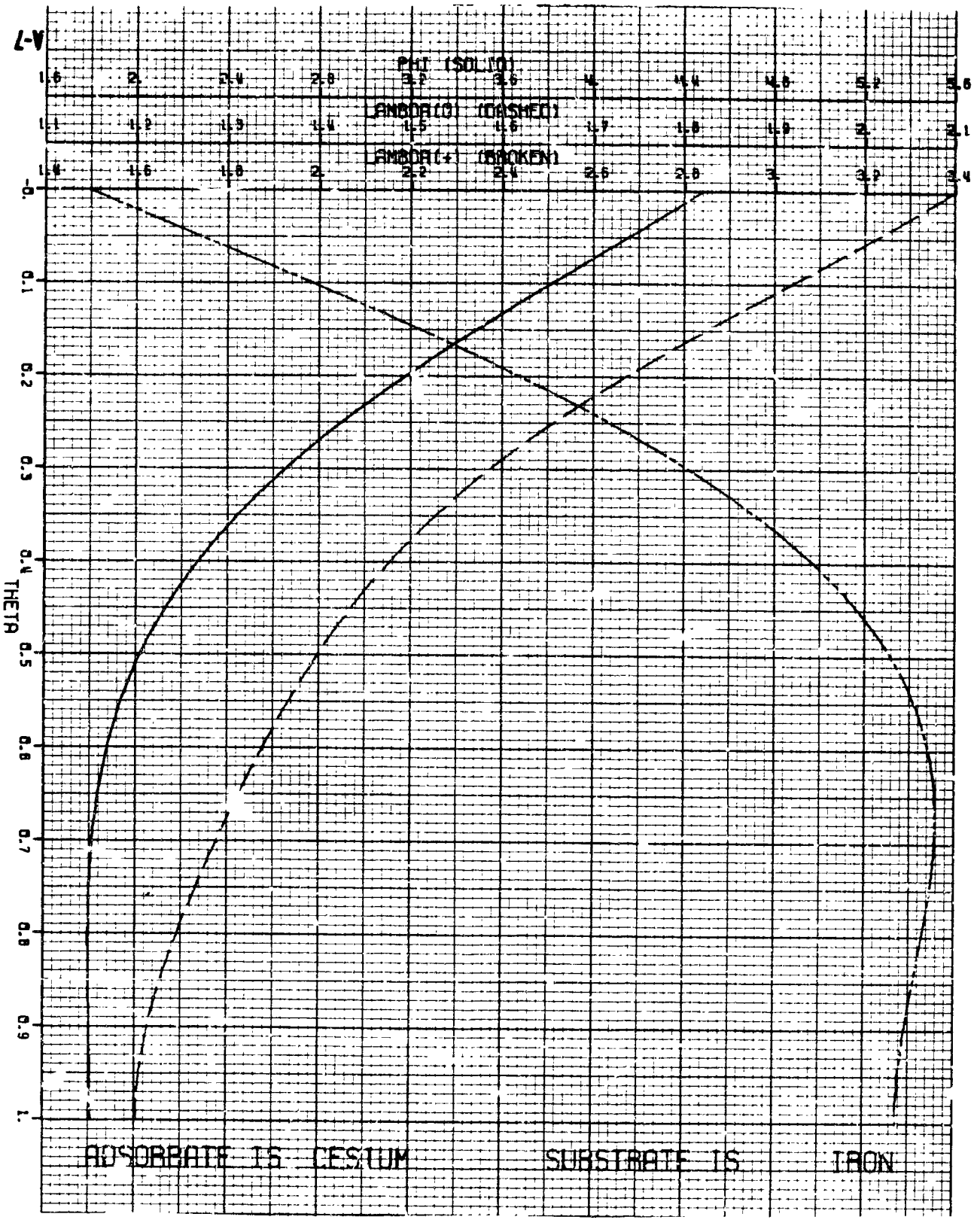
L-V
PHI (SOLID)
LANGOR(D) (DASHED)
LANGOR(+) (BROKEN)
THETA
ADSORBATE IS CESIUM
SUBSTRATE IS IRON

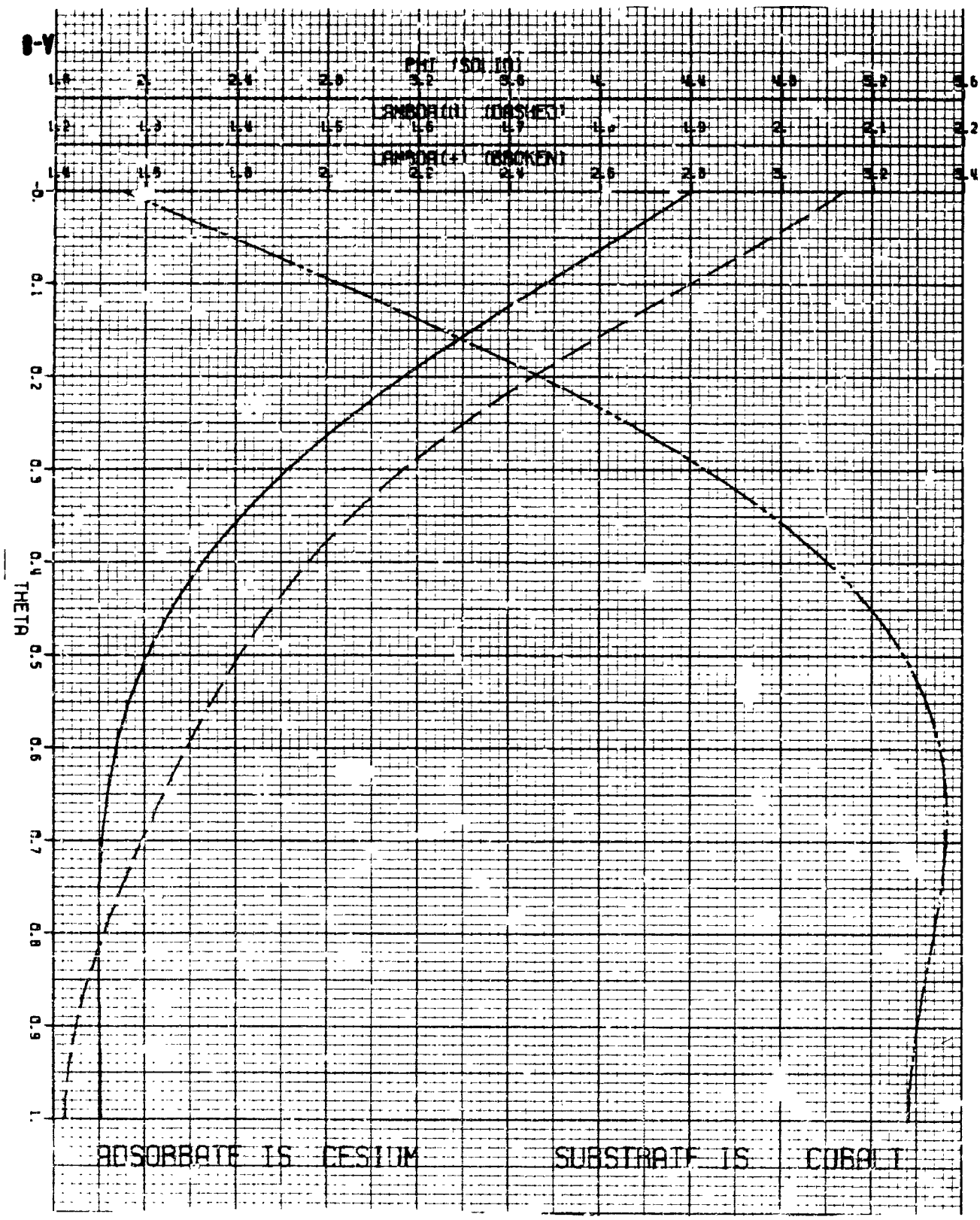
B-V
THETA
ABSORBATE IS CESIUM
SUBSTRATE IS COBALT

6-V

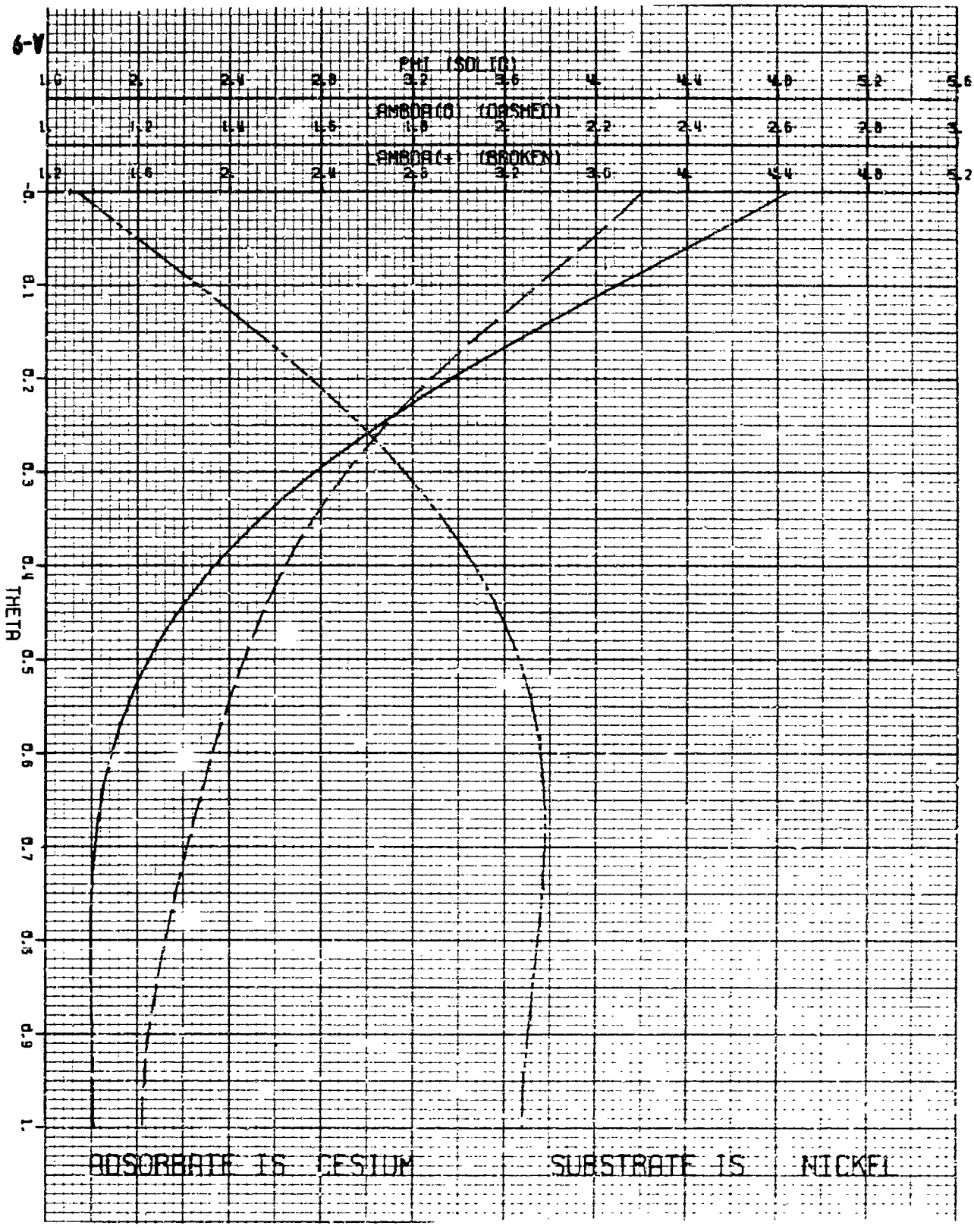
PHI (SOLID)
ANSORB(O) (DASHED)
ANSORB(+) (BROKEN)
THETA
ADSORBATE IS CESIUM
SUBSTRATE IS NICKEL

ADSORBATE IS CESIUM
SUBSTRATE IS COPPER
PHI (SOLID)
ANODE(D) (DASHED)
ANODE(+) (BROKEN)
DELTA

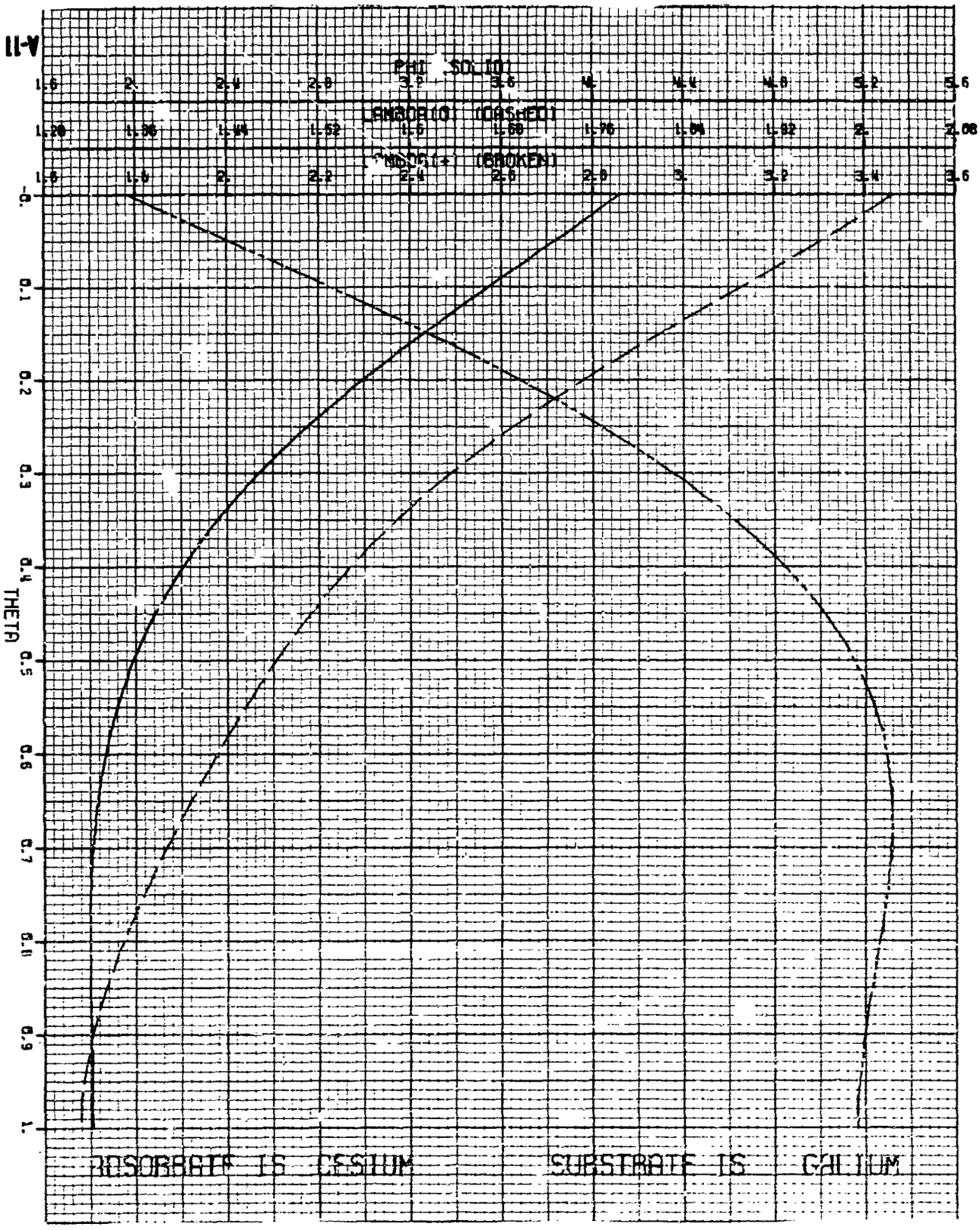
PHI .SOLID)
ENERGY(D) (CASHED)
PHI(+) (BROKEN)
THETA
ADSORBATE IS CESIUM
SUBSTRATE IS GALLIUM

THETA
PHI (SOLID)
ENDOTE(+ SMOOTH)
ENDOTE(O) (DASHED)
A-12

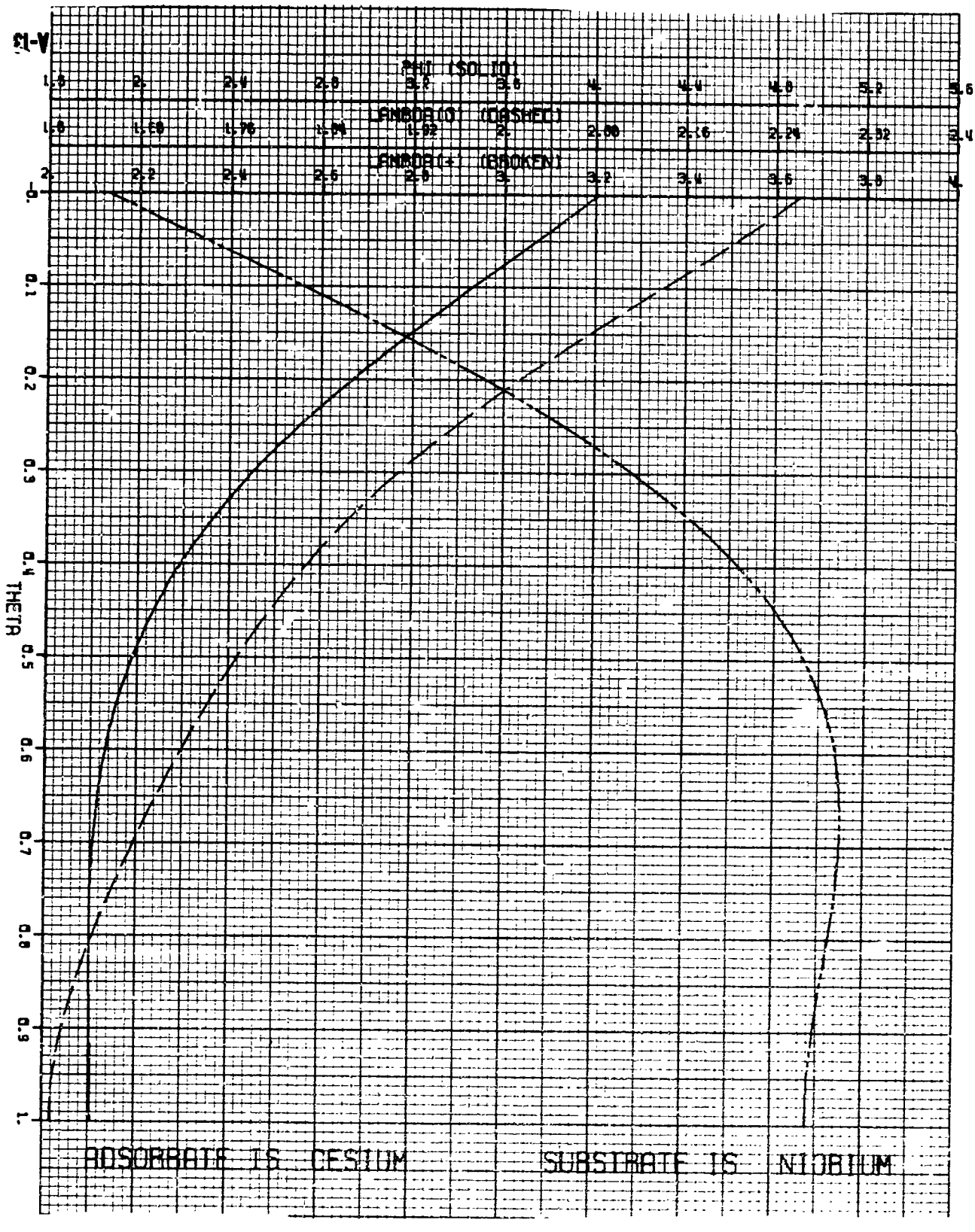
PHI (SOLID)
ANROOT(O) (DASHED)
ANROOT(+) (BROKEN)
THETA
ADSORBATE IS CESIUM
SUBSTRATE IS NIOBIUM

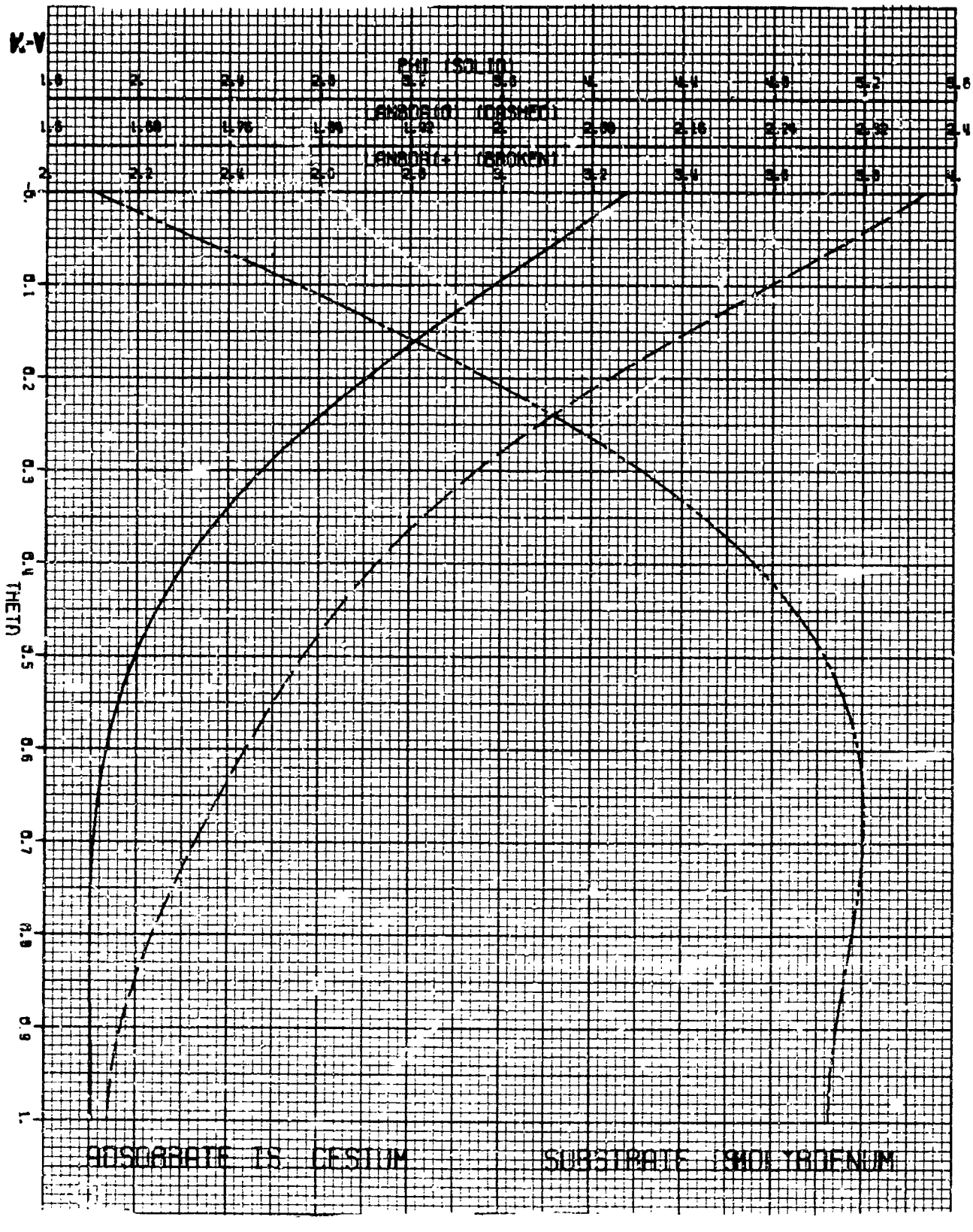
K-V
PHI (SOLID)
ANODE(0) (DASHED)
ANODE(+) (BROKEN)
THETA
SUBSTRATE IS CESIUM
SUBSTRATE IS MOLYBDENUM

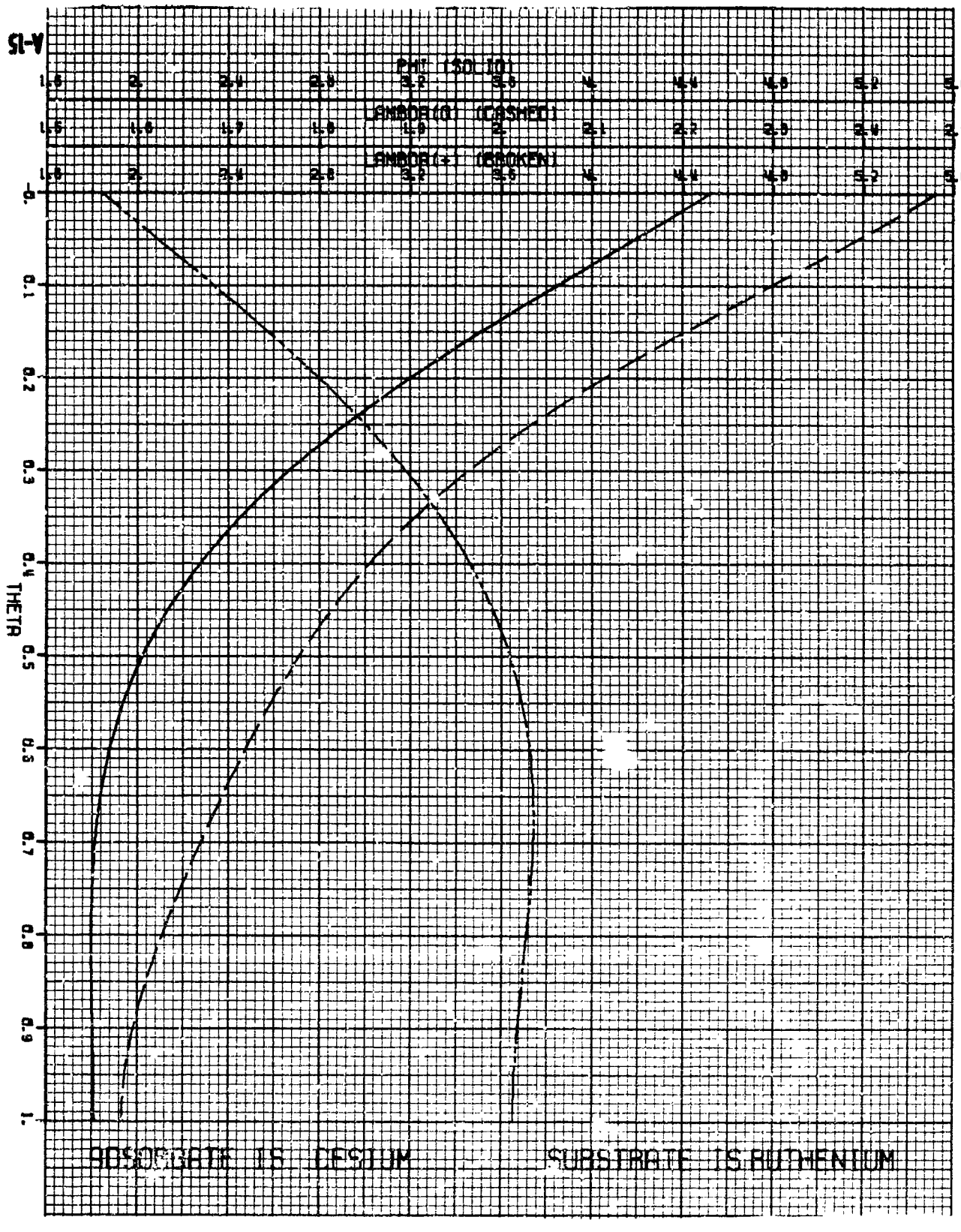
A-15
PHI (SOLID)
LANGOR(0) (DASHED)
LANGOR(+) (BROKEN)
THETA
ADSORBATE IS CESIUM
SUBSTRATE IS RUTHENIUM

ADSORBATE IS CESIUM
SUBSTRATE IS RHODIUM
THETA
0.9
0.8
0.7
0.6
0.5
0.4
0.3
0.2
0.1
0.

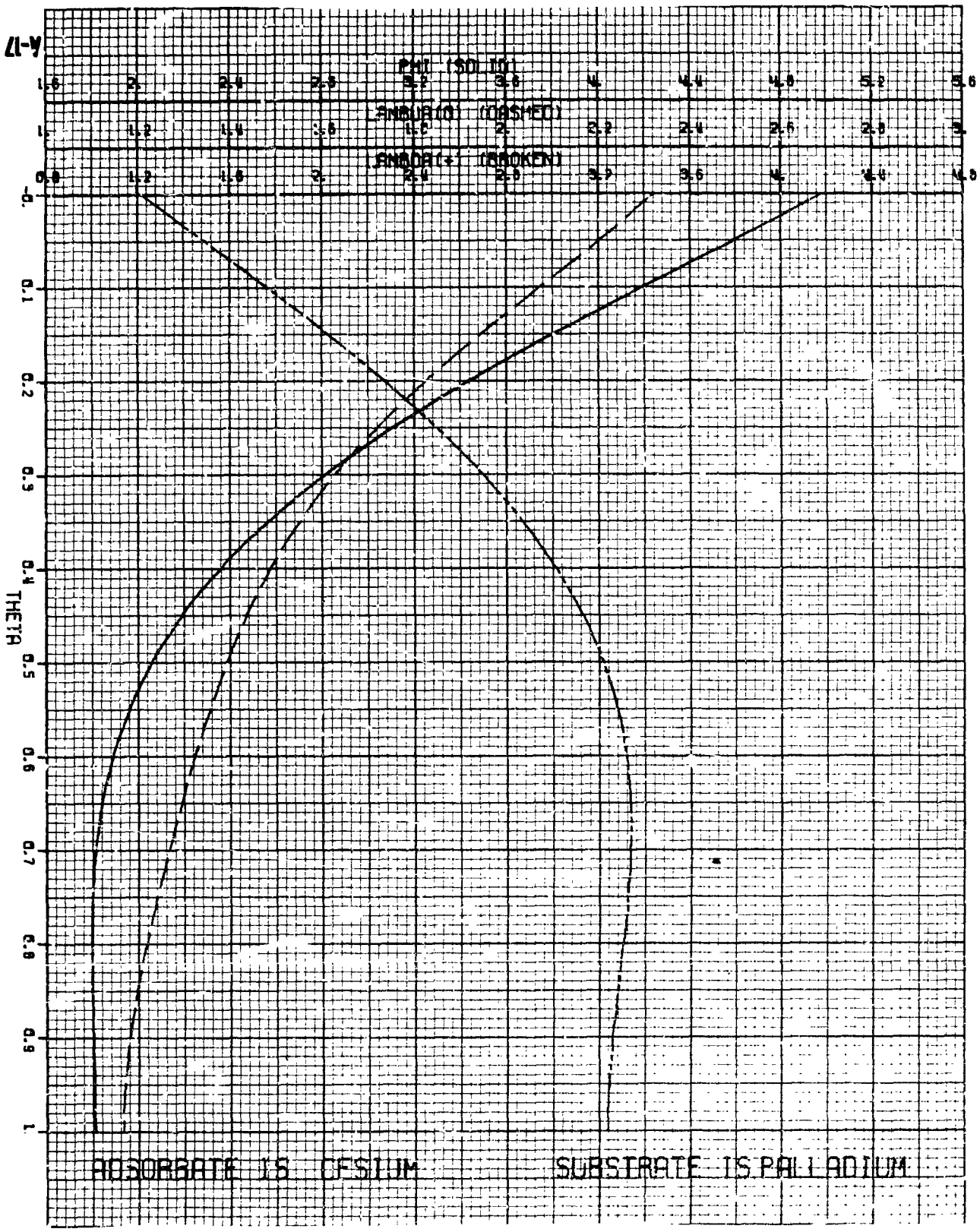
(1-Y
PHI (SOLID)
ANBUR(O) (WASHED)
ANBUR(+) (BROKEN)
THETA
ADSORBATE IS CESIUM
SUBSTRATE IS PALLADIUM

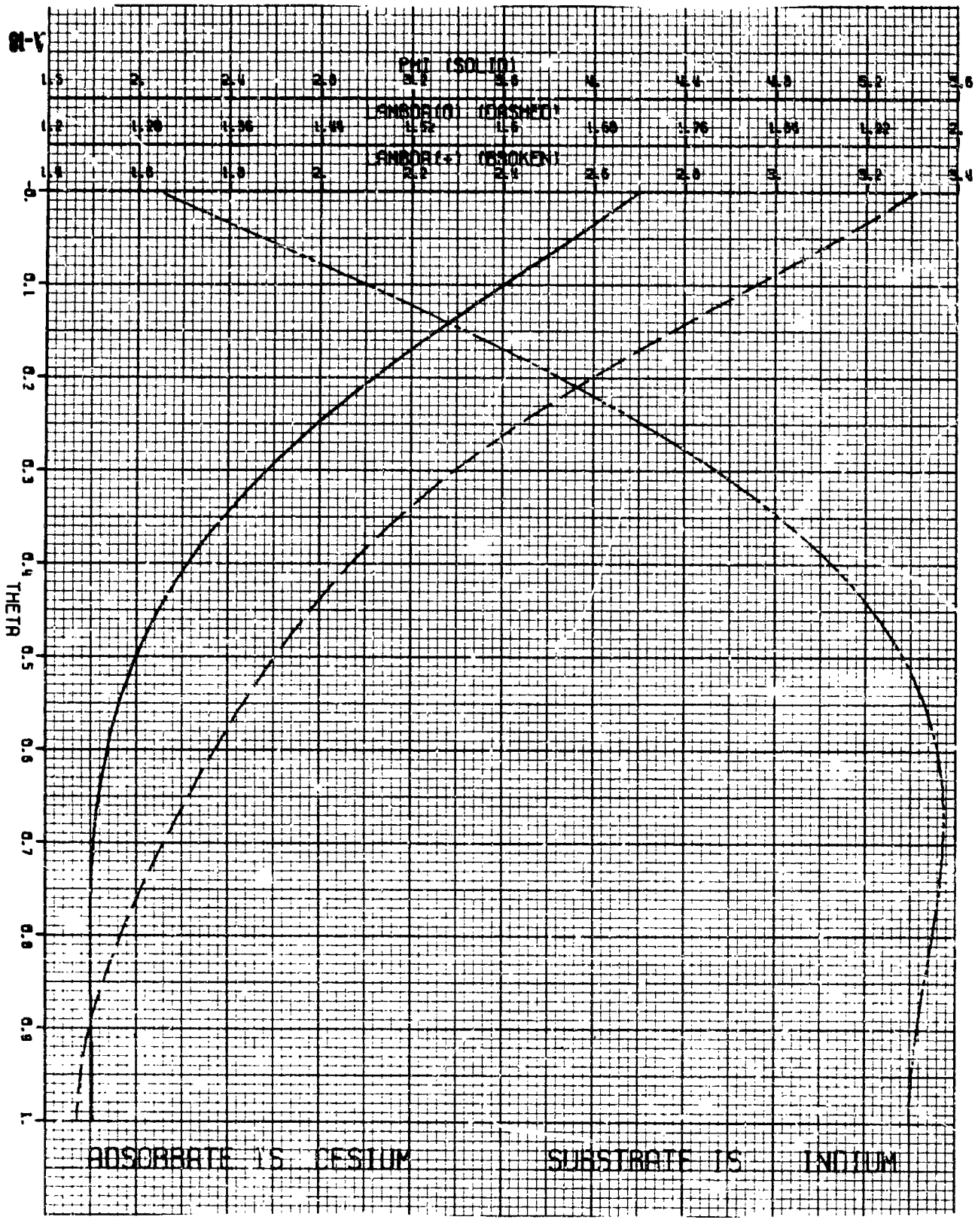
PHI (SOLID)
ANODE(0) (DASHED)
ANDOR(+) (BROKEN)
THETA
ADSORBATE IS CESIUM
SUBSTRATE IS INDIUM

THETA
PHI (SOLID)
LAMBDA(+) (BROKEN)
LAMBDA(0) (DASHED)
SUBSTRATE IS CESIUM
SUBSTRATE IS TIN

ADSORBATE IS CESIUM
SUBSTRATE IS HAFNIUM
THETA

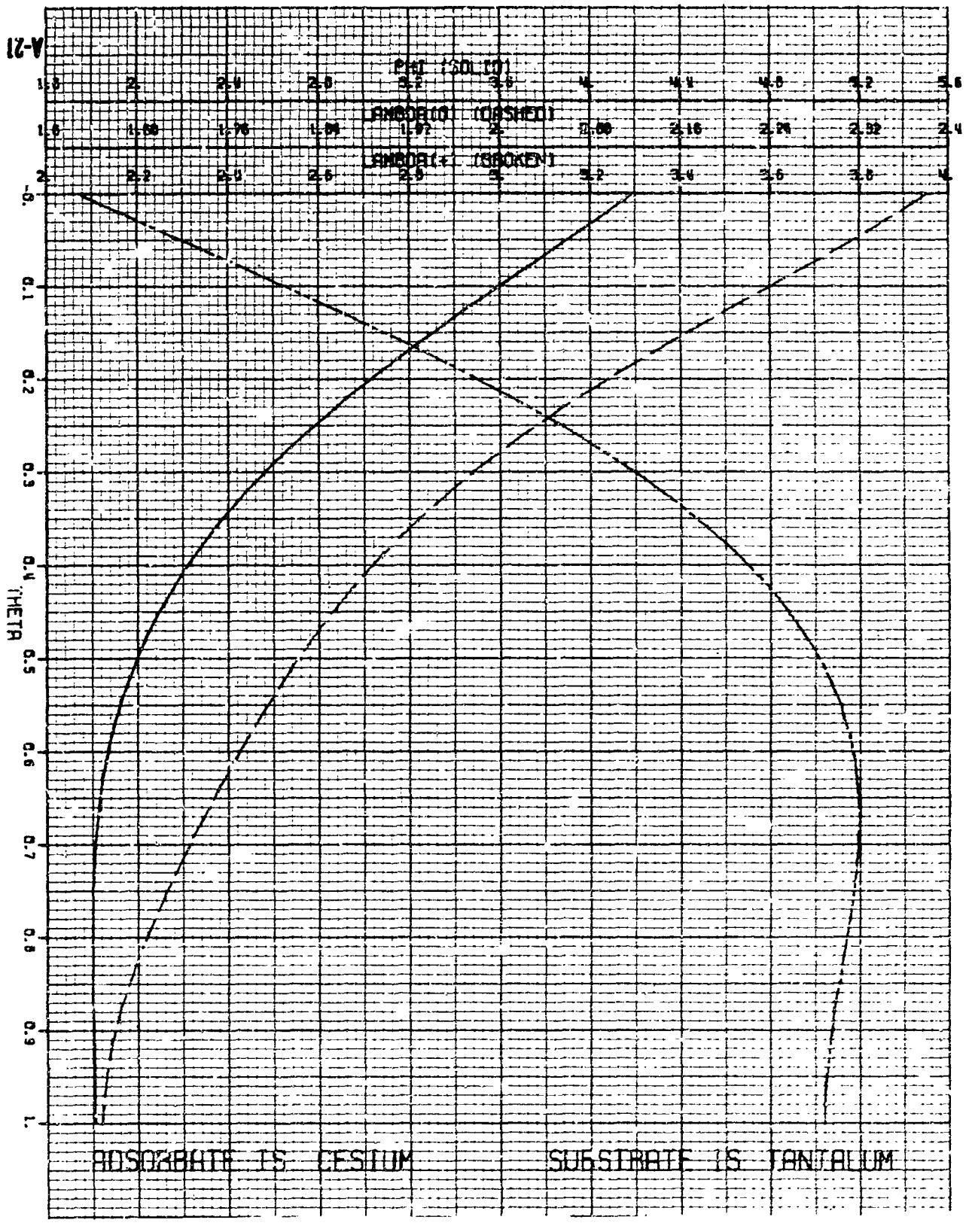
PHI (SOLID)
ANBOR(0) (DASHED)
ANBOR(+) (BROKEN)
THETA
ADSORBATE IS CESIUM
SUBSTRATE IS TANTALUM

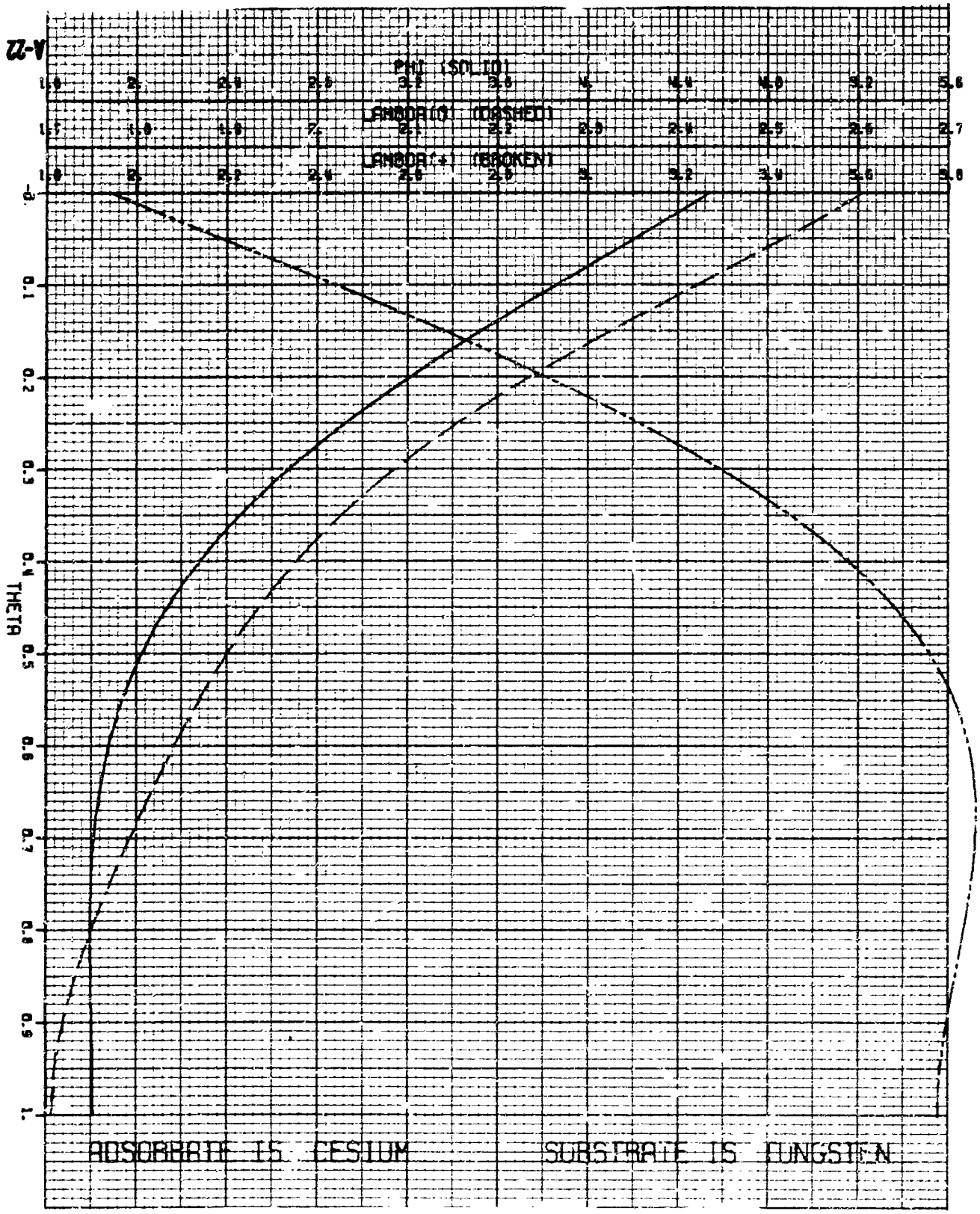
II-V
PHI (SOLID)
LAMBDA(0) (DASHED)
LAMBDA(+) (BROKEN)
THETA
ADSORBATE IS CESIUM
SUBSTRATE IS TUNGSTEN

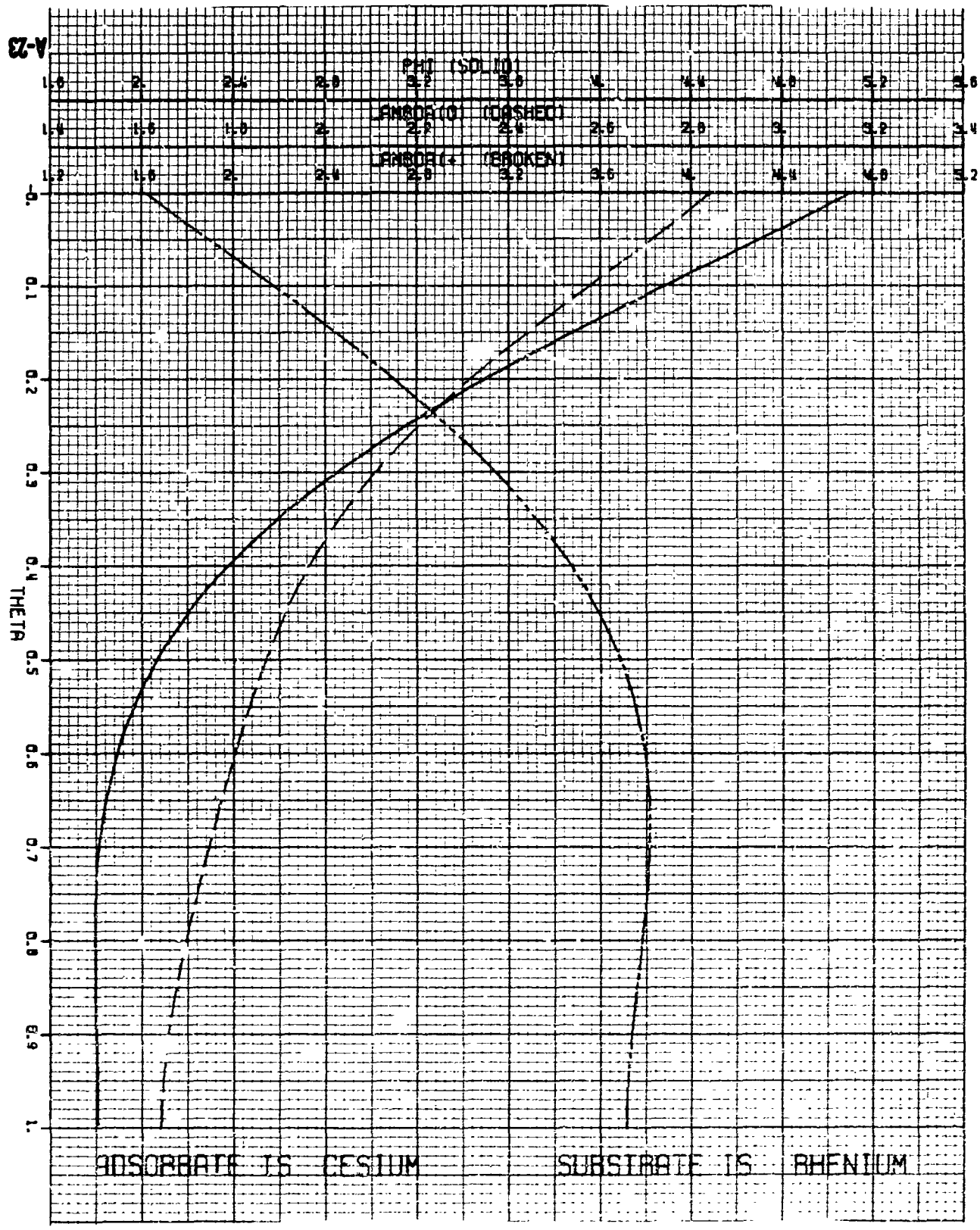
PHI (SOLID)
ANGDA(0) (DASHED)
ANGDA(+) (BROKEN)
THETA
ADSORBATE IS CESIUM
SUBSTRATE IS RHENIUM

SUBSTRATE IS OSMIUM
ADSORBATE IS CESIUM
THETA

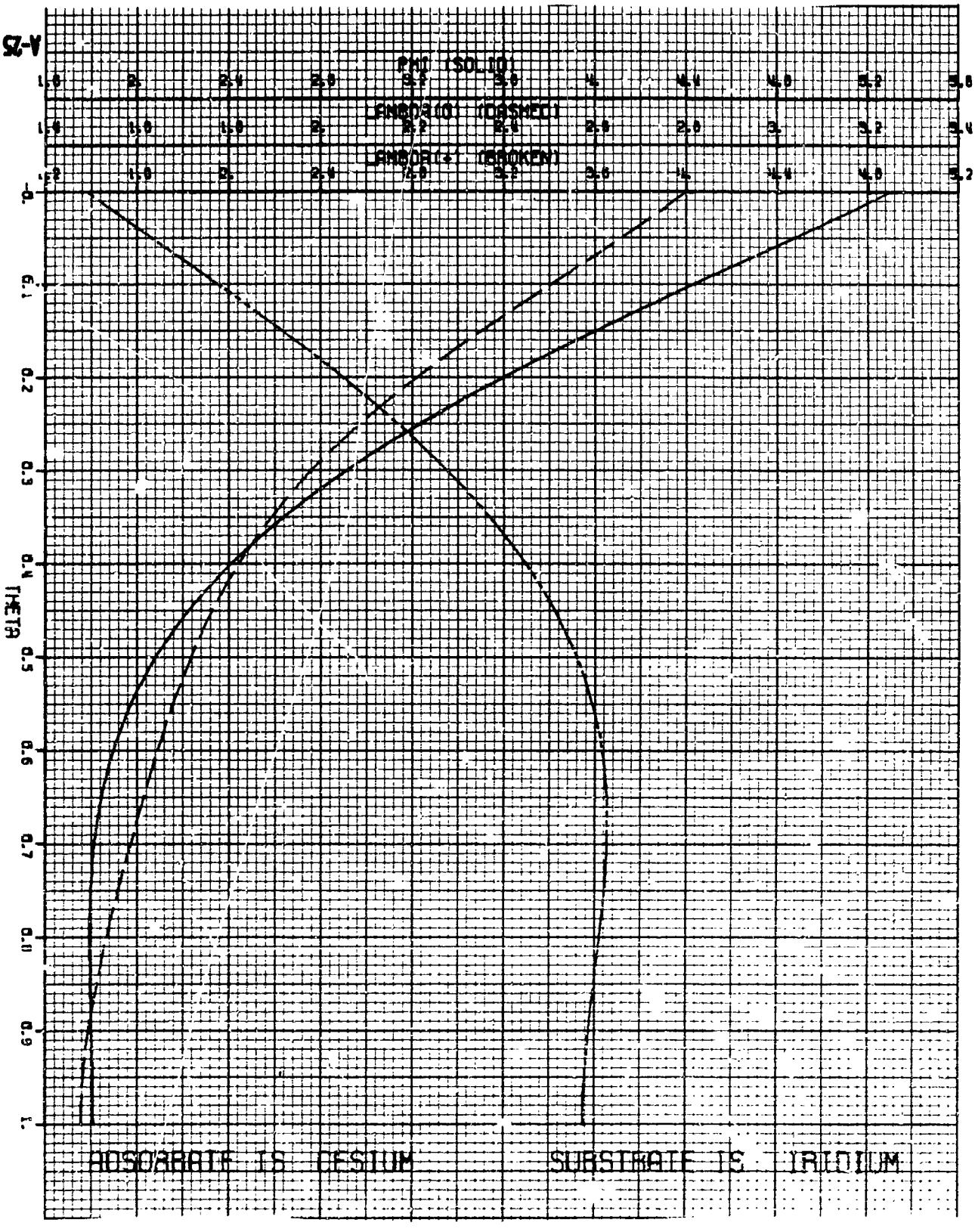
A-25
PNT (SOLID)
LINE(3(0) (DASHED)
LINE(0(+) (BROKEN)
THETA
ADSORBATE IS CESIUM
SUBSTRATE IS IRIDIUM

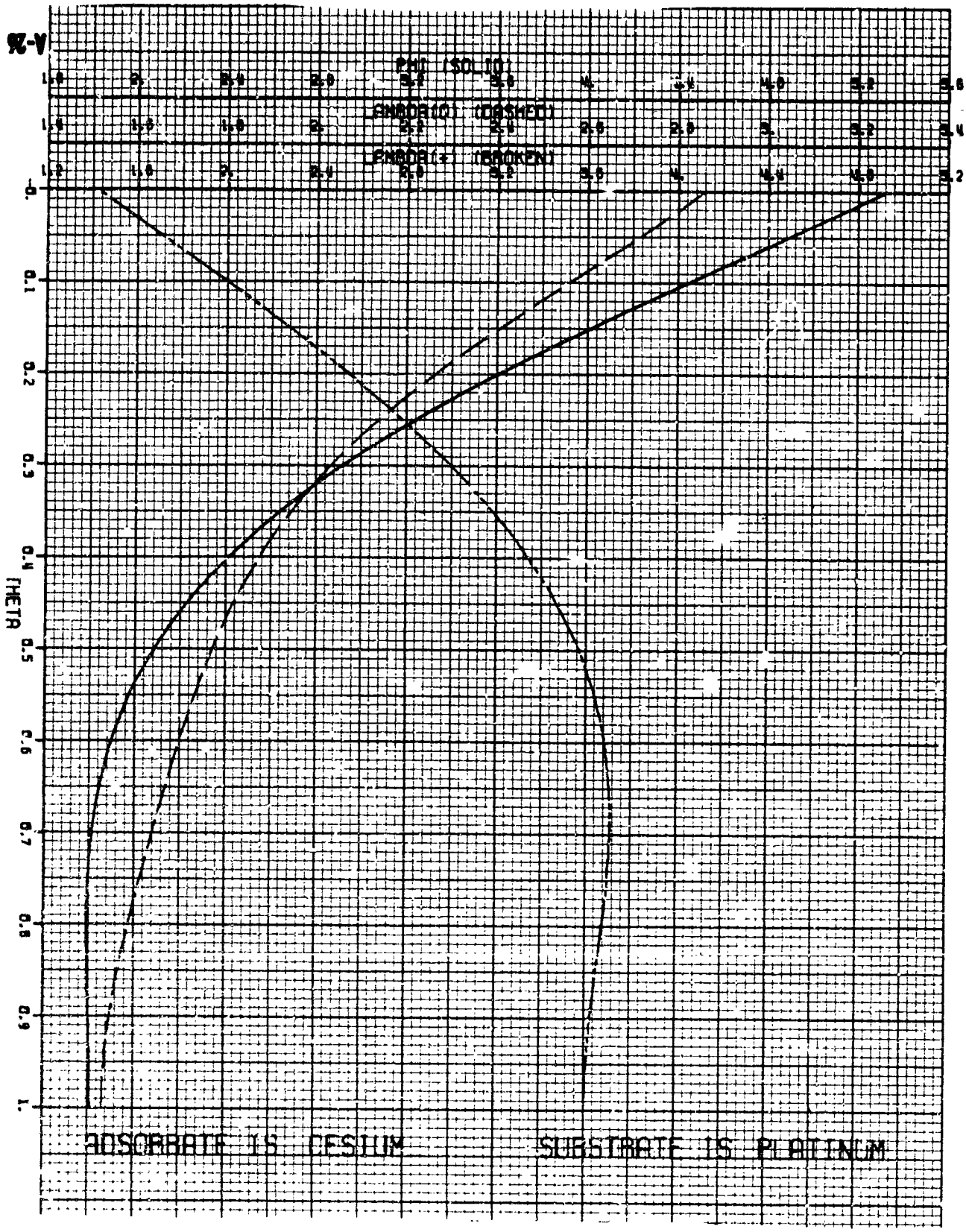
K-V
PHI (SOLID)
ENERGY(O) (DASHED)
ENERGY(+) (BROKEN)
THETA
ADSORBATE IS CESIUM
SUBSTRATE IS PLATINUM

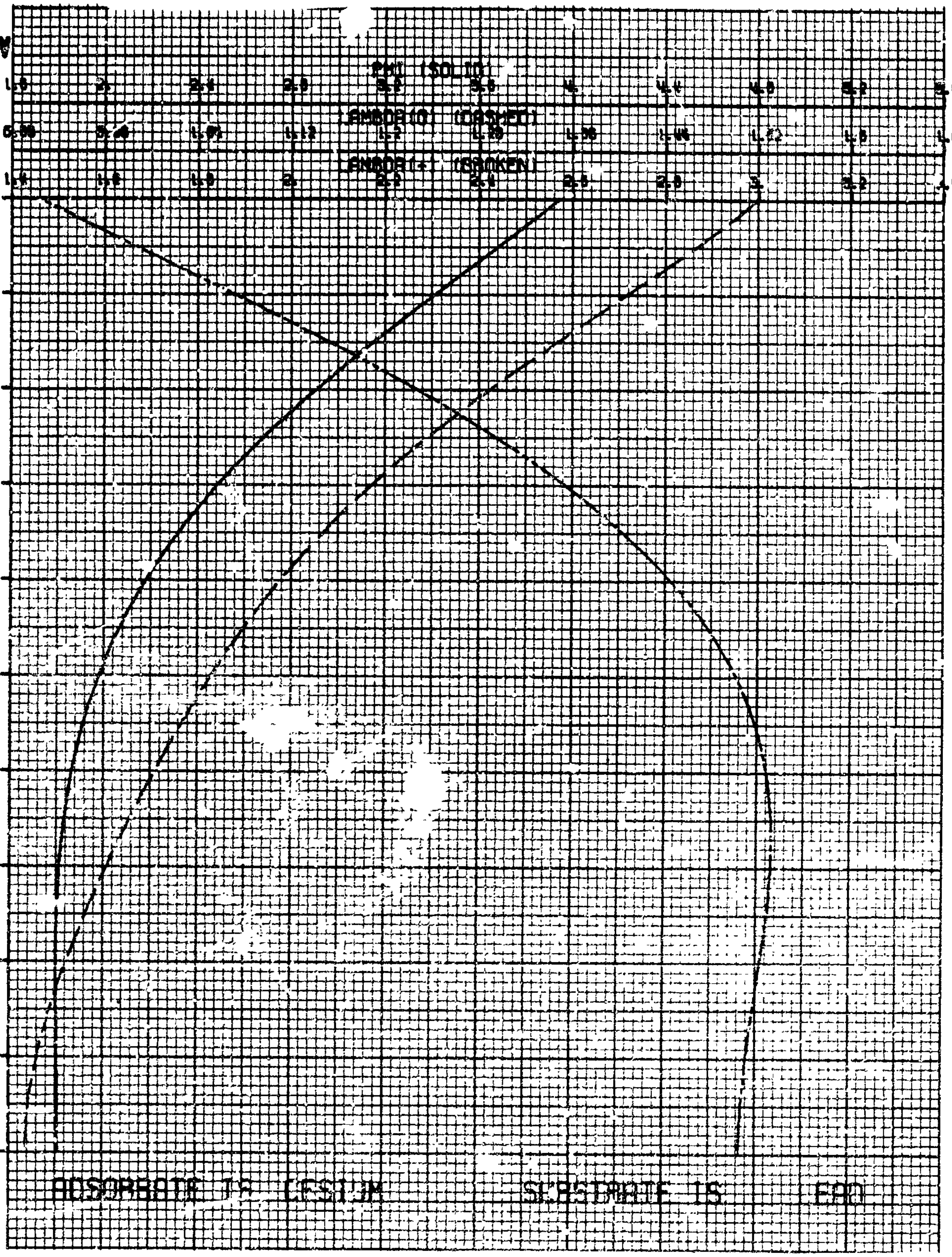
PHI (SOLID)
LAMBDA(0) (DASHED)
LAMBDA(+) (BROKEN)
THETA
ADSORBATE IS CESIUM
SUBSTRATE IS
ERO